



TECHNISCHE
UNIVERSITÄT
WIEN

D I P L O M A R B E I T

Point source stimulation of dendrites of a pyramidal cell in Python

ausgeführt am

Institut für
Analysis und Scientific Computing
TU Wien

unter der Anleitung von

**ao. Univ.Prof. Dipl.-Ing. DDDr.
Frank Rattay**
und
Dipl.-Ing. Dr. Andreas Fellner

durch

Tomislav Dolic

Matrikelnummer: 01525225

Contents

Kurzfassung	i
Abstract	iii
Acknowledgements	iv
Glossary	v
1 Introduction	1
1.1 Neuronal Structure	1
1.1.1 Cell Membrane	2
1.1.2 Channel types	4
1.2 Action potential	5
1.2.1 AP Propagation	7
1.3 Resting membrane voltage	8
1.4 Pyramidal Neuron	11
1.4.1 Synaptic Integration	12
1.5 Electrical stimulation	15
1.5.1 Point-source electrode	17
2 Model	19
2.1 Hodgkin Huxley model	20
2.1.1 ODE	21
2.1.2 Subthreshold stimulation, time-domain	22
2.1.3 Cable equation	24
2.2 Geometrical Realization	26
2.2.1 Discretization in NEURON	30
2.2.2 Activating function	31
2.2.3 Blocking artifacts	36
3 Methodology	39
3.1 Channel types	39
3.1.1 Na^+	42
3.1.2 K_f	43
3.1.3 K_s	43
3.1.4 I_h	44
3.1.5 Leakage channel	44
3.1.6 Ca^{2+}	44
3.1.7 Temperature adjustment	46

Contents

3.2	Channel Distribution	47
3.2.1	Apical Dendrites	49
3.2.2	Soma	52
3.2.3	Basal dendrites	53
3.2.4	Axon	53
3.3	NEURON extracellular mechanism	54
3.4	Morphology	54
3.4.1	Spines	55
3.4.2	Soma	55
3.4.3	Axon	58
3.4.4	Axon Hillock	60
3.4.5	Dendrites	62
4	Results	63
4.1	Intracellular stimulation	63
4.2	Extracellular stimulation	74
4.2.1	Long-range distance	74
4.2.2	Mid-range distance	80
4.2.3	Lateral to soma	85
5	Discussion	89
5.1	Summary	89
5.2	Outlook	90
	Bibliography	91

Kurzfassung

Die elektrische Stimulation neuronaler Zellen ist ein aktiv erforschtes Gebiet. Es ist von Interesse, unter welchen Umständen elektrische Stimulation ein Aktionspotential (AP) auslösen kann. Anders als bei der intrazellulären Stimulation, bei der Strom direkt in die Zelle injiziert wird, erlaubt die extrazelluläre Stimulation eine flexiblere Position der Elektrode außerhalb der Zelle. Andererseits erfordert diese auch mehr Aufmerksamkeit, zumal da viele Phänomene auftreten können wie man sie so bei der intrazellulären Stimulation nicht vorfindet. Diese Phänomene führen zur Bildung sogenannter Aktivierungsbereiche und zu neuen Möglichkeiten der neuronalen Stimulation. Im Zuge der Erregung bilden sich sogenannte Hyper- als auch Depolarisationszonen aus, die interessante Konsequenzen für diese Arbeit haben. In dieser Arbeit wurde ein von [Almog and Korngreen \(2014\)](#) eingeführtes Kompartiment-Modell einer realen L5 Pyramidenzelle verwendet. Im Allgemeinen machen Pyramidenzellen einen Großteil der erregbaren Neuronenfamilie im Gehirn aus. Sie bilden mit einem Anteil von zwei Dritteln aller Neuronen in der Großhirnrinde von Säugetieren die Mehrheit, was sie zu einem wichtigen Bestandteil kognitiver Prozesse macht. Die Pyramidenzelle wurde in *Python* rekonstruiert. Die Schnittstelle zum Modell diente dann auch als High Level API zur Software *NEURON* basierend auf der HOC Interpretersprache. Die Ionenkanaldynamik basiert auf dem Hodgkin Huxley (HH)-Formalismus ([Hodgkin and Huxley, 1952](#)). Das Axon wurde künstlich konstruiert da das Papier keine optimierten Resultate für das Axon bereitstellte. Daher wurden homogene Ionenkanalwerte von Natrium, Kalium und Leckagekanälen von [Mainen and Sejnowski \(1996\)](#) übernommen. Im Gegensatz zu früheren Modellen enthält dieses zusätzlich eine Kalzium Ionenkanal Dynamik. Dies ist ein sehr wichtiges Merkmal da es ermöglicht Effekte wie die synaptische Integration in den apikalen Dendriten zu untersuchen und Kalzium getriebene AP-Erzeugung, auch Kalzium spike genannt, zu beobachten. Im Falle einer intrazellulären Stimulation werden wir die Wirkung der Kalzium getriebenen AP-Erzeugung in den apikalen Dendriten untersuchen sowie ihren Einfluss auf die AP-Form des Soma.

Für den Fall der extrazellulären Stimulation untersuchen wir den Einfluss der Elektrodenpositionierung in großer und mittlerer Entfernung sowie lateral zum Soma. Im letzteren Fall konzentrieren wir uns auf den Einfluss auf die basalen Dendriten, das Soma sowie das Axon. Durch die Anwendung von Lang- und Mittelstrecken Stimulation sind wir auf einige interessante Ergebnisse gestoßen. In großer Entfernung, führte anodische Erregung zu einer Depolarisation der Region um das Soma herum. Aufgrund der hohen Erregbarkeit des Axonhügels, führte dies bevorzugt zur Initiierung eines AP. Auf der anderen Seite führte die kathodische Stimulation zur Erregung der apikalen Dendriten in der Nähe der Elektrode und folglich zur Bildung von Kalzium spikes. Nachdem die Elektrode seitlich zum Soma positioniert wurde, hat man festgestellt dass kathodische Stimulation zur Erregung des Axon-Anfangssegments führte. Trotz der Erregung konnte in den basalen Dendriten kein AP initiiert werden, obwohl man davon ausgeht dass die Dendriten die Initiierung eines

Kurzfassung

APs im Axon-Anfangssegment begünstigen. Gleichzeitig wurde das Axon durch kathodische Stimulation hyperpolarisiert. Weiters führte die anodische Stimulation zur Erregung des am weitesten entfernten Ranvier-Schnürring und gleichzeitig zur Hyperpolarisation von Strukturen in der Region des Soma.

Abstract

Electrical stimulation of neuronal cells is an actively researched area. It is of interest under what circumstances electrical stimulation can initiate an action potential (AP). Unlike in the case of intracellular stimulation where current is injected through a patch clamp directly into the cell, extracellular stimulation allows for a more flexible position of the electrode outside of the cell. Extracellular stimulation also needs more attention since there are many more phenomena that may occur, unlike in the case of intracellular stimulation. Those phenomena on the other hand lead to more selectivity of activation regions and new opportunities for neuronal stimulation. During stimulation zones of hyper-, as well as depolarization come into appearance which have interesting consequences for this thesis. A compartmental model of a real L5 pyramidal cell that was introduced by Almog and Korngreen (2014) was used in this thesis. In general pyramidal neurons make a big share of the excitatory family of neurons. They settle for two thirds of all neurons in the mammalian cerebral cortex which makes them an important part for cognitive processes. The pyramidal neuron was reconstructed in a *Python* programmed framework, serving as a high-level API to the software *NEURON* based on the HOC interpreter language. Ion-channel dynamics were based on the Hodgkin Huxley (HH) formalism (Hodgkin and Huxley, 1952). The axon was constructed artificially since the paper did not focus on peeling procedures for the axon. Therefore they did not provide any morphological data, except well-known homogenous settings of sodium, potassium and leakage channels according to Mainen and Sejnowski (1996). Unlike earlier models, this one incorporated sensitive calcium ion-channel dynamics. This is a very important feature that allows studying effects like synaptic integration in the apical dendrites and calcium-driven AP-generation, also called calcium spike. In the case of intracellular stimulation, we will study the effect of calcium-driven AP-generation in the apical dendrites as well as their influence on soma AP form. In the case of extracellular stimulation we study the influence of electrode positioning in long- and mid-range distance, as well as lateral to the soma. Regarding the latter, we focus on the influence on basal dendrites, the soma, and the axon. By applying long- and mid-range distance stimulation, we encountered some interesting results: Anodic stimulation led to depolarization of the region around the soma in long-range distance. Given the high excitability of the axon initial segment, this led to its excitation. On the other hand, cathodic stimulation led to excitation of apical dendrites in the near neighbourhood of the electrode and consequently to generation of calcium spikes. When the electrode was positioned lateral to the soma we encountered that cathodic stimulation led to excitation of the axon initial segment. Nevertheless, no AP could be triggered in the basal dendrites although as a matter of fact the dendrites facilitated AP-initiation in the axon initial segment. At the same time, the axon was hyperpolarized by cathodic stimulation. On the other hand, anodic stimulation led to excitation of the most distant node of the axon and simultaneously to hyperpolarization of structures in the somatic region.

Acknowledgements

I want to thank professor Dr. Frank Rattay for giving me clear instructions at the very early stage of this project and literature to foster through. He also gave me useful hints on how to make simulations and observe phenomena during trials. Given that this topic was quite new for me as a mathematician, it was very helpful to me to have the goals clarified. This allowed me to focus on learning the related theory in order to interpret the sought after results more precisely. I experienced Dr. Rattay as a calm and sympathetic supervisor. He considered my state of knowledge and made amendments such that I was still able to search for valuable results and conclusions!

Furthermore I want to thank Dr. Andreas Fellner who helped me in the early stages of the project. Getting used to the NEURON HOC-interpreter language and transferring the whole model into a self-built python API, augmenting it with the extracellular mechanism, was a challenge. I am thankful that Dr. Fellner provided me with useful code snippets and hints on how to implement the morphology from which I could start off my journey. Since the first meeting he unhesitatingly offered me his support whenever his help was needed!

Most of all I want to thank my parents who made it possible to pursue my interests in life. Starting from an early age, they instilled my interest for mathematics and physics which led to studying the former. They have always been an interesting source of knowledge and inspiration to me!

Glossary

V_m	Membrane voltage
V_e	Extracellular voltage
V_i	Intracellular voltage
V_{rest}	Resting membrane voltage
R_i	Axial intracellular resistance
R_e	Axial extracellular resistance
R_m	Membrane resistance
C_m	Membrane capacitance
c_m	Specific membrane capacitance, area-related
r_m	Specific membrane resistance, area-related
r_i	Specific intracellular interaxial resistance, length-related
E_m	Electric field across membrane
E_{ion}	Reversal potential of ion-species ion
R	Gas constant
F	Faraday constant
T	Temperature in Kelvin
$[I]_i$	Intracellular concentration of ion I in unit mol/m^3
$[I]_e$	Extracellular concentration of ion I in unit mol/m^3
P_i	Permeability of the membrane for ion-species i
$R_{transfer}$	Extracellular electrical transfer resistance
$X_{transfer}$	Extracellular electrical transfer conductance
g_{chan}	Specific electrical conductance for ion-channel chan
G_{chan}	Density distribution of ion-channel chan, along the cell
i	Specific current density
NEURON	Software, based on the HOC-Interpreter Language
Python	High level Interpreter Language
section	Subunit of the neuronal cell in the view of NEURON
segment	Smallest discretized subunit of a neuronal cell, in the view of NEURON
compartment	Synonym for segment
$V_{m,n}$	Membrane voltage at n-th compartment
$I_{n,injected}$	Current injected into n-th compartment

Glossary

Δx	Length of a segment
d	Diameter
A	Area, either cross-sectional or coating
Activating function	Function that evaluates if a certain neuronal section is susceptible to AP-initiation, in case of extracellular stimulation
strength duration relation	Relation of time duration and minimal current strength it takes to excite a structure
strength distance relation	Relation of distance and minimal current strength it takes to excite a structure
somatic path	Given a section in NEURON, it defines the path of predecessor sections towards the soma
Electrotonic length constant $\tilde{\lambda}$	Measure of how good an intracellular voltage deflection may influence its neighbourhood locally
Time constant τ	Measure of how fast a voltage deflection may evolve in the time-domain, at one specific place
synaptic integration	Process of summing up several stimuli in the apical dendrites
subthreshold	Region of membrane voltage where no Action potential, facilitated through activation of ion-channels, is observed
AP	Action potential
BAC	Backpropagation-activated calcium driven spike firing
CV	Coefficient of variation: Statistical measure of deviation, given a set of trials
EPSP	Excitatory postsynaptic potential
FWHM	Full width half maximum of a signal
FCM	Fohlmeister Miller
IC_{50}	Half maximal inhibitory concentration
SDuR	Strength duration relation
SDR	Strength distance relation
HH	Hodgkin Huxley

1 Introduction

1.1 Neuronal Structure

A neuronal cell is an electrically excitable structure whose main purpose is to transfer electrical signals. In its simplest form, its structure looks like in [Figure 1.1](#). Most of the information and conclusions are derived from [Zhang \(2019\)](#).

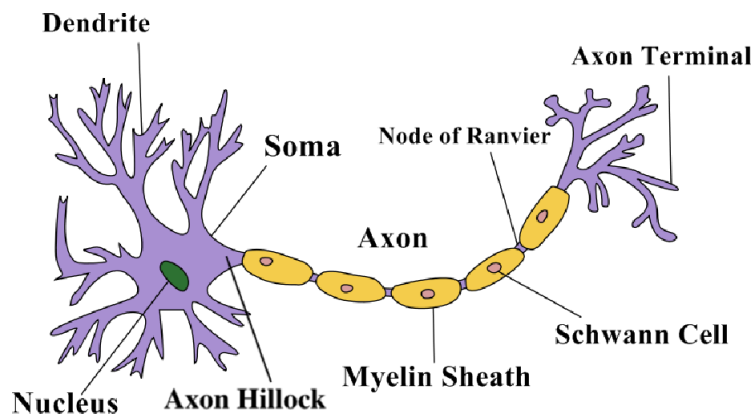


Figure 1.1: Morphology of a neuronal cell: The *soma* consists of the cell *nucleus* of the neuronal cell. Usually it has a diameter of about $20\mu m$. Proximal to it, the *axon hillock* starts and cones into the axon. It is a highly excitable structure in terms of high density of voltage-gated sodium channels, making it the first candidate for initiation of an action potential (AP) (see [Section 1.2](#)). Basically, an AP is a propagating electrical signal. Dendrites are recipients of synaptic signals and have a strongly branched structure in order to increase their surface. They also do so by use of so-called *spines*, small protrusions along the surface of the membrane (see [Figure 1.2](#)). The *axon* itself has a special structure and is divided into regions. The axon is additionally surrounded by *myelin sheaths*. The structure of myelin sheaths is interrupted by sections of small length called *nodes of Ranvier*. Unlike the myelinated sections of the axon, the nodes hold a high density of sodium channels. Later, we will see that while the myelin increases the velocity of signal propagation, the nodes facilitate its propagation by exchange of charged particles. The *myelin* is rich of lipids and is formed by Schwann cells. The *Axon Terminal* consists of presynaptic buttons. Source: [Zhang \(2019\)](#)

Dendrites facilitate the generation of electrical activity in the somatic region, especially in the axon hillock. In case an AP is generated in the neuronal cell, it then propagates along

the axon finally arriving at the axon terminal. The axon terminal consists of presynaptic buttons which are usually attached to some other target neuron. In case a signal arrives at the axon terminal, neurotransmitter are released. These neurotransmitter are exchanged between the presynaptic membrane and the postsynaptic membrane of the target neuron. The small space between the two is called *synaptic cleft*. Subsequently, this either leads to excitation or inhibition of the target neuron.

The myelin sheaths which wrap around the axon increase the velocity of signal transmission due to its greater thickness of lipid insulation. This greater insulation leads to less loss of charge carrier as well as to decreased membrane capacitance. The nodes of Ranvier amplify the propagating signal.

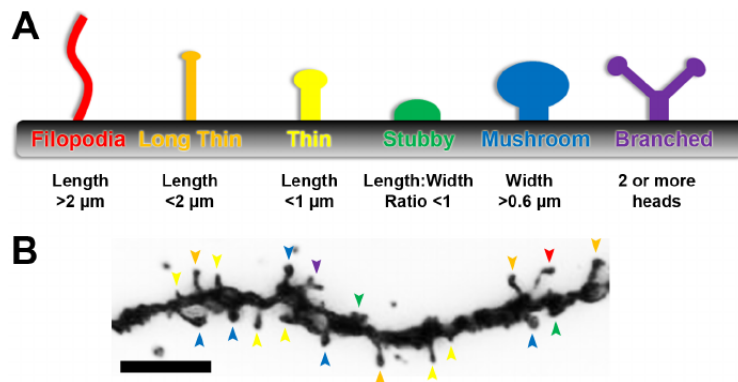


Figure 1.2: Spines: Obviously there exist many different types of spines, each serving some different functionality. Nevertheless, all of them aim to catch presynaptic signals better. They do so by increasing the dendrites biochemically active area. Depending on the geometry and type of neuronal cell, they develop different forms. Source: ¹

1.1.1 Cell Membrane

In order to understand the dynamics of signal propagation fully, we must take a look at the neuronal cell membrane itself in order to study its specific properties. [Figure 1.3](#) shows a simplified picture of the membrane.

¹<https://doi.org/10.1371/journal.pone.0107591>

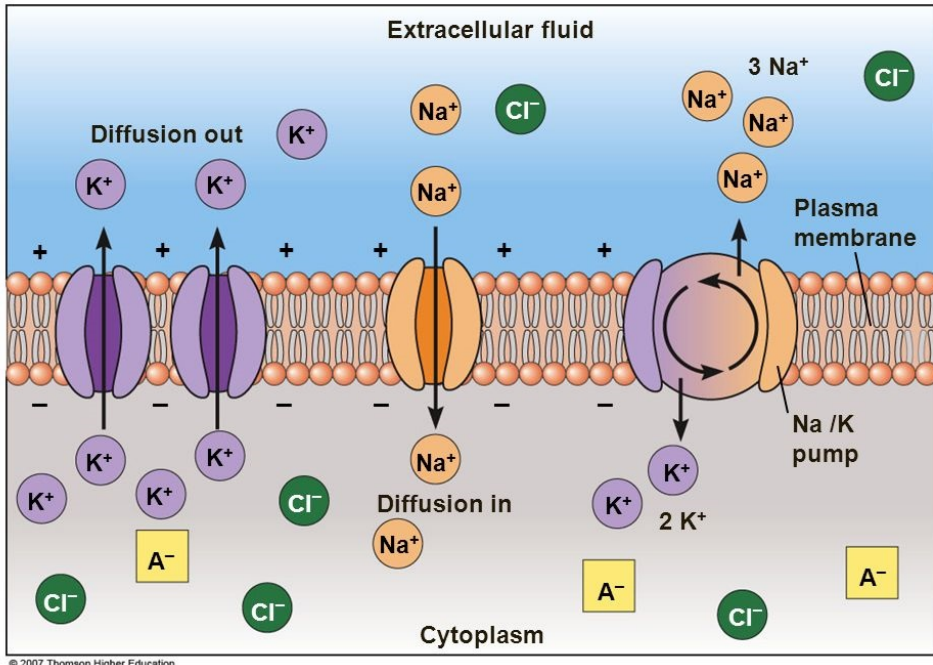


Figure 1.3: Cell membrane: The membrane consists of so-called ion-channels which are permeable for a specific ion species or even a mixtures of them. The ion channels are embedded into a matrix of a phospholipid bilayer. The channels provide the possibility of ion exchange between intra- and extracellular space. The intracellular space is also called cytoplasm. The exchange of sodium and potassium ions plays a key role when it comes to signal propagation. Ion-pumps are in charge of maintaining a non-zero *concentration gradient* perpendicular to the membrane. This is done by exchange of ions which leads to a disbalance of ion concentration between cytoplasm and extracellular fluid. The disbalance in concentration also leads to a disbalance of charge. Put together, this process leads to an electric field across the membrane. The difference of voltage between intra and extracellular space is defined by $V_m = V_i - V_e$ and is called the *membrane voltage*. The value of V_m at *resting state* is analyzed in Section 1.3. Resting state defines the situation when a neuron is not excited. Source: ²

Referring to Figure 1.3, ion-pumps maintain a non-zero concentration gradient of ion species between cytoplasm and extracellular space. They do so by exchanging ions against their concentration gradient. This process consumes energy which is covered through recovery of Adenosinetriphosphate (ATP). The mechanism behind this process is thoroughly sketched in Figure 1.8. So-called leakage channels are present in the membrane. Through the leakage of ions, this leads to a loss of charge along the concentration gradient (see Section 1.1.2). Therefore, ion pumps must run permanently in order to compensate for this loss of charge. This process consequently leads to a resting state. The membrane voltage at resting state is $V_{rest} = V_{i,rest} - V_{e,rest}$. V_{rest} is negative.

²Thomson Higher Education; 2007; Chap.42:Voltage-Activated Ion Channels

Let us consider the case of a mammalian cell. Its concentration of each ion-species is listed in [Figure 1.4](#). By application of [Equation Goldman](#), we can conclude the resting membrane voltage to be $V_{rest} \approx -65mV$. The physical mechanism behind this process is explained in [Section 1.3](#).

Ion	Intracellular Concentration [M]	Extracellular Concentration [M]
Na^+	$5\text{-}15 \times 10^{-3}$	145×10^{-3}
K^+	140×10^{-3}	5×10^{-3}
Mg^{2+}	0.5×10^{-3}	$1\text{-}2 \times 10^{-3}$
Ca^{2+}	10^{-7}	$1\text{-}2 \times 10^{-3}$
H^+	7×10^{-8} (pH 7.2)	4×10^{-8} (pH 7.4)
Cl^-	$5\text{-}15 \times 10^{-3}$	110×10^{-3}

Figure 1.4: Typical ion concentrations in- and outside a Mammalian Cell.

Source: [Alberts et al. \(2017\)](#)

1.1.2 Channel types

There are different ion-channel types present in the membrane of a neuronal cell. In the following we list some of them. Constants are interpreted in view of [Section 1.3](#).

- **Leakage Channel:** This type of channel has an almost constant permeability. From the perspective of the HH formalism, this translates to a constant specific membrane resistance of that specific channel. Many of them are selectively permeable for one specific ion-species and therefore can only facilitate the motion along the concentration gradient for that specific ion-species. Some of them may also be deactivated by chemical ligands although not being ligand-gated channels.
- **Ligand-gated channels** This type of channel is activated by docking of neurotransmitter onto receptors which populate the extracellular surface of the membrane. Roughly there are two types of neurotransmitter/receptor pairs. Glutamate docks onto AMPA receptors which facilitates the flux of sodium ions into- as well flux of potassium ions out of the cell. GABA docks onto GABAA receptors, facilitating the flux of chloride ions Cl^- into the cell. The direction of flux for a specific ion-species is determined by its reversal potential E_{ion} across the membrane. In the case of $E_{ion} > 0$ this leads to influx, and for $E_{ion} < 0$, to outflux of ions.
- **Voltage-gated channels** This type of channel plays an important role in the case of excitation through application of electrical stimulation. Usually the condition $V_m - V_{thre} > 0$ must hold true for some threshold membrane voltage $V_{thre} > V_{rest}$, in order to activate this channel. We will see that there exist several types of these channels. They differentiate each other by the ion-species they are permeable for. Furthermore, voltage-gated channel may also be activated at different threshold levels. In this thesis for example, we will use high and medium threshold voltage-gated calcium channels. Furthermore, there also exist channels which are voltage-gated but at the same time, depend on the intracellular concentration of some other ion-species.

The interplay of sodium and potassium voltage-gated channels within the course of a propagating AP is described in Section 1.2.

- **Mechanically-gated channels** This type of channel opens upon application of physical force onto the membrane. For example, they are important from the perspective of sensoric input over the skin.

As we have seen, there exist many more ion-channels than the ones for passage of sodium and potassium ions. The composition of the different ion channel types amongst each other may also differ in different parts of the cell. This in turn leads to varying V_{rest} along the neuron.

1.2 Action potential

Most of this chapter is based on Rattay (1990) and Hodgkin and Huxley (1952), if not stated otherwise. Referring to Rattay (1990) and Hodgkin and Huxley (1952) an *action potential* (AP) can be defined as a deflection of the membrane voltage V_m above 0mV for some minimal time duration. This process of excitation is produced by a stimulus. The stimulus triggers the activation of ligand-, voltage gated or even some other type of ion-channels. In the following we see a detailed description.

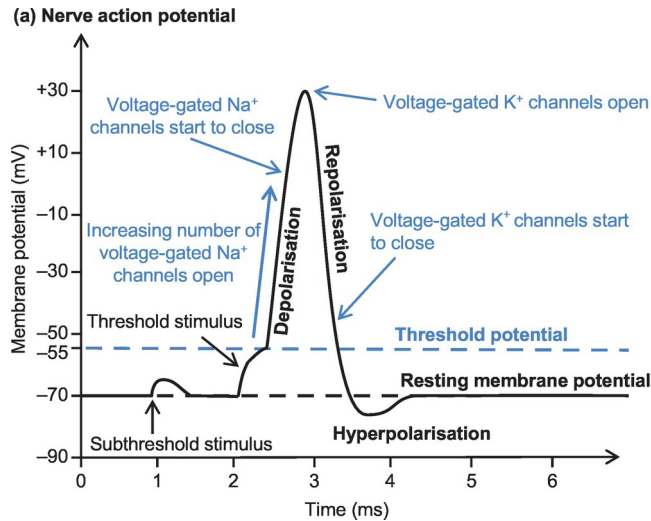


Figure 1.5: Action potential: The membrane potential $V_m = V_i - V_e$ is plotted on the y-axis. Two consecutive stimuli are considered. Chronologically, the first one does not manage to reach threshold potential $V_{thre} = -55\text{mV}$ and consequently fails to initiate an AP. The second one manages to do so. The very first phase after threshold voltage has been reached is called depolarization. In this phase, sodium channels open. Due to the positive reversal potential E_{Na} of sodium ions, an influx of latter into the cell is observed. At some point, the ion channels close, hindering the sodium ions from further influx into the cell. At the same time, the potassium channels open initiating the process of *repolarization*. Given the negative reversal potential E_K of potassium, this leads to outflux of positively charge potassium ions which leads to recovery of the membrane voltage towards resting voltage V_{rest} . After a short period, the potassium channels close their gates. The subsequent phase is called *hyperpolarization*.

Source: Chambers et al. (2019)

The sodium channel type has the possibility to inactivate itself. This is not simply done by closing the activation gates, but rather activation of the so-called *inactivation gate*. This happens in the early stages of the repolarization phase. The situation is sketched in Figure 1.6.

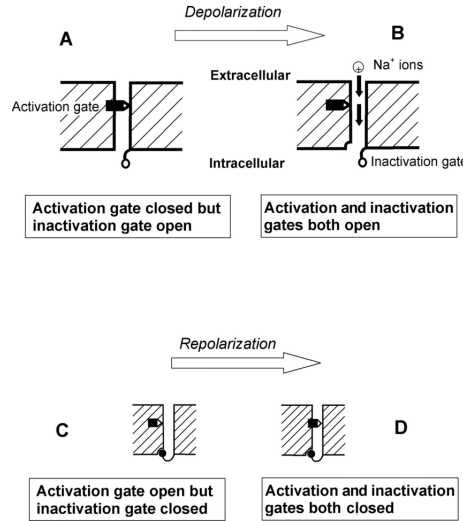


Figure 1.6: Sodium channel gates: The influence of the action potential onto the sodium gates is sketched. a) At the very beginning, $V_m = V_{rest}$ holds true, and the activation gate remains closed. b) As soon $V_m > V_{thre}$ is reached, the activation gate opens and allows for influx of sodium ions during the phase of depolarization. c) As soon depolarization reaches a certain level, the inactivation gate closes. This stops sodium ions from further influx into the cell and devolves into the repolarization process d) During the repolarization process the activation gates also close. Both stay closed until resting state is restored. Source: [Booker et al. \(2003\)](#)

1.2.1 AP Propagation

In this section we use conclusions and information based on [Rattay et al. \(2002\)](#). We saw that each part of the neuron may experience the temporal evolution of an AP. AP propagation is defined as the traveling of the AP along and maybe across a neuronal structure. As an example, the evolution of an AP in the human cochlear neuron is sketched in [Figure 1.7](#).

Refractory Period After an AP has been generated locally, for a certain period it is not possible to initiate a second one at the same place. This is due to the fact that after an AP has occurred, sodium channels remain in their inactivated state for some small time period. This period during which no further AP can be initiated is called *absolute refractory period*. Nevertheless an AP may be initiated even before expiry of the absolute refractory period at higher threshold voltage. This shorter time period is called *relative refractory period*.

Electrotonic length constant Referring to [Rattay \(1990\)](#), the *electrotonic length constant* gives us a quantification of how far a deflection of the membrane voltage may influence its neighbourhood. [Equation electrotonic length constant](#) gives a measure of this behaviour. In contrast to this, [Equation time constant](#) gives us a measure of how fast the temporal evolution of an AP may happen.

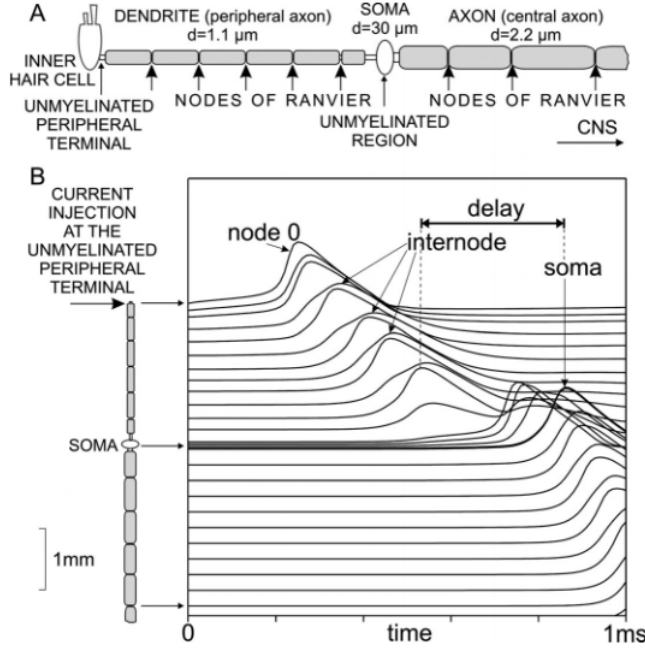


Figure 1.7: Human cochlear neuron: Current was injected through a patched clamp into the first node of the peripheral axon. This led to excitation and furthermore to AP initiation in the first node. The generated AP subsequently propagates towards the soma and is passed to the axon. The signal gets amplified each time it passes a node of Ranvier. Source: [Rattay et al. \(2002\)](#)

1.3 Resting membrane voltage

Most of the section is based on results from [Goldman \(1943\)](#). The resting membrane voltage V_{rest} is defined as the voltage when the neuronal section is at rest and no signal is transmitted. V_{rest} is determined by the difference of ion concentrations in- and outside the cell membrane. We will see that this disbalance leads to twofold gradients which in turn determine V_{rest} . We already encountered the fact that $V_{rest} < 0$ is maintained by the exchanging mechanism of ion-pumps. The ion-species we focus on while deriving subsequent conclusion are sodium (Na^+), potassium (K^+), chloride (Cl^-) and calcium (Ca^{2+}). Given that the concentration gradient between in- and extracellular space is non-zero, [Equation Goldman](#) will give us a formula for determining V_{rest} . Each ion species experiences a force. The forces are of twofold nature and listed as followed.

1. Ions are charged particles. A disbalance in charge between in- and extracellular space always leads to an electric field which in turn creates an electrical force upon the charged particles. The gradient of that electric field is called *electrical gradient*.
2. Due to the difference of concentrations between in- and extracellular space, the solutions aim to equalize this difference. This in turn produces a gradient which is called *concentration gradient*. In short: The underlying principles are of thermodynamic

nature and well studied. The root cause of this phenomenon is due to the fact that entropy of any given system always tends to increase.

[Goldman \(1943\)](#) explains the mechanism and its consequences in detail. It describes the impact of both beforementioned gradients onto movement of ions across the membrane. In the following we denote the total flux of ions across the membrane.

$$J = \sum_{i \in \{ion_{species}\}} j_i \quad (\text{total flux})$$

j_i denotes the flux of i -th ion species and is defined in [Equation molar flux](#). Although not obvious, it also incorporates the impact of the ion pumps which is expressed in the presence of an electric field E_m across the membrane and its resulting drift-term $j_{i,drift}$. One assumption that may be made is that $J = 0$ holds true. This states the condition that in and outgoing amount of ions are equal and a dynamic equilibrium is sustained. Several ion-pumps maintain the two resulting gradients. One of the ion-pumps is the calcium-ATPase. It facilitates the efflux of calcium-ions out of the cell ([Destexhe A, 1993](#)). The other one is the sodium/potassium-ATPase pump ([Pivovarov A. S., 2018](#)). The process of ion exchange in the case of sodium and potassium is illustrated in [Figure 1.8. Equation molar flux](#) determines the molar flux of i -th ion species across the membrane.

$$j_i(z) := j_{i,drift}(z) + j_{i,diffusion}(z) \quad (\text{molar flux})$$

$z \in [0, d]$ parameterizes the membrane with thickness d . The molar flux consists of two components. $j_{i,drift}$ accounts for the flux caused by the electric field across the membrane which is induced by charge separation. $j_{i,diffusion}$ accounts for the share of ion flux due to the concentration gradient. The concentration gradient is also described by Fick's Law of diffusion. It makes the degree of diffusion linearly dependent on the density gradient across the membrane. According to [Goldman \(1943\)](#) the components may be defined as,

$$\begin{aligned} j_{i,diffusion}(z) &:= -z_i u_i RT \frac{d[n_i]}{dz} = -D \frac{d[n_i]}{dz} \\ j_{i,drift}(z) &:= -z_i^2 n_i u_i F \frac{dV_m}{dz} \\ [n_i] &= \frac{\text{mol}}{\text{m}^3} \dots \text{concentration of the } i\text{-th ion species at point } z \\ [z_i] &= \pm 1 \dots \text{valence of } i\text{-th ion} \\ [R] &= \text{JK}^{-1} \text{mol}^{-1} \dots \text{gas constant} \\ [F] &= \text{C mol}^{-1} \\ [T] &= \text{K} \end{aligned}$$

$D := z_i u_i RT$ denotes the diffusion coefficient with unit $[D] = \frac{\text{m}^2}{\text{s}}$ which is determined by Fick's first law. Drift of ions is obviously dependent on the electric field $E_m(z) = \frac{dV_m}{dz}$ that is present across the membrane. u_i denotes the mobility of the specified ion

species. [Equation molar flux](#) is a differential equation for $[n_i](z)$, the concentration of i-th ion-species across the membrane at point z . The distribution of V_m along the membrane may not be linear. Consequently, the electric field $E_m(z)$ may not be constant which would otherwise lead to a straightforward solution. Therefore, the field may be determined in terms of a Poisson's equation for V_m which reads as,

$$\frac{d^2V}{dz^2} = -\frac{4\pi}{\epsilon}\rho(z)$$

$\rho(z)$ denotes the distribution of charge along the membrane. It is defined by,

$$\rho(z) = F \left(\sum z_i n_i(z) + \hat{N}(z) \right)$$

\hat{N} denotes the concentration of fixed ions in the membrane at point z . The first term denotes the contribution of mobile ions. The membrane as a whole should be electrically neutral which reads as the condition,

$$\int \rho dx = 0$$

We can make the assumption that the membrane mainly consists of dipolar ions which are close to their isoelectrical point. The isoelectrical point is defined as the pH-value at which the net charge of a dipolar molecule diminishes to zero and where the distortion forces of the electric field along the membrane at low currents is minimized ([Goldman, 1943](#)). As a consequence, we may assume that $\rho \equiv 0$ and it follows that $E_m(z) \equiv E_m$ for some constant E_m . This simplifies [Equation molar flux](#) to an ODE of the form,

$$j_i(z) = -z_i^2 n_i(z) u_i F E_m - z_i u_i RT \frac{d[n_i]}{dz}, \quad [n_i](0) = n_{i0} \quad (1.1)$$

Since we will not go too far into detail of the derivation process we can summarize: [Equation 1.1](#) for each ion species separately combined with the condition $J = 0$ in [Equation total flux](#), leads to determination of [Equation Goldman](#). This also means that the ion-pumps maintain a dynamic equilibrium of ion-exchange across the membrane. [Equation 1.1](#) is an ODE with initial value n_{i0} . n_{i0} denotes the intracellular ion concentration of i-th ion species.

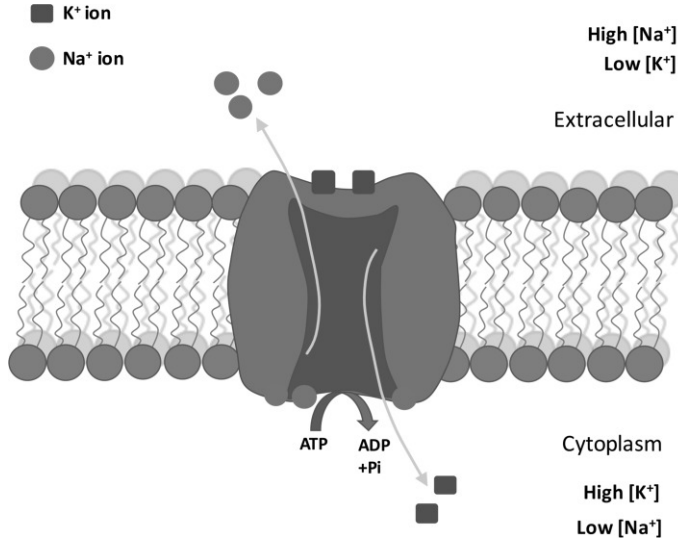


Figure 1.8: Sodium/potassium-ATPase pump: The ion pump maintains an asymmetric exchange of ions. Concretely the figure shows an efflux of 3 sodium ions for each 2 potassium ions. The energy for this process is delivered by exploitation of one ATP molecule. The voltage dependent gates do have a higher permeability for potassium ions in the phase of outflux than they do for sodium ions in phase of influx. This observation goes hand in hand with the fact that processes of repolarization and hyperpolarization evolve in a fast pace. Source: [Pivovarov A. S. \(2018\)](#)

The resting membrane voltage V_{rest} is determined by,

$$V_{rest} = \frac{RT}{F} \ln \left(\frac{\sum_i^n P_i [ion_i^+]_{out} + \sum_i^n P_i [ion_i^-]_{in}}{\sum_i^n P_i [ion_i^+]_{in} + \sum_i^n P_i [ion_i^-]_{out}} \right) \quad (\text{Goldman})$$

P_i denotes the ionic permeability of i-th ion-species. $[ion_i^\pm]_{in}$ denotes the intracellular ion concentration of positively as well as negatively charged ions of species i. $[ion_i^\pm]_{out}$ denotes the extracellular counterpart. V_{rest} is called the resting potential. Applying this same equation for only one ion species leads to determination of the *reversal potential*,

$$E_{ion} = \frac{RT}{z_{ion} F} \ln \left(\frac{[ion]_{out}}{[ion]_{in}} \right). \quad (\text{Reversal Potential})$$

$z_{ion} \in \{-1, 1, 2\}$ denotes the ion-charge

1.4 Pyramidal Neuron

In this work we will focus on a Layer 5 pyramidal neuron. Information in this section is based on [Spruston \(2008\)](#) and [Bekkers \(2011\)](#). [Figure 1.9](#) shows a picture of a L5 pyramidal

neuron. It is mostly found in the cerebral cortex of mammals but also occurs in subcortical areas like the hippocampus amygdala. Obviously there are many types of pyramidal neurons. Their slightly differing geometrical structure may hint to different functionalities and roles in the corresponding parts of the brain. Most of pyramidal neurons are part of the excitatory family of neurons and are furthermore *projection neurons*. This means that the cells possess long axons usually ranging to regions outside the brain. Several diseases can be attributed to faulty evolution of pyramidal neurons. For example, in patients with epileptic disorder the neurons are far too excitable and the main herd region of this kind of dysfunctionality is found in areas of the brain where a lot of interconnected pyramidal neurons are present. The Alzheimer disease in contrary destroys these, leading to degradation of cognitive abilities and memory loss.

1.4.1 Synaptic Integration

Pyramidal neurons populate almost two thirds of all neurons in the cerebral cortex. Given its frequent occurrence in the family of excitatory neurons we may verify plausibility of the existence of the highly branched apical dendrites as followed.

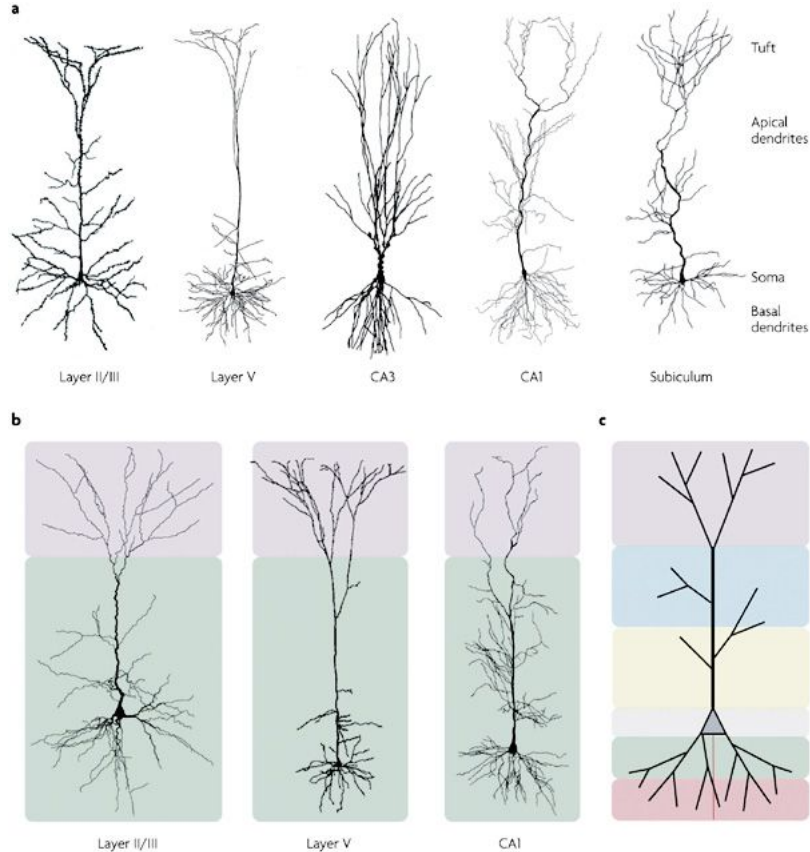
In the context of pyramidal neurons, *synaptic integration* in the apical tuft defines the process of nonlinear summing up of successive excitation which either occurs in a small enough time-window for one considered neuronal section, or when two propagating signals merge at one point. The first one is referred to as *temporal summation* and the latter is called *spatial summation*. Temporal summation may for example occur when a train of excitatory postsynaptic potentials (EPSP) passes the same neuronal section in a short time. Spatial summation may occur in case two signals merge at one point where a neuron branches. This nonlinear summation may lead to surpassing of threshold-levels consequently generating an AP that propagates towards the pyramidal soma and is passed further to the axon. This behaviour models selectivity for stimulation applied at the apical tuft. One may think of it like this: Enough activity must be present temporal and local in order to fire an AP.

I_h

In connection to synaptic integration in the apical tuft we anticipate the existence of the hyperpolarization subthreshold activated current I_h (Larkum et al., 2009). Its channel density increases towards the apical tuft with further distance from the soma. This also hints to its important role for AP propagation in the apical tuft. Simply spoken, the presence of the I_h ion-channel makes it harder for signals originating from the apical tuft to propagate further to its neighbourhood. We may also find an explanation why initiated APs may travel always towards the soma instead of backwards to the top, under the assumption that the AP itself is initiated in the apical tuft. The explanation is twofold.

- **Branching:** Spatial summation can only take place towards the soma. This is because of the fact that two branched apical dendrites can only merge to one, with decreasing distance to the soma. This consequently leads to amplification of their activity.
- **Greater hyperpolarization:** Since specific I_h current increases towards the apical

tuft with greater distance to the soma, it is easier to depolarize neighbours which are closer towards the soma than those that are more distant.



Nature Reviews | Neuroscience

Figure 1.9: Morphology of the pyramidal neuron: There are many subtypes of pyramidal neurons. As suggested by its name, the soma has the form of a pyramid. In the left lower part an example of a L5 pyramidal neuron is visualized. The dendrites are divided into two species, the basal dendrites surrounding the soma and the apical dendrites which are characterized by a highly branched structure. The region of apical dendrites has high vertical spatial extension. Its top is called the apical tuft. The axon is not drawn. Usually it originates from the soma and is either pointing downwards or lateral from the soma away. Source: [Spruston \(2008\)](#)

NMDA

[Larkum et al. \(2009\)](#) investigate the importance of n-methyl-D-aspartate (NMDA)-synapses for the process of synaptic integration in the apical tuft. Allegedly the local recruitment of NMDA-synapses and therefore generation of NMDA spikes in thin dendrites of the apical tuft leads to calcium spike generation in branching points of the apical dendrites. Its

activity was amplified after blocking I_h . This hints to the inhibiting features of I_h 's hyperpolarizing subthreshold nature. [Figure 1.10](#) shows that simultaneous strong synaptic NMDA-stimulation at two sites within the same branch of the apical tuft, provided that the distance between the two of them is close enough, led to nonlinear superposition of both spikes. This led to a higher activity than it would have been the case when both sites were on different or parallel branches.

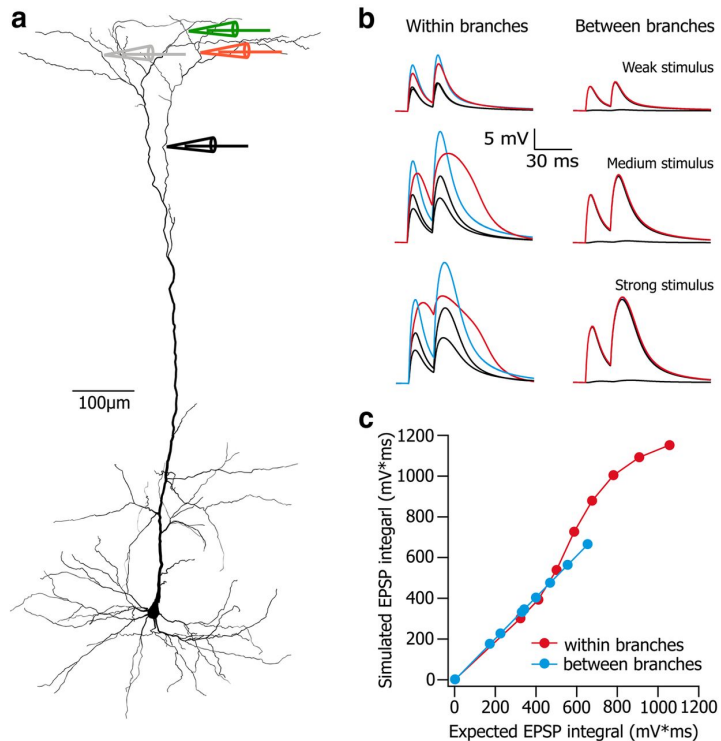


Figure 1.10: Synaptic Integration: The process of synaptic integration is sketched. a) Electrode placement through patch-clamp technique along the reconstructed L5 pyramidal cell at four places. The same model was used in this thesis to deduct some results. b) NMDA spikes were evoked at (green) and (orange) placements marking the case of "within branches". Both had a distance of $26\mu m$ to each other. The black traces illustrate activation of both electrodes separately. The red one illustrates the event of simultaneous stimulation from both electrodes and the resulting trace at their branching-point. For comparison and enlightning the fact of nonlinear synaptic integration, the blue trace equals the sum of both black traces. The stronger the stimuli was, the stronger was the expression of the nonlinear behaviour. When stimulation was applied between branches, no such superposition was observed regardless of stimuli strength. c) An EPSP was simulated at $150\mu m$ underneath the orange electrode. The effects of nonlinear superposition are now obvious, comparing the expected and simulated results of the trace of the EPSP. Source: [Almog and Korngreen \(2014\)](#)

1.5 Electrical stimulation

The main focus in this work will be on electrical stimulation of a pyramidal cell. We refer to the sources of information Rattay et al. (2002) and Rattay (1990), concerning electrical nerve stimulation.

There are two types of electrical stimulation.

- **Intracellular stimulation:** It is realized by injecting current through a patch-clamp directly into a cell. Structures are excited through the increase of V_i .
- **Extracellular stimulation:** It is realized by an electrode placement which is embedded into the extracellular medium. The electrode produces an electric field and consequently indirectly stimulates the cell membrane by increasing its membrane voltage V_m .

In Chapter 4 we will study the effect of both stimulation types onto excitation of a L5 pyramidal cell. The main goal is to achieve the condition $V_m \geq V_{thre}$ with $V_m = V_i - V_e$ and therefore to initiate an AP at some place.

In contrast to intracellular stimulation, the situation for extracellular stimulation looks different. Since it is possible to place the electrode at much greater distance from the membrane, this gives us more possibilities for AP initiation. We are able to initiate an AP either with anodic or cathodic stimulation. More about that matter is discussed in Section 2.2.2.

When we consider a square-wave impulse, not only the strength is of importance when it comes to AP initiation, but also the exposure time as well as temperature of the medium. The curve that describes the minimal strength for AP initiation is called the *strength duration relation* (SDuR) which is sketched in Figure 1.11.

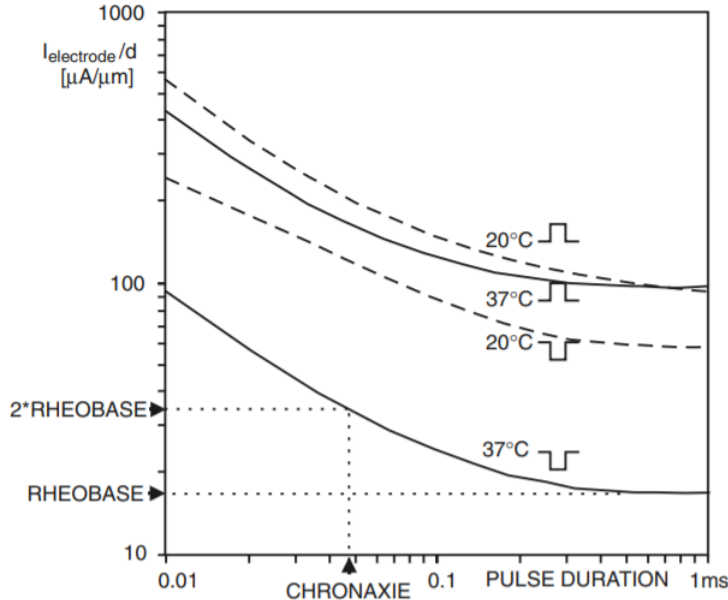


Figure 1.11: Strength duration relation (SDuR): The plot depicts the strength duration relation of the trial [Figure 1.7](#). A fiber with diameter d is stimulated extracellularly at a distance of $\Delta x = 100d$ above a node. The curves are given for two temperatures. One with $20\text{ }^{\circ}\text{C}$ (dashed lines) and the other one for $37\text{ }^{\circ}\text{C}$ (full lines). Obviously, a cathodic impulse initiates an AP at a lower threshold, than it is the case for the anodic counterpart. The difference between anodic and cathodic stimulation is more pronounced for greater temperatures. *Rheobase* defines the minimal necessary current strength in order to initiate an AP. *Chronaxie* defines the time duration of stimulus which is needed in order to initiate an AP at twofold *Rheobase* current strength. The current strength is defined by the relation $I_{electrode}/d$. This makes the observation independent of the diameter of considered neurite.

Another measure for accessing the features of extracellular stimulation is the evaluation of the *strength distance relationship* (SDR). It gives the relation between minimal threshold current for AP initiation as a function of given distance. [Mahnam et al. \(2009\)](#) states a slightly different interpretation of the SDR. It says,

*"The strength distance relationship (SDR) quantifies the relationship between the stimulus amplitude and the extent of neuralactivation around the electrode, although traditionally it was defined based on measurements from a single neuron, i.e., the threshold current for excitation of a neuron as a function of the distance between the electrode and the neuron"*³

For our purposes it suffices to stick to the usual definition. Nevertheless, the paper is of interest since it gives us a theoretical functional approximation of the threshold current

³ [Mahnam et al. \(2009\)](#)

from the perspective of the new interpretation. We will just enlighten its key findings for demonstration purpose. The *Refractory interaction* method was used for assessment of the theoretical approximation of the SDR. Simply spoken, the method searches for a polynomial

$$I_{th}(r) = I_0 + kr^2, \quad (1.2)$$

with distance r from the electrode. The constants are defined as the minimal threshold current I_0 and inclination factor $k = \left[\frac{\mu A}{mm^2} \right]$. The threshold current I_{th} is made quadratically dependent of the distance r . We should bear in mind that this approximation only holds true for small distance r . Furthermore, depending on the concrete setting k may also have high variation. Determination of the factors I_0 and k is part of the refractory interaction method. Without going too deep into detail, it does so by applying excitation through two spatially separated electrodes A and B . It is assumed that both are point electrodes producing a spherical electric field. Then, two steps are made to determine the sought after constants.

1. Current I_a is applied through electrode A . The maximal radial distance r_a from the center of electrode A is measured, for which neuronal activity in form of AP initiation is still detected. Let us call r_a the activation radius of electrode A .
2. Define the distance between both electrodes as L . From the perspective of electrode B we do following steps
 - a) Determine $I_{min,B}$, the minimal current which has to be applied through electrode B in order to achieve activation radius $r_{b,min} = L - r_a$ and therefore no overlapping of activation regions between both electrodes.
 - b) Determine $I_{max,B}$, the minimal current which has to be applied through electrode B in order to achieve activation radius $r_{b,max} = L + r_a$ and therefore full overlapping of activation regions between both electrodes.

Overlapping of respective activation radii is assessed by the Refractory interaction technique. The idea behind this is the following. After neurons were excited till the point of AP initiation by electrode A , they are not responsive to stimuli applied by electrode B for some refractory period, provided that they also lay within the sphere with radius r_b surrounding the electrode B . This procedure concludes two equations, therefore two conditions which are solvable for k and I_0 . This method was used to determine the SDR for peripheral motor nerve fiber with the results $k = 27\mu A/mm^2 \pm 19\%$ and $I_0 = 49\mu A \pm 17\%$. Relative error of r_a and r_b were 11 %. The paper also mentions results from other works which point to even cubic growing behaviour.

1.5.1 Point-source electrode

In this thesis we will always assume to have an almost perfect point-source electrode and isotropic extracellular specific resistance $\rho_e \approx 5050\Omega cm$, if not stated otherwise. Referring to [Rattay \(1990\)](#), the extracellular voltage generated by a point source in distance r by application of stimulation current $I_{el} = [A]$ evaluates to

$$V_e = \frac{\rho_e I_{el}}{4\pi r} = R_e(r)I_{el}. \quad (1.3)$$

Figure 1.12 sketches a concrete situation.

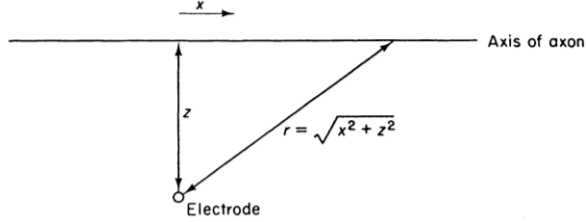


Figure 1.12: Here we consider a concrete situation of one point along the axon with distance r from point-source. For simplicity we consider the two-dimensional case with $r = \sqrt{x^2 + z^2}$. Source: [Rattay \(1990\)](#)

The extracellular voltage obviously declines in the manner $1/r$ which means that a twofold increase in distance leads to a halving of extracellular voltage. Since we have an isotropic medium with its specific conductivity ρ_e which is independent of the direction, this leads to a spherical electric field produced by the point-source.

2 Model

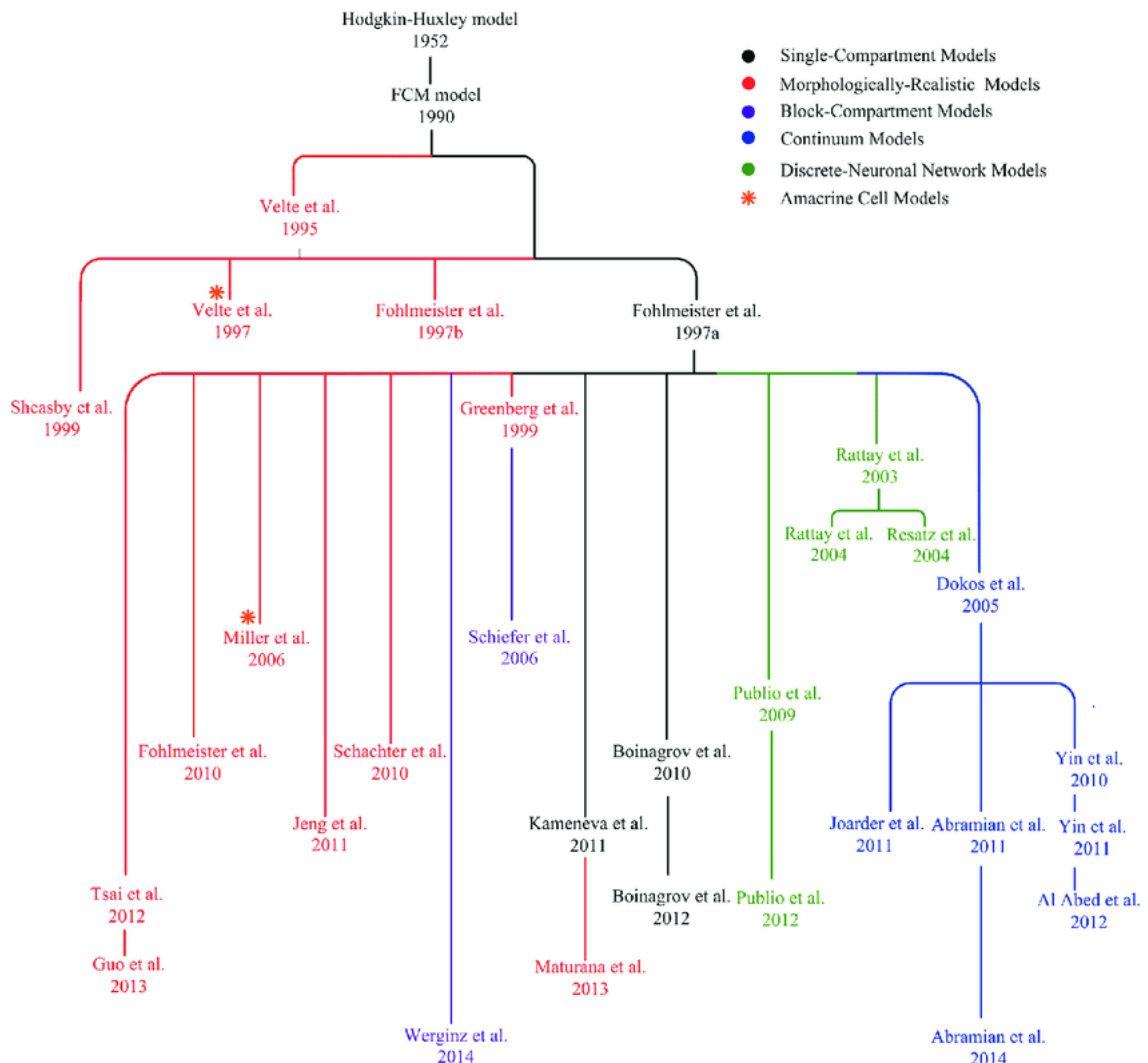


Figure 2.1: The Fohlmeister-Coleman-Miller (FCM) model family: The depiction shows an overview over all the different developments originating from the Hodgkin-Huxley model. This thesis is occupied with the numerical realization of such neuronal models (green subtree). Source: Guo et al. (2014)

2.1 Hodgkin Huxley model

Before we may dive deeper into understanding the model used in this thesis, we must understand the *Hodgkin Huxley* formalism (HH) first. It was developed in [Hodgkin and Huxley \(1952\)](#). Ion channels are interpretable in form of parallelly wired nonlinear resistors. From the perspective of the mathematical representation of the HH formalism, dynamics of ion-channels are modeled by gating functions which are non-linearly dependent on the membrane voltage. It can be defined as follows,

$$i_{ion}(V_m, t) = G_{ion} \prod_{x \in \mathcal{G}} x(V_m, t)^{k_x} (V_m - E_{ion})$$

The equation describes the specific ion current as a function of nonlinear gating functions $x(V_m, t)$, the reversal potential E_{ion} and maximal ion conductivity G_{ion} . Many channels have more than one gating function. In general gating function may also occur as polynomials ($k_x \in \mathbb{N}_+$). Usually, one of the gating functions models the opening behaviour while the other one models its closing behaviour. \mathcal{G} defines the set of all gating functions for considered ion species. The temporal evolution of $x(V_m, t)$ is defined by,

$$\dot{x}(V_m) = \alpha_x(V_m)(1 - x) + \beta_x(V_m)x$$

$\alpha_x(V_m)$ and $\beta_x(V_m)$ are functions which solely depend on V_m . The concrete realization of the functions will be discussed in Chapter 3. [Figure 2.2](#) depicts the electrical realization of the cell membrane for a HH-like model. The membrane lipid bilayer is modeled as a parallel circuit of capacitance C_m and a leakage channel with resistance R_m .

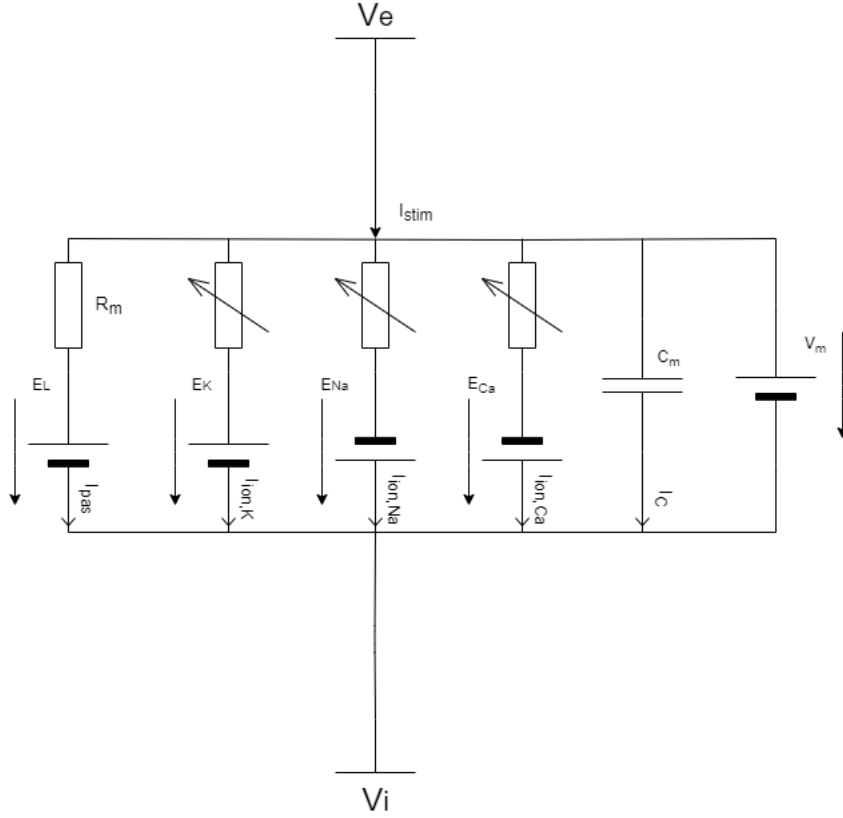


Figure 2.2: HH-like model: The membrane is replaced by an equivalent circuit diagram. Since the ion channels have nonlinear behaviour they can be modeled by variable resistance. The leakage channel is represented by a constant resistance since it models the inherent feature of the membrane itself to leak charge. C_m is the capacitance determined by the lipid bilayer in the neuronal membrane. For myelinated structures like the axon, values of $R_m * C_m$ are smaller than usual. E_{ion} denotes the reversal potential for each ion-channel which can be determined by [Equation Goldman](#). Reversal potentials are maintained through exchange of ions by the mechanisms of ion-pumps. $V_m = V_i - V_e$ denotes the membrane voltage and equals to V_{rest} at resting state.

2.1.1 ODE

From the perspective of [Figure 2.2](#) and by application of Kirchhoff's first Law we can deduct the defining equations for the temporal evolution of V_m ,

$$i_{stim}(t) = c_m \frac{dV_m}{dt} + \sum_k^n i_{ion,k}(V_m(t), t) + i_{pas}(t), \quad V_m(0) = V_{rest}. \quad (2.1)$$

[Equation 2.1](#) describes is given in terms of current densities. We applied Kirchhoff's first Law onto the circuit [Figure 2.2](#) and divided it by some prespecified area A_s . A_s refers to the coating area of some specific segment that is part of the neuronal structure. We shall

later determine what a segment exactly is. c_m defines the specific membrane capacitance, r_m the specific membrane resistance and $i_{ion,k}$ the current density for ion species of type k . i_{pas} denotes the leakage current density. i_{stim} is the current density with which the neuronal segment is excited. By use of the HH-formalism and some fundamental physics we can derive following substitutions,

$$\begin{aligned} i_c &= c_m \frac{dV_m}{dt}, \\ i_{ion,k} &= g_{ion}(V_m)(V_m - E_{ion}), \\ i_{pas} &= \frac{(V_m - E_L)}{R_m * A_s}. \end{aligned}$$

The chosen units are $[i_{ion,k}] = \frac{A}{cm^2}$, $[V] = mV$, $[c_m] = \frac{F}{cm^2}$ and $[t] = s$. This circuit can only represent one small part of the whole neuronal cell. The subunit to which we refer the density values to is called a segment. We shall see later that each segment is also connected parallelly to some neighboring segment (see [Equation cable equation](#)). This interconnection represents the spatial expansion of considered neuronal structure. Taking into account the spatial expansions of the cell and consequently the existence of many more segments, we can determine the membrane voltage of each segment separately. This leads to the discretized version of [Equation 2.1](#) for n-th segment which reads as,

$$i_{stim,n}(t) = c_m \frac{dV_{m,n}}{dt} + \sum_k^n i_{ion,k}(V_{m,n}(t), t) + i_{pas,n}(t), \quad V_{m,n}(0) = V_{rest,n} \quad (2.2)$$

In the model used in this thesis r_m and c_m are choosen to be uniform. The values will only differ for the nodes of Ranvier and the myelin sheaths of the axon. Since we have seen that $i_{ion}(V_m, t)$ non-linearly depends on V_m , [Equation 2.1](#) can not be solved analytically. The use of a numerical method for solving ODEs is indicated.

2.1.2 Subthreshold stimulation, time-domain

Despit the nonlinear nature of the underlying ODE, we can still get an idea of how the temporal solution looks like in a specific segment. We just consider the case of subthreshold stimulation when no ion-channel is activated. Consequently we can focus on membrane properties like r_m and c_m which are almost independent from V_m and solve [Equation 2.1](#) analytically. The path of solving the equation is motivated by results from [Rattay \(1990\)](#). We will consider the case of square wave stimulation $i_{stim}(t)$. For the sake of simplicity we set $V = V_i - V_e - V_{rest}$, measuring voltage deflections from resting state. This is due to the fact that ion pumps are always at work trying to maintain the resting condition $0 = V_m - V_{rest}$. Therefore we can rewrite

$$\tilde{i}_{stim}(t) = c_m \frac{dV_m}{dt} + \frac{V_m(t)}{r_m},$$

to

$$i_{stim}(t) = \tilde{i}_{stim}(t) - \underbrace{\frac{V_{rest}}{r_m}}_{=const.} = c_m \frac{dV}{dt} + \frac{V(t)}{r_m}. \quad (2.3)$$

We used the substitution,

$$i_{pas}(t) = \frac{V_m(t)}{r_m}.$$

$r_m = \frac{R_m}{A_s}$ denotes the specific membrane resistance. In the course of discretization we shall see later what this area exactly looks like. First we deduct the homogeneous solution V_h of [Equation 2.3](#) by setting $i_{stim} \equiv 0$ and reordering summands,

$$\begin{aligned} c_m \frac{dV_h}{dt} &= -\frac{V_h(t)}{r_m} \\ \frac{\frac{dV_h}{dt}}{V_h(t)} &= -\frac{1}{c_m r_m} \\ \Rightarrow V_h(t) &= V_0 e^{-\frac{1}{\tau} t} \quad \text{with initial value } V(0) = V_0 \end{aligned} \tag{2.4}$$

We introduce the definition of [Equation time constant](#),

$$\tau = r_m c_m. \quad (\text{time constant})$$

It measure how fast the temporal evolution of V proceeds. The last equation shows some important implications. The greater the resistance or either capacitance, the greater τ and the slower the temporal evolution gets. As an example let us consider the insulating sheath of the myelinated axon. Although r_m is by far greater than anywhere else in the neuron, c_m overcompensates the increased resistance in terms of [Equation time constant](#). This consequently leads to an overall faster temporal evolution of a propagating signal. Due to the high membrane resistance there is also less loss of charge along the myelin sheaths of the axon. We recall that the injected square-wave current is constant and non-zero for some time period which can be defined as,

$$i_{stim}(t) = \begin{cases} 0 & 0 \leq t \leq t_0 \\ I & t_0 \leq t < t_1 \\ 0 & t_1 \leq t \end{cases}$$

with some constant value I . Therefore, we study the case of how the solution looks like right before stimulation starts, during the process of excitation and afterwards. We can deduct the particular solution by making the Ansatz $V_p(t) = C(t)V_h(t)$ and evaluate it by substitution in [Equation 2.3](#) to,

$$\begin{aligned} V'_p(t) &= C'V_h(t) - \frac{1}{\tau}V_p(t) = -\frac{1}{\tau}V_p(t) + \frac{i_{stim}(t)}{c_m}, \\ \Rightarrow C'(t)V_h(t) &= \frac{I}{c_m} \mathbb{1}_{[t_0, t_1]}, \\ \Rightarrow C(t) - C(0) &= \int_0^{t_0} 0 dt + \frac{1}{V_0} \int_{t_0}^t \frac{I}{c_m} \mathbb{1}_{[t_0, t_1]} e^{\frac{t}{\tau}} dt. \end{aligned}$$

The overall solution is given by $V(t) = V_h(t) + V_p(t)$. Obviously for $0 < t < t_0$, $C(t) = 0$ holds true. Out of continuity, this concludes $C(0) = 0$ and we can proceed with,

$$C(t) = \begin{cases} 0 & 0 \leq t \leq t_0 \\ \frac{I r_m}{V_0} \left(e^{\frac{t}{\tau}} - e^{\frac{t_0}{\tau}} \right) & t_0 \leq t < t_1 \\ \frac{I r_m}{V_0} \left(e^{\frac{t_1}{\tau}} - e^{\frac{t_0}{\tau}} \right) & t_1 \leq t \end{cases}$$

This leads to the particular solution,

$$V_p = C(t)V_h = \begin{cases} 0 & 0 \leq t \leq t_0 \\ I r_m e^{-\frac{t}{\tau}} \left(e^{\frac{t}{\tau}} - e^{\frac{t_0}{\tau}} \right) & t_0 \leq t < t_1 \\ I r_m e^{-\frac{t}{\tau}} \left(e^{\frac{t_1}{\tau}} - e^{\frac{t_0}{\tau}} \right) & t_1 \leq t \end{cases}$$

Further we can deduct qualitative boundaries of the solution, sketching the asymptotic behaviour of temporal evolution.

$$V_p(t) = \begin{cases} 0 & 0 \leq t \leq t_0 \\ e^{-\frac{t}{\tau}} \theta(e^{\frac{t}{\tau}}) \equiv \theta(1) & t_0 \leq t < t_1 \\ \theta(e^{-\frac{t}{\tau}}) & t_1 \leq t \end{cases}$$

We can conclude that even during stimulation with continual current influx, V_m would still deviate asymptotically to some constant value. As soon as stimulation halts, V_m exponentially declines to zero.

2.1.3 Cable equation

With reference to [Rattay \(1990\)](#) we introduce a diffusional partial differential equation which describes the interconnection between segments visualized in [Figure 2.3](#) in the subthreshold-case. For our purpose we assume constant intracellular resistance $R_i = R_{n-1} = R_n = R_{n+1}$ and constant membrane resistance R_m for the subthreshold-case. The aim is to derive an equation which also shows the spatial evolution of voltage along the neuronal cell. We will also deduct the value of the *electrotonic length constant* λ . Its value quantifies how strong a voltage deflection locally may influences its neighbourhood and how far this deflection spreads. It also determines how fast a possible AP in the suprathreshold case may "jump" from one segment to the other, determining the spatial velocity of signal propagation, next to the value of [Equation time constant](#) which determines the temporal evolution in the segment itself. We shall see later that λ is determined solely by the values of R_i and R_m .

Interestingly the case of subthreshold stimulation mimics the evolution of a non-propagated *electrotonic potential*. By definition, this is a voltage deflection that propagates along the axon without any process of amplification. For example,

- An excitatory postsynaptic potential (EPSP) that does not reach threshold voltage V_{thre} and therefore fails to activate ion-channels on its journey to the soma.

- Myelinated sections of the axon where a signal propagates purely through the mechanism of eletrotonic conduction, getting amplified at the nodes of Ranvier.

The diffusional partial differential equation reads as followed.

$$\frac{1}{R_i + R_e} \frac{\partial^2 V}{\partial x^2} = C \frac{\partial V}{\partial t} + \frac{V}{R_m}, \quad (\text{cable equation})$$

We defined $V = V_i - V_e - V_{rest}$ since we are only interested in the deflections from the resting state. We are going to solve this equation by the *separation Ansatz* $V(x, t) = g(x)v(t)$. Applying it to [Equation cable equation](#) leads to,

$$\begin{aligned} g''(x)v(t) &= (R_i + R_e)Cv'(t)g(x) + v(t)g(x) \underbrace{\frac{R_i + R_e}{R_m}}_{\lambda^2}, \\ \Rightarrow \frac{g''}{g} - \lambda^2 &= (R_i + R_e)C \frac{v'}{v}. \end{aligned}$$

This obviously only works for $v(t) < 0$ or $v(t) > 0$ which is no restriction since we can always apply an affine translation $V(x, t) - a$ such that $V(x, t) - a < 0$ or $V(x, t) - a > 0$ holds true and solve this one. Since both sides are independent of each other, both have to be equal to some constant value k . We can now solve both sides separately and recompose the solution at the end. Now, both differential equations are of ODE-type. First we solve for the time-domain.

$$\begin{aligned} k &= (R_i + R_e)C \frac{v'(t)}{v(t)} \Big| \int dt, \\ \ln(v(t)) &= \frac{k}{(R_i + R_e)C} t \Rightarrow v(t) = v_0 e^{\frac{k}{(R_i + R_e)C} t} = v_0 e^{\frac{k}{\lambda^2 R_m} t} = v_0 e^{\frac{k}{\lambda^2 \tau} t}, \end{aligned}$$

with initial value v_0 and substitution $\tau = R_m C$. Since $\lim_{t \rightarrow \infty} v(t)$ should not diverge, we can directly conclude that $k \leq 0$ has to hold true. Now we want to solve for $g(x)$,

$$\frac{g''}{g} - \lambda^2 = k.$$

Obviously we only have a homogeneous component of the solution. We conclude,

$$\Rightarrow g'' = (k + \lambda^2)g \Rightarrow g(x) = g_0 e^{\pm \sqrt{k+\lambda^2} x}$$

The solution only makes sense for real exponents. Further $\lim_{x \rightarrow \infty} g(x)$ should not diverge, but decline. This is the reason why we can set $g(x) = g_0 e^{-\sqrt{k+\lambda^2} x}$ with the condition $k \geq -\lambda^2$. By backcomposition to $V(x, t) = g(x)v(t)$ we can conclude the overall solution by,

$$V(x, t) = v_0 g_0 e^{-\sqrt{k+\lambda^2} x} e^{\frac{k}{\lambda^2 \tau} t} \quad V(x, 0) = V_0(x), \quad (2.5)$$

for some given initial function $V_0(x)$. Still, the constants v_0, g_0 and k are unknown. $v_0 * g_0$ can be set by an initial condition. Each $-\lambda^2 \leq k \leq 0$ gives a different solution. Setting $k = 0$ leads to the steady state solution

$$V(x, t) = v_0 g_0 e^{-\sqrt{\lambda^2}x}$$

and to the only possible initial condition,

$$V_0(x) = V_0 e^{-\sqrt{\lambda^2}x} \quad \text{for some constant } V_0.$$

If we had chosen $k = -\lambda^2$ this would conclude a solution in the time domain which we already deducted [subsection 2.1.2](#). Obviously the spatial evolution is highly dependent on the factor λ . We can now determine [Equation electrotonic length constant](#),

$$\tilde{\lambda} = \frac{1}{\lambda} = \sqrt{\frac{R_m}{R_i + R_e}}. \quad (\text{electrotonic length constant})$$

The constant describes the spatial decline of the steady-state solution. Now it is also clear why a high enough value of R_m is important in the context of AP-propagation in the myelinated sections of the axon. While the AP is amplified at the nodes of Ranvier, it is conducted purely electrotonic in the myelinated sections. If $\tilde{\lambda}$ were too small, this would lead to a fast attenuation of the signal and therefore failure of reaching V_{thre} in the nodes of Ranvier.

2.2 Geometrical Realization

Referring to [Meffin et al. \(2012\)](#) there are two possibilities of geometric modelling of the neuronal cell, for the purpose of discretization.

- **longitudinal:** Its equivalent circuit diagram is sketched in [Figure 2.3](#). It is also the geometry of choice when it comes to a representation in NEURON.
- **transversal:** Its equivalent circuit diagram is sketched in [Figure 2.4](#). Naturally, this could be used for a closed structure like the soma for example.

According to [Meffin et al. \(2012\)](#) it turns out that both representations have slightly differing parameter like electrotonic length constant λ and time constant τ . For our purposes we will use the longitudinal representation of the cell throughout the thesis.

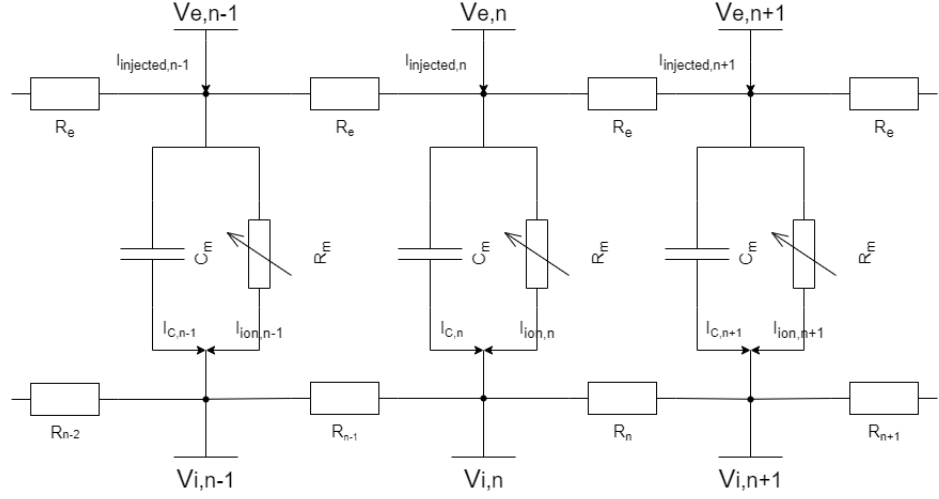


Figure 2.3: Longitudinal Compartment model: The graph depicts a longitudinal realization of the neuronal cell. The neuron is discretized into compartments which are represented by an electrical RC parallel connection. The lipid bilayer of the membrane is represented by capacitance C_m and the constant part of overall resistance R_m . Ion-channel dynamics account for the varying nature of R_m . Each compartment is interconnected to its neighbour by interaxial resistances through extracellular (R_e) and intracellular (R_i) space. $V_{m,n} = V_{i,n} - V_{e,n}$ denotes the discretized membrane voltage at n -th compartment. Considering an extracellular stimulation with current strength $I_{injected}$ leads to its distribution through an extracellular mechanism (see Figure 2.6) to each one of the compartments. Each share is denoted by $I_{injected,n}$.

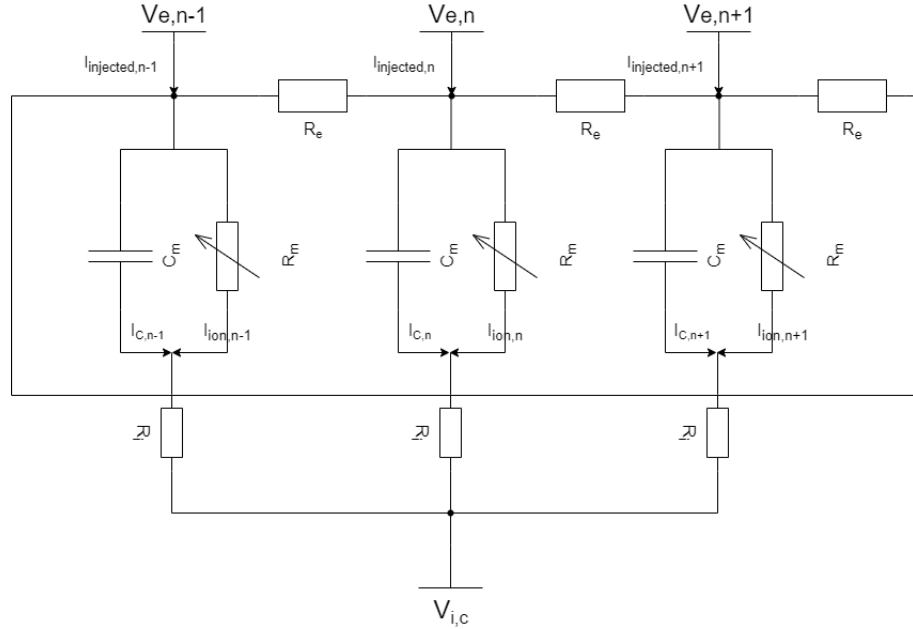


Figure 2.4: Transversal Compartment model: The graph depicts a transversal model with 3 compartments. Its use may be indicated for structures like the soma. In the case of the soma, the star connection point with voltage $V_{i,c}$ would geometrically match its center.

Figure 2.5 gives us a geometrical interpretation of both representations as well as their peculiarities.

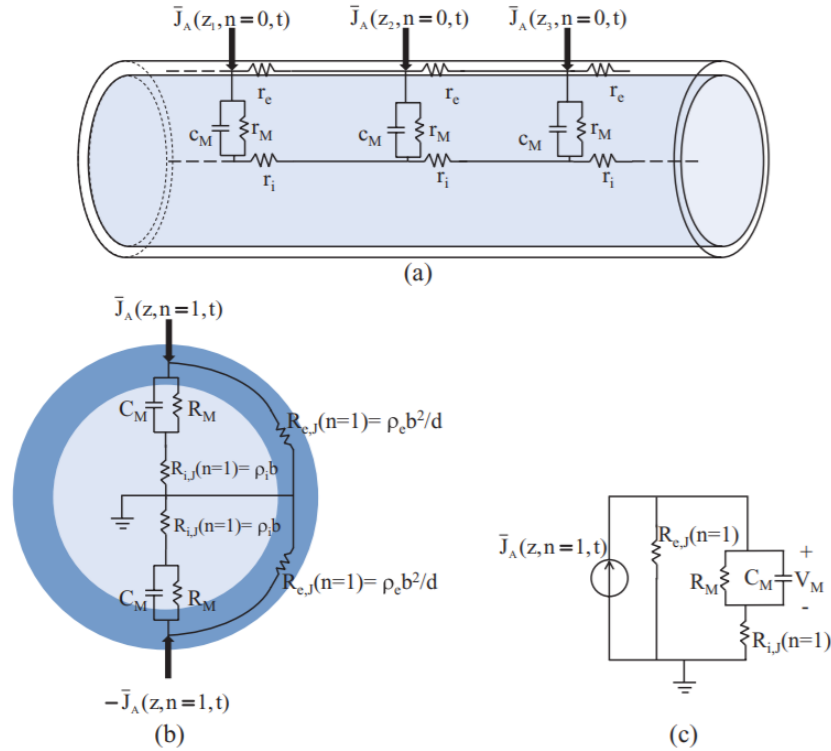


Figure 2.5: Geometrical comparison: The figure shows the geometrical interpretation of both representations. $\bar{J}_A(z, n, t)$ denotes the current strength at different compartments. n determines the mode of representation. z determines the position along the neuron. In the longitudinal case of representation z could be parametrized by a line. In the case of transversal representation we could make use of spherical coordinates in order to parametrize z . a denotes the radius of the neurite (light blue). b denotes the radius of the outer cylinder. The width of the shell between both is defined as $d = b - a$. a) Longitudinal mode: r_e denotes the extracellular resistance. r_i denotes the intracellular resistance. Obviously, all of the values are not of type density. b) Transversal mode: $R_{i,j}$ and $R_{e,J}$ denote intra- as well as extracellular resistances. c) The depiction shows the representation of the transversal realization in form of an electrical equivalent circuit. Source: Meffin et al. (2012)

Referring to Figure 2.5 there are several things to mention.

- a) Both interaxial resistances r_i and r_e can easily be evaluated in the Euclidean space for some given compartment length Δx and specific values of resistance. Assuming a cylindrical section with neurite radius a , we must first evaluate its cross-sectional area A in order to calculate r_i . From its value $A = a^2\pi$, in correspondence with the specific intracellular resistance $\rho_i = [\Omega m]$ it can be concluded that $r_i = \frac{\Delta x \rho_i}{A}$. For calculation of the extracellular resistance r_e we only have to consider extracellular cross-currents in a small cylindrical shell with width $d = b - a > 0$, surrounding the neurite. The shell is confined by the membrane and outer cylinder with radius b .

Since $d \ll a, b$ and $\rho_e \gg 1$ holds true, the extracellular resistance is quite big and consequently negligible. Still it can be calculated by consideration of the small cross-sectional area $A_{sheath} = (b^2 - a^2)\pi = (b - a)(b + a)\pi$ of the shell. From there we may conclude $r_e = \frac{\Delta x \rho_e}{A_{sheath}}$.

Values of r_M and c_M can be calculated by using the circumference $U_{cover} = 2a\pi$ of the neurite as well as incorporating specific values of membrane capacitance $c_m = [F/cm^2]$ and that of membrane resistance $r_m = [\Omega cm^2]$. We can then conclude that $c_M = c_m U_{cover} \Delta x$ and $r_M = r_m / (\Delta x U_{cover})$ holds true.

- b) It is recommended to use spherical coordinates when it comes to the evaluation of values for specific resistance parameters. The situation for the simplified case of only two compartments is visualized.

2.2.1 Discretization in NEURON

In view of the software NEURON the neuronal cell is divided into so-called sections and furthermore into its smallest subunits, the segments.¹ NEURON makes use of the longitudinal geometrical representation of the cell. The segments are usually modeled in a cylindrical fashion. As we shall see later, they can also be modeled by truncated cones. Figure 2.6 visualizes the schematic picture of such a discretization.

¹compartment is a synonym for segment

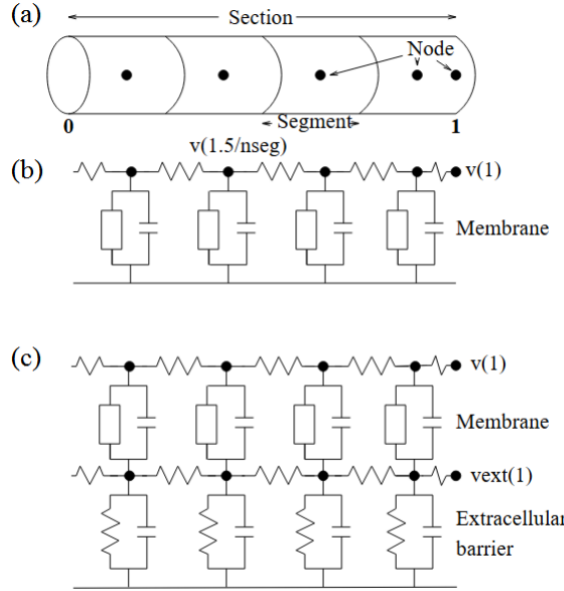


Figure 2.6: Morphology in NEURON: The neuronal cell is divided into so-called sections and further into its smallest units, the segments. Each segment represents an electrical circuit. a) The figure shows the discretized representation of a cylindrical section in NEURON. b) The depiction shows the representation of the equivalent circuit diagram c) NEURON allows for augmentation with an extracellular barrier in order to be able to simulate the distribution of injected current I_{stim} over all the different segments. The values of resistance and capacitance in the extracellular barrier may vary since each compartment has a different distance to the source. Source: [Hines \(1993\)](#).

2.2.2 Activating function

From the perspective of extracellular stimulation the *Activating function* is a handy numerical method for determining candidates of excitation. It also incorporates information about the geometry of considered section. It is studied in [Rattay \(1990\)](#) and [Rattay et al. \(2002\)](#) by its explorer Dr. Frank Rattay. For the purpose of demonstration, f_n is visualized for the electric field, generated by a point-source.

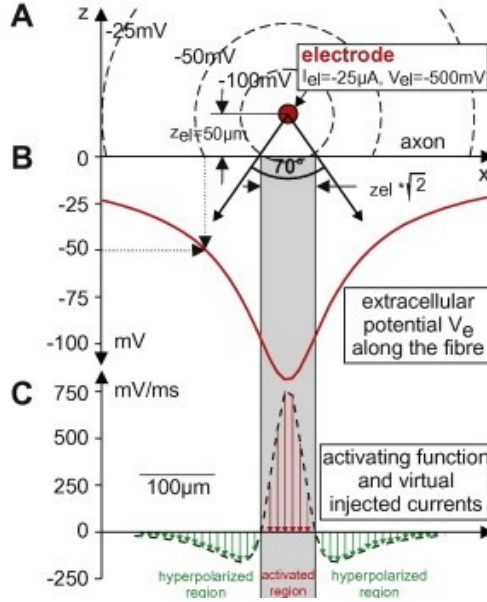


Figure 2.7: Activating function: The figure depicts the evaluation of the Activating function for some horizontal neurite and cathodic stimulation with strength $I_{el} = -25\mu A$, $V_{el} = -500mV$. A) The stimulation is realized by a point soure electrode in a two-dimensional plane with coordinates $(x_{el}, z_{el}) = (0, 50\mu m)$. Setting the electrode distance $r = \sqrt{(z - z_{el})^2 + x^2}$ and evaluation of [Equation 1.3](#) concludes $V_e(r)$. The spatial distribution of extracellular voltage is sketched in B). C) The graph shows the Activating function as well as zones of activation ($f > 0$) and hyperpolarization ($f < 0$). Given a spherical voltage distribution we can determine the region of activation by a law. In this specific case the width is always $z_{el}\sqrt{2}$. In a general context it is defined as the 70 ° field of view onto the membrane. Source: [Rattay et al. \(2012\)](#)

We deduct the mathematical representation of the Activating function for one specific segment by making use of the longitudinal representation. We assume that $R_e \gg 1$ and that consequently cross-currents can be neglected. By application of Kirchhoff's first Law onto the network sketched in [Figure 2.3](#) we can write,

$$I_{injected,n} = \underbrace{C_n \frac{d(V_{i,n} - V_{e,n})}{dt}}_{=I_{C,n}} + I_{ion,n} + \frac{V_{i,n} - V_{i,n-1}}{R_{n-1}} + \frac{V_{i,n} - V_{i,n+1}}{R_n}.$$

We can now make the transition to the reduced voltage $V_n = V_{i,n} - V_{e,n} - V_{rest,n}$ since the ion-pumps equalize any deflection from resting state. This behaviour can also be visualized in [Figure 2.3](#) by augmenting it with a parallelly connected voltage source for each compartment. Furthermore we can also assume that resting voltage is everywhere the same. Then we can proceed with,

$$\frac{dV_n}{dt} = \left(-I_{ion,n} + \frac{V_{n-1} - V_n}{R_{n-1}} + \frac{V_{n+1} - V_n}{R_n} + I_{injected,n} \right) / C_m + \underbrace{\left(\frac{V_{e,n-1} - V_{e,n}}{R_{n-1}} + \frac{V_{e,n+1} - V_{e,n}}{R_n} \right) / C_m}_{f_n}. \quad (2.6)$$

f_n determines the direction $V_n(t)$ is headed to at time $t = 0$. As already said, this equation is in simplified form using the discretization in longitudinal form. If we would have used the transversal form, there could be even more terms in f_n . From the perspective of [Figure 2.4](#), had we used a transversal model with m compartments, f_n would be composed by $m - 1$ terms.

Now we want to analyze the function under a concrete setting. Let us consider the trial from [Figure 2.8](#). We inject a square-wave current $I_{injected}$ for some time period $t_{duration}$. Furthermore we assume that after a time period of $t_{duration} > t > 5\tau$ we are still in the subthreshold-case. $\tau = r_m c_m$ denotes the time constant under the assumption that membrane properties are homogeneous. For simplicity we assume constant intracellular resistance $R_i = R_{n-1} = R_n$. We can make two case distinctions for different values of t and analyze what role f_n is assigned to.

- **t=0:** We inject a square-wave current at $t = 0$. We assume that membrane voltage is everywhere equal at resting state which is denoted by $V_{n-1} = V_n = V_{n+1}$. Since C_m poses almost no resistance for volatile voltage changes we can conclude that $I_{injected,n}(t = 0) \approx I_{C,n}(t = 0)$. Subsequent application of Kirchhoff's first Law concludes $I_{ion,n}(t = 0) \approx 0$. We can proceed with,

$$\frac{dV_n}{dt}|_{t=0} = I_{injected,n}/C_n + f_n.$$

The first term may be quite small due to the subthreshold-case, leading to superior meaningfulness of f_n .

- **t=5*\tau:** τ also determines the transient decline behaviour of the RC-circuit. As soon as $t > 5\tau$ holds true and some time has passed, we can conclude $I_C \leq I_{injected,n}/e^5 \approx 0$.

This is due to the sloping nature of the capacitor current which is determined by $e^{-t/\tau}$. Application of Kirchhoff's first Law concludes the equation $-I_{injected,n} + I_{ion,n} \approx 0$.

From there we can proceed with,

$$\begin{aligned}\frac{dV_n}{dt}|_{t=5\tau} &= \left(\frac{V_{n-1} - V_n}{R_{n-1}} + \frac{V_{n+1} - V_n}{R_n} \right) / C_m + f_n \\ &= \left(\frac{V_{i,n-1} - V_{i,n}}{R_{n-1}} + \frac{V_{i,n+1} - V_{i,n}}{R_n} \right) / C_m.\end{aligned}$$

Therefore we can conclude that after some time has passed, the growth behavior of V_n is determined by the intracellular voltage distribution. To be more precise, growth behaviour is determined by the second difference coefficient of the intracellular voltage distribution. The intracellular space is assumed to be a conductive medium, especially from the perspective of the HH formalism which augments it even with an intracellular resistance R_i . Therefore, the cell tries to compensate any superimposed field in the attempt to keep its inner field-free. This in turn leads to an intracellular electric field who points into the opposite direction. We suspect that this compensating behaviour may help to smooth out the discretized function $V(x)|_{t=t_0}$ for greater times t_0 . This may also be underpinned by the subthreshold-cases from [Figure 2.8](#) for each successive timestep. In each of the trials, the curves are smoothed until the moment an AP starts to be generated through opening of sodium channels.

A more representative form of f_n may be determined without dealing too much with the surrounding geometry. We do so by focusing on the membrane properties. For simplicity and because of the fact that it coincides with most of used models, we assume constant intracellular resistance $R_{n-1} = R_n = R_{n+1} = R_i$. By use of expressions from [Figure 2.5](#) with slightly differing variable names, we can substitute $R_i = \frac{\Delta x \rho_i}{a^2 \pi}$ and $C_m = c_m \Delta x 2a\pi$. Inserting them into f_n leads to,

$$\begin{aligned}f_n &= \left(\frac{V_{e,n-1} - V_{e,n}}{R_{n-1}} + \frac{V_{e,n+1} - V_{e,n}}{R_n} \right) / C_m = \frac{V_{e,n-1} - 2V_{e,n} + V_{e,n+1}}{R_i C_m} \\ &= \frac{V_{e,n-1} - 2V_{e,n} + V_{e,n+1}}{\Delta x^2 c_m \rho_i 2a\pi / (a^2 \pi)} = \\ &= \frac{a}{2c_m \rho_i} \underbrace{\frac{V_{e,n-1} - 2V_{e,n} + V_{e,n+1}}{\Delta x^2}}_{\text{2nd difference coefficient}}.\end{aligned}$$

In case we have a closed expression for $V_e(x)$ we can directly switch to the continuous case,

$$f_n = \frac{a}{2c_m \rho_i} \frac{\partial^2 V_e}{\partial x^2}.$$

For example, $x(t)$ could be a parametrized line along a given geometry.

Differences between anodic and cathodic extracellular stimulation

By virtue of the Activating function we can visualize the differences between anodic and cathodic stimulation. Cathodic stimulation may be interpreted as the right choice for

neuronal excitation since it increases V_m for structures next to the electrode. Still, anodic stimulation also manages to do so but in a different fashion. Unlike the case of cathodic stimulation, its Activating function has a bimodal distribution of activation regions. The comparison is sketched in [Figure 2.8](#).

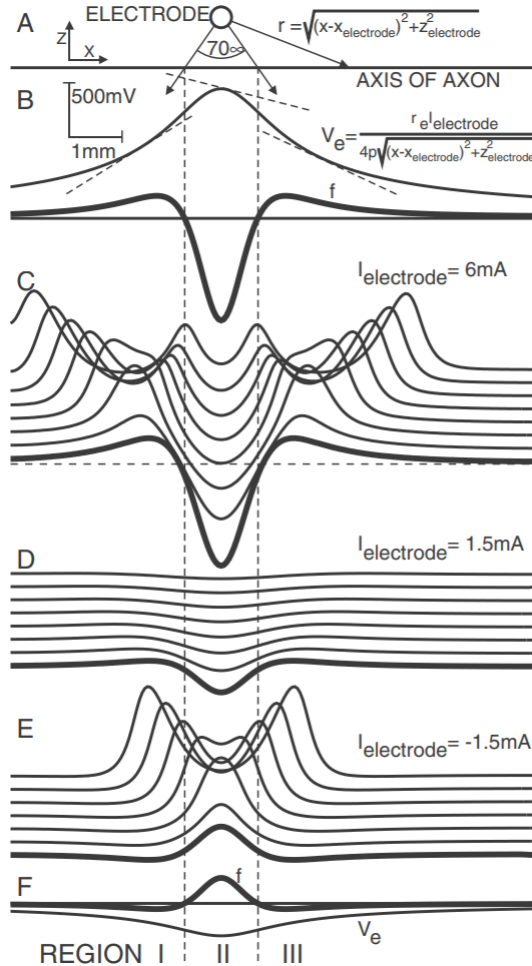


[Figure 2.8: Activating function: Cathodic/Anodic comparison.](#)

Stimulation environment: HH-model, 29 °, $\rho_e = 0.3 \text{ k}\Omega\text{cm}$.

Setting: Unmyelinated axon with a monopolar electrode. Vertically shifted snapshots of V_n were taken every 100 μsec for different current strengths.

A) Electrode placement, C-D) Anodic stimulation, E) Cathodic stimulation, F) Regions of activation and hyperpolarization in the case of cathodic stimulation,
Source: [Rattay et al. \(2002\)](#)

Referring to [Figure 2.8](#) a few things should be mentioned:

- B** The graph shows the comparison of extracellular voltage distribution (thin line) and the Activating function (thick line).

- C-D** The Rheobase current for anodic stimulation is $6mA$. The thick line represents $V_n(t = 0)$ and emphasizes the similarity to the Activating function f_n which obviously has a bimodal distribution of activation regions.
- E** The cathodic Rheobase equates to $-1.5mA$ and is therefore approximately 4 times lower than that for the anodic case.
- F** RegionI and RegionIII denote regions of hyperpolarization ($f < 0$). RegionII denotes the region of activation ($f > 0$).

2.2.3 Blocking artifacts

During stimulation several situations may occur which prohibit either generation or propagation of an AP. We will shed lights on both.

Anodal Surround Block

The *Anodal Surround Block* phenomenon describes the situation where an AP is generated but fails to propagate further. It was first discovered by Dr. James B. Rank ([Ranck J. B., 1975](#)). The phenomenon occurs for high current strength and at close distance to the electrode. It can be best visualized by evaluation of the Activating function. For example, in the case of cathodic stimulation the regions of hyperpolarization bordering to that of activation, hinder a potentially generated AP from further propagation. The initiated AP fails to propagate through the regions of hyperpolarization. Such a case is visualized in [Figure 2.7](#).

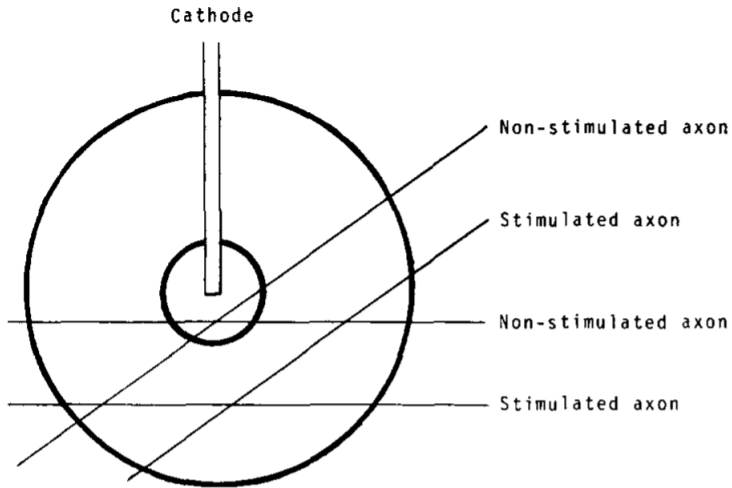


Figure 2.9: Anodal Surround Block: A point-source electrode with cathodic current strength is depicted. We can determine regions where anodal surround block occurs. For axons passing the inner sphere, any AP that propagates fails to continue its journey along the path. The outer sphere denotes the lower threshold of stimulation strength. The ratio of radii between inner and outer-sphere is 1:4. The dimension of the shells are determined by extracellular resistance and the diameter of axon. The dimensions are larger for axons with larger diameter. This leads to the phenomenon that thinner parts of a neuron may be stimulated in a region where thicker one experience anodal surround block.
Source: [Ranck J. B. \(1975\)](#)

Referring to [Figure 2.9](#), [Ranck J. B. \(1975\)](#) states that an 8-fold increase in current is equivalent to a 4-fold decrease in distance towards the point-source. Outer and inner shell of the spherical surfaces determine the *stimulation window*. The stimulation window is the strength distance relation augmented by an upper threshold curve for anodal surround block. It also hints to why the simulation window increases in size for greater distance to the electrode.

Upper Threshold

The upper threshold is a blocking phenomenon where in contrast to the anodal surround block, no AP is generated at all. From the perspective of the Activating function, the AP fails to be generated in activated regions of the Activating function. The upper threshold current for that to happen is obviously even higher than that of anodal surround block. The phenomenon was discovered in [Boinagrov et al. \(2012\)](#). It can be described from the perspective of *current reversal*, although the upper threshold may appear even before current reversal occurs. Current reversal describes the process where membrane voltage surpasses the reversal potential of some specific ion-species. This leads to movement of that specific ion species against the direction of its electrochemical gradient. For example, positively charged sodium ions are accelerated towards the extracellular space which consequently hinders an AP initiation. It is best described from the perspective of

the HH-formalism.

$$i_{Na} = g_{Na}(V_m)(V_m - E_{Na}),$$

denotes the sodium current through the membrane. $g_{Na}(V_m)$ is the specific conductivity for sodium ions. The sodium reversal potential equates to $E_{Na} \approx 60mV$. As soon $V_m > E_{Na}$ is reached through high enough stimulation strength, this leads to $i_{Na} > 0$ and therefore to current reversal.

3 Methodology

The model used to deduct results in Chapter 4 is mainly based on morphological data provided by Almog and Korngreen (2014). The features of ion channel dynamics were studied in Keren et al. (2005, 2009). The HH formalism is used for modelling the dynamical properties of the membrane. The setup of two voltage-gated calcium channels is based on findings from nucleated patch-clamp experiments. One calcium channel is a medium threshold voltage activated channel (MVA) with high inactivating time constant τ . The second one is a high threshold voltage activated channel (HVA). Two calcium-gated potassium channels were also included. The first one represents a calcium-gated small conductance potassium channel (K_{SK}). The second one represents a calcium-gated large conductance potassium channel (K_{BK}). An artificial axon was constructed based on Mainen and Sejnowski (1996), since no experimental data was available on neither the ion channel dynamics nor the geometry. Nevertheless, some features of the axon were part of a constraining procedure in Keren et al. (2005). The shift in threshold values for the activating and inactivating gating variables of the sodium channel were recorded and their final values optimized. The values were denoted by $N_{a,shift,act}$ and $N_{a,shift,inact}$.

Due to the abundant presence of calcium channels dynamics in combination with a more detailed distribution of latter, the model offers a good experimental template. That is especially the case when excitability of dendrites in the apical tuft is studied. It gives us a new way to approach the matter since AP initiation and generation of calcium spikes in the apical tuft is owed to the activation of voltage-gated calcium channels. This is in contrast to the process of AP-initiation in the somatic region, prompted by the activation of sodium channels.

3.1 Channel types

All of the ion channels are described in terms of the their gating variables from the perspective of the HH formalism. Hereinafter we will define each of them for the concrete model implementation. Keren et al. (2005) provides four ion channel dynamics.

1. voltage-activated sodium
2. voltage-activated potassium
3. hyperpolarization activated (I_h)
4. leakage

They have in common to solely describe the movement of potassium and sodium ions across the membrane. Almog and Korngreen (2014) managed to find a proper distribution

of voltage-gated calcium channels as well as calcium-gated potassium channels along the apical dendrites. We shall see that for distant apical dendrites the subgroup of calcium channel types plays an important role in the course of de- and hyperpolarization in the aftermath of an AP or dendritic spike. The voltage-gated calcium channels also have a greater inactivation constant. This leads to a different form of the AP curve than it would have been the case for excitation sites close to the soma. Anticipating the existence of a hyperpolarization activated ion channel I_h which is permeable for sodium and potassium ions we can use [Equation Goldman](#) to determine the reversal potentials.

- $E_{Na} = 60mV$
- $E_K = -100mV$
- $E_{Ih} = -30mV$
- $E_{Ca} = 130mV$

E_{pas} together with the other passive membrane parameters were constrained by a constraining procedure in [Almog and Korngreen \(2014\)](#). [Table 3.1](#) shows the deducted parameters of the procedure which will be used over and over again.

3 Methodology

	Parameter	Unit	Cell 5	Average	CV
0	Distance	μm	413	454	nan
1	R_a	Ωcm	120	96	0.2
2	R_m	Ωcm^2	25.812	18.314	0.45
3	C_m	$\mu\text{F}/\text{cm}^2$	0.60	0.68	0.16
4	E_{pas}	mV	-47.8	-48.3	0.03
5	$G_{Ih,dend}$	$\text{pS}/\mu\text{m}^2$	118	115	0.24
6	$I_{h,x1/2}$	μm	352	419	0.14
7	$I_{h,slope}$	$1/\mu\text{m}$	-0.014	-0.016	0.26
8	$G_{Ih,soma}$	$\text{pS}/\mu\text{m}^2$	2.51	2.24	0.45
9	$G_{Ks,dend}$	$\text{pS}/\mu\text{m}^2$	3.79	6.13	0.76
10	$K_{s,slope}$	$1/\mu\text{m}$	-0.092	-0.078	0.16
11	$G_{Ks,soma}$	$\text{pS}/\mu\text{m}^2$	206	220	0.17
12	$G_{Kf,dend}$	$\text{pS}/\mu\text{m}^2$	28	28	0.2
13	$K_{f,slope}$	$1/\mu\text{m}$	-0.012	-0.018	0.48
14	$G_{Kf,soma}$	$\text{pS}/\mu\text{m}^2$	332	294	0.16
15	$G_{Na,soma}$	$\text{pS}/\mu\text{m}^2$	352	284	0.52
16	$G_{Na,dend}$	$\text{pS}/\mu\text{m}^2$	56	81	0.47
17	Na_{dist}	μm	481	583	0.17
18	$Na_{shift,act}$	mV	-11.0	-10.1	0.09
19	$Na_{shift,inact}$	mV	-9.6	-10.2	0.06
20	$P_{HVA,soma}$	$\mu\text{m}/\text{s}$	0.9	66.9	1.08
21	$P_{HVA,dend}$	$\mu\text{m}/\text{s}$	1.56	1.39	0.64
22	$Ca_{HVA,dist}$	μm	10	63	0.93
23	$Ca_{HVA,shift,act}$	mV	-4.5	-8.8	0.31
24	$Ca_{HVA,shift,inact}$	mV	-7.1	0.8	6.4
25	$P_{MVA,soma}$	$\mu\text{m}/\text{s}$	31.5	72.4	0.79
26	$P_{MVA,dend}$	$\mu\text{m}/\text{s}$	4.9	13.3	0.73
27	$Ca_{MVA,dist}$	μm	925	487	0.69
28	$Ca_{MVA,shift,act}$	mV	-9.7	-8.4	0.36
29	$Ca_{MVA,shift,inact}$	mV	-2.1	-2.6	2.37
30	$G_{SK,soma}$	$\text{pS}/\mu\text{m}^2$	3.18	3.05	0.23
31	$G_{SK,dend}$	$\text{pS}/\mu\text{m}^2$	0.52	0.65	0.76
32	SK_{dist}	μm	239	453	0.39
33	$G_{BK,soma}$	$\text{pS}/\mu\text{m}^2$	0.64	1.93	0.7
34	$G_{BK,dend}$	$\text{pS}/\mu\text{m}^2$	1.23	1.85	0.93
35	BK_{dist}	μm	28	84	1.31
36	$G_{pas,node}$	$\text{pS}/\mu\text{m}^2$		0.02	
37	$C_{m,myelin}$	$\mu\text{F}/\text{cm}^2$		0.04	
38	$G_{Na,node}$	$\text{pS}/\mu\text{m}^2$		30000	
39	$G_{Ks,node}$	$\text{pS}/\mu\text{m}^2$		1500	
40	$G_{Kf,node}$	$\text{pS}/\mu\text{m}^2$		1000	

Table 3.1: Constrained Parameters: Set of best constrained values was chosen from Almog and Korngreen (2014). Cell 5 refers to the fifth trial. (see next page)

Table 3.1 (*previous page*): "CV" represents the coefficient of variation for a set of five trials and is determined for each parameter. "Distance" denotes the distance between soma and recording site along the apical dendrite which was used in considered trial for the constraining procedure. "Average" denotes the average value of each parameter for the set of five trials. R_a is the specific length-related interaxial resistance of the intracellular space. R_m and C_m denote the specific membrane properties. The meaning of all the other parameters is derived from the context in Section 3.2 and Section 3.1. An artificial axon according to [Mainen and Sejnowski \(1996\)](#) is used since no constrained data was available for it. Therefore, the axons properties are listed without any value for CV and Average.

3.1.1 Na^+

Na^+ is a voltage-gated sodium conductance channel. It is the main driver of the AP initiation process in the soma and the region surrounding it. Its importance for the process of AP initiation declines with further distance from the soma along the apical dendrites. Its flow equations are described as follows.

$$g_{Na} = G_{Na} m^3 h,$$

$$m_\infty = \frac{1}{1 + e^{-\frac{V_m+36}{28}}}, \quad \tau_m = 0.058 + 0.114 e^{-(\frac{V_m+36}{28})^2}$$

$$h_\infty = \frac{1}{1 + e^{-\frac{V_m+66}{6}}}, \quad \tau_h = 0.28 + 16.7 e^{-(\frac{V_m+66}{6})^2}.$$

The variables m and h refer to the activating and inactivating gates. The rate of increase is determined by their time constants τ_m and τ_h . Referring to [Hodgkin and Huxley \(1952\)](#) we can rewrite it into a different form for the purpose of demonstration,

$$\alpha_m(V_m) := \frac{m_\infty}{\tau_m}, \quad \beta_m(V_m) := \frac{1 - m_\infty}{\tau_m},$$

$$\alpha_h(V_m) := \frac{h_\infty}{\tau_h}, \quad \beta_h(V_m) := \frac{1 - h_\infty}{\tau_h},$$

$$\frac{dm}{dt} = \alpha_m(V_m)(1 - m) + \beta_m(V_m)m,$$

$$\frac{dh}{dt} = \alpha_h(V_m)(1 - h) + \beta_h(V_m)h.$$

We can also conclude the ion current density,

$$i_{Na} = g_{Na}(V_m - E_{Na}).$$

3.1.2 K_f

K_f denotes the voltage-gated fast inactivating potassium conductance channel. It is activated for increasing V_m which initiates the repolarization process after AP initiation. Due to the negative reversal potential $E_K < 0$, opening of potassium channels leads to outflux of K^+ which in turn decreases the membrane voltage.

$$g_{Kf} = G_{Kf} a^4 b,$$

$$a_\infty = \frac{1}{1 + e^{-(\frac{V_m+47}{29})^2}}, \quad \tau_a = 0.34 + 0.92 e^{-(\frac{V_m+71}{59})^2},$$

$$b_\infty = \frac{1}{1 + e^{\frac{V_m+66}{10}}}, \quad \tau_b = 8 + 49 e^{-(\frac{V_m+73}{23})^2}.$$

Its ion current density is defined by,

$$i_{Kf} = g_{Kf}(V_m - E_K).$$

3.1.3 K_s

K_s denotes the voltage-gated slow inactivating potassium conductance channel. As the name suggests, it has a high inactivating time constant. This channel is obviously the main driver of the repolarization and hyperpolarization process. Its flow equations are stated as follows,

$$g_{Ks} = G_{Ks} r^2 (0.5s_1 + 0.5s_2),$$

$$\frac{dr}{dt} = \alpha_r(V_m) (1 - r) + \beta_r(V_m) r,$$

with,

$$\alpha_r(V_m) = \frac{0.0052(V_m - 11.1)}{1 - e^{-\frac{V_m-11.1}{13.1}}}, \quad \beta_r(V_m) = 0.02 e^{-\frac{V_m+1.27}{71}} - 0.005$$

$$s_{1,\infty} = s_{2,\infty} = \frac{1}{1 + e^{\frac{V_m+58}{11}}},$$

$$\tau_{s1} = 360 + (1010 + 23.7(V_m + 54)) e^{-(\frac{V_m+75}{48})^2},$$

$$\tau_{s2} = 2350 + 1380 e^{-0.011 V_m} - 210 e^{-0.03 V_m}.$$

The ion current density is given by,

$$i_{Ks} = g_{Ks}(V_m - E_K).$$

Na^+ and K_s are the main driver of the de- and repolarization process for regions proximal to the soma. Referring to [Almog and Korngreen \(2014\)](#) this behaviour changes with further distance along the apical dendrite where the group of calcium type channels plays a superior role when it comes to generation of dendritic AP.

3.1.4 I_h

I_h denotes the hyperpolarization activated cation conductance (Berger et al., 2001). It is permeable for sodium and potassium ions and activated in the subthreshold-case (Des-texte A, 1993). Therefore its reversal potential is in-between both and may be determined by [Equation Goldman](#). Since its membrane density increases with further distance from the soma it has a main impact on the membrane features of apical dendrites and consequently on synaptic integration in the apical tuft. Its flow equations read as follows,

$$g_{Ih} = G_{Ih} o, \\ o_\infty = \frac{1}{1 + e^{\frac{V_m + 91}{6}}}, \quad \tau_o = \frac{1}{0.004 e^{-0.25 V_m} + 0.088 e^{0.062 V_m}}.$$

Its ion current density is given by,

$$i_{Ih} = g_{Ih} (V_m - E_{Ih}).$$

3.1.5 Leakage channel

The leakage channel accounts for the amount of leaking charge across the membrane. As we already know it may be represented by a constant specific membrane resistance r_m and capacitance c_m . Its reversal potential is denoted by E_{pas} . The membrane parameters as well as the reversal potential were subject to the constraining procedure in [Almog and Korngreen \(2014\)](#).

$$g_{pas} = \frac{1}{r_m}, \quad i_{pas} = g_{pas} (V_m - E_{pas}). \quad (3.1)$$

3.1.6 Ca^{2+}

The subgroup of the next five channels consists of two voltage-gated calcium channels, two calcium-gated potassium channels and one calcium extrusion pump mechanism. These channel types play a key role in the process of AP initiation along the apical dendrite. They also play a superior role when it comes to the understanding of regenerative calcium and sodium spikes in the apical dendrite, synaptic integration and backpropagation-activated calcium driven spike firing (BAC).

Ca_{HVA}

This channel denotes the high threshold voltage activated calcium channel type. Consequently it is activated at higher voltage levels. Its flow equations read as follows,

$$p_{HVA} = P_{HVA} \alpha_\infty^2 \beta_\infty, \\ \alpha_\infty = \frac{1.1}{1 + e^{-\frac{V_m + 14}{10}}}, \quad \tau_\alpha = \frac{0.97}{\cosh(0.032(V_m + 26))}, \\ \beta_\infty = \frac{0.75}{1 + e^{\frac{V_m + 23}{7}}}, \quad \tau_\beta = \frac{70}{\cosh(0.047(V_m - 20))}.$$

We notice that the flow equations are given in terms of permeability values.

3 Methodology

Ca_{MVA}

This channel is activated at medium threshold voltage levels. It has a high inactivating time constant that is in the milliseconds region. We shall see later that the membrane density for this channel type decreases along the apical dendrite. Still this happens in a slower manner than it is the case for its counterpart, the HVA channel. It is the main driver of AP depolarization for regions in the distal apical dendrites. Its flow equations read,

$$p_{MVA} = P_{MVA} \alpha_\infty^2 \beta_\infty,$$

$$\alpha_\infty = \frac{1}{1 + e^{-\frac{V_m+23}{7}}}, \quad \tau_\alpha = \frac{5.5}{\cosh(0.032(V_m + 23))},$$

$$\beta_\infty = \frac{1}{1 + e^{\frac{V_m+79}{8}}}, \quad \tau_\beta = \frac{771}{\cosh(0.047(V_m + 79))}.$$

The following two channels are calcium-gated potassium channels. They are activated after a depolarization process has occurred in the apical dendrites, with successful calcium spiking. They are activated by influx of calcium ions into the cell and modeled directly by taking the intracellular calcium ion concentration $[Ca^{2+}]_i$ into account. It is a counterpart to the potassium channels already presented, whose purpose is to repolarize a cell after a sodium driven AP has occurred in the somatic region.

K_{BK}

It denotes the calcium-gated large conductance potassium channel. According to Sun et al. (2003), a fast transient potassium current is activated by calcium entry. Calcium enters through preceding activation of HVA channels which are also referred to as L- and N-type calcium ion channels. Its flow equations are,

$$g_{SK} = G_{BK} \alpha_\infty,$$

$$\alpha = 1.3^4 [Ca^{2+}]_i^4,$$

$$\alpha_\infty = \frac{\alpha}{\alpha + 0.06}, \quad \tau_\alpha = \frac{1}{\alpha + 0.06}.$$

K_{SK}

It denotes the calcium-gated small conductance potassium channel. Its flow equations are,

$$g_{BK} = G_{BK} \alpha_\infty^3 \gamma_\infty^2 \beta_\infty,$$

$$\alpha_\infty = \frac{1}{1 + e^{-\frac{V_m+29}{6.2}}}, \quad \tau_\alpha = \frac{1000.505}{e^{\frac{V_m+86}{10}}},$$

$$\gamma_\infty = \frac{1}{1 + \frac{0.001}{[Ca^{2+}]_i}}, \quad \tau_\gamma = 1.$$

This channel has a high time constant and explains the characteristic and dominant behaviour in the aftermath of a calcium-spike.

Ca^{2+} -pump

The dynamics of calcium exchange are based on results from [Destexhe A \(1993\)](#). It models a calcium ATPase fueled extrusion mechanism which is dependent on the intracellular calcium concentration. The exchange of calcium ions is modeled to take place only within a thin shell of depth d underneath the membrane. At each timestep, the specific calcium current I_{Ca} is assessed and used in order to determine the change in ion concentration within the thin shell. The flow equations read,

$$\begin{aligned} [\dot{C}a]_{influx,i} &= -\frac{k}{2Fd} I_{Ca} \quad \text{with,} \\ F &= 96489 \frac{C}{mol}, \\ k &= 1e4, \\ d &= 0.01\mu m, \\ [I_{Ca}] &= \frac{\mu A}{cm^2}. \end{aligned}$$

The variable k denotes the unit conversion factor, F the Faraday constant. The mechanism for the pump-extrusion reads as follows,

$$\begin{aligned} [\dot{C}a]_{ATPase,i} &= \frac{[Ca]_{rest} - [Ca]_i}{\tau} \quad \text{with,} \\ [Ca]_{rest} &= 10^{-5} mmol, \quad \tau = 80ms. \end{aligned}$$

$[Ca]_{rest}$ is the intracellular calcium concentration at resting state. Obviously, $[Ca]_{rest}$ is a stable hyperbolic fixed point of the ODE. τ denotes the rate of calcium removal and was adjusted to cortical neurons. When we put both mechanisms together we get,

$$[\dot{C}a]_i = [\dot{C}a]_{influx,i} + [\dot{C}a]_{ATPase,i} \quad (3.2)$$

as the flow equation for the evolution of $[Ca]_i$.

3.1.7 Temperature adjustment

According to [Hodgkin and Huxley \(1952\)](#) the velocity of dynamics increases with higher temperature. For this specific model it is calculated by,

$$f = q_{10}^{\frac{t-t_{record}}{10}}.$$

This means that each of the time constants has to be divided by f to get adapted to the new temperature. t_{record} denotes the temperature in degree at which each of the trials was recorded ([Almog and Korngreen, 2014](#)). We list the values of q_{10} and t_{record} for each of the channels.

	$t_{record}(degree)$	q_{10}
Na^+	21	2.3
K_f	21	2.3
K_s	21	2.3
I_h	21	2.3
$CaHVA$	24	4
$CaMVA$	24	1
K_{BK}	22	3
K_{SK}	22	3

Table 3.2: The values for temperature adjustment: Surprisingly the dynamics of the calcium pump as well as MVA channel were not scaled by the temperature guessing from the source code.¹

3.2 Channel Distribution

One big advantage of the model used in this thesis is that it allows for a non homogeneous channel distribution along the apical dendrites. The functions usually were linearly interpolated by providing two supporting values. The supporting values were constrained by the constraining procedure and are listed in Table 3.1. An overview of all distribution functions along the apical dendrites is sketched in Figure 3.1.

¹ <https://senselab.med.yale.edu/ModelDB/showModel?model=151825&file=/Demo/#tabs-2>

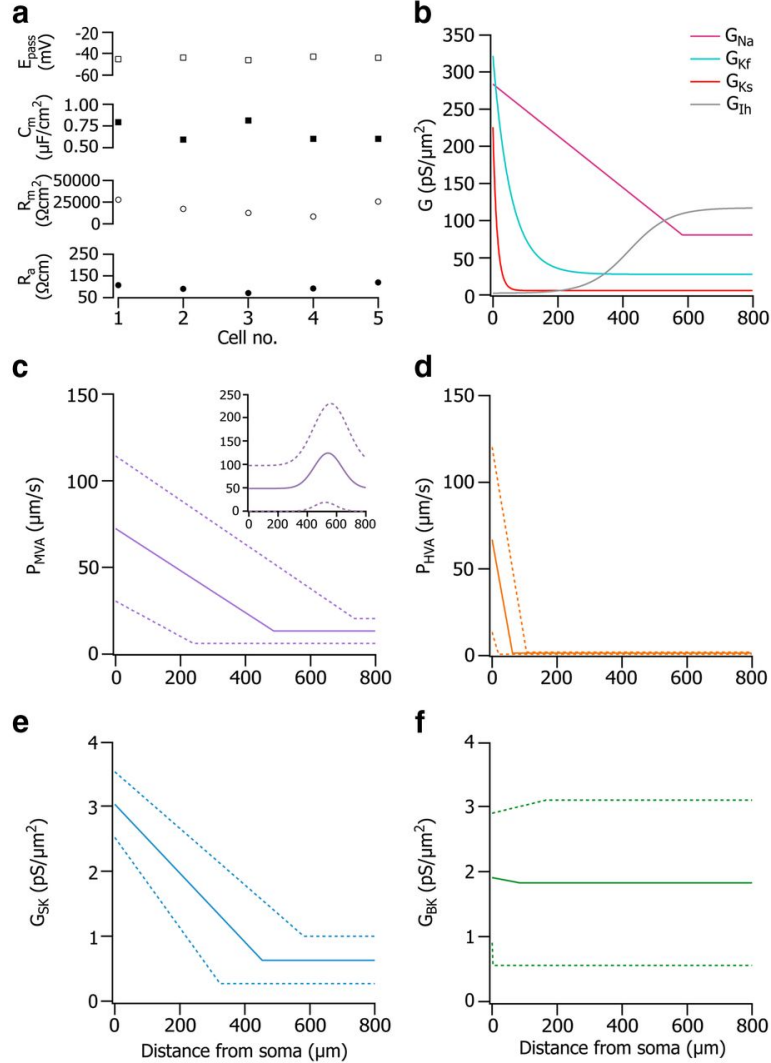


Figure 3.1: Channel distributions along the apical dendrites. **a)** The constraining procedure was applied to five different cells. The constrained values for the passive membrane parameter set are plotted. Remaining plots show the distributions for the best chosen parameter set from Table 3.1. **b)** The share of sodium channels decreases linearly and comes to a halt at $600 \mu m$. The amount of repolarizing potassium channels decreases exponentially. The amount of hyperpolarization activated channels increases in a sigmoidal fashion towards the apical tuft. All of the subsequent plots include their respective confidence interval ($\alpha = 0.1$). **c, d)** Voltage-gated calcium channel distribution. Overlaid inside c) we see a gaussian distribution function which can be ignored. **e, f)** Small and large conductance calcium gated potassium channels. Source: Almog and Korngreen (2014)

Throughout the following explanations we refer to values specified in [Table 3.1](#). The density distribution for the leakage channel is uniform except for the axon where we used artificial parameters according to [Mainen and Sejnowski \(1996\)](#).

3.2.1 Apical Dendrites

Let us take a look at the channel distributions along the apical dendrites. For all of the interpolated density functions, x denotes the distance between the center of soma and the chosen position on the apical section.

I_h

The distribution of the hyperpolarization activated channel I_h is determined by,

$$G_{I_h}(x) := G_{I_h,soma} + \frac{G_{I_h,dend}}{1 + e^{I_{h,slope}(x - I_{h,x1/2})}}$$

It is defined by an increasing sigmoidal curve whose value halts at approximately $120\text{pS}/\mu\text{m}^2$. [Berger et al. \(2001\)](#) observe that the high density of I_h channels in the apical tuft leads to a higher attenuation of spontaneous excitatory postsynaptic potentials (sEPSPs) along the apical dendrite. Blockage of this channel led to less attenuation by 17 percent for somatopetal (towards soma) and 47 percent for somatofugal (from soma away) sEPSPs in both, apical as well as basal dendrites. It is also shown that in the blocked state, trains of sEPSPs showed temporal summation in contrast to the case when I_h was present. On the other hand [Williams and Stuart \(2000\)](#) observe some interesting phenomena that also coincide with the ones already mentioned. They are summarized as follows.

1. Linear increase of I_h channel density along the apical dendrite with a rising constant of $9\frac{\text{pA}}{\mu\text{m}}$ was observed.
2. In the case of blockage of I_h channels, a higher degree of temporal summation of EPSPs and therefore a higher degree of synaptic integration occurred, with increasing distance to the soma.
3. In the case of blockage of I_h channels, a higher Full Width at Half Maximum (FWHM) of somatically recorded simulated EPSPs, generated by dendritic current injection was observed. It increased with further distance from the soma.
4. In the case of presence of I_h channels, somatically recorded arriving EPSP signals showed constant FWHM which was independent from dendritic injection site. The degree of synaptic integration also remained constant.
5. The rising time of somatically recorded signals of arriving EPSP which were initiated at dendritic injection site, increased with further distance from the soma. This behaviour was independent from the presence of I_h channels.
6. Injection of trains of EPSP signals with varying injection strength: The degree of synaptic integration was evaluated by the integral of the time voltage course of somatic recording. This led to following observations,

3 Methodology

- a) Presence of I_h channels led to a linear increase of the integral and V_m time course.
- b) Blockage of I_h channels led to a nonlinear increase of the integral and V_m time course.

The observed phenomena are visualized in [Figure 3.2](#) and [Figure 3.3](#).

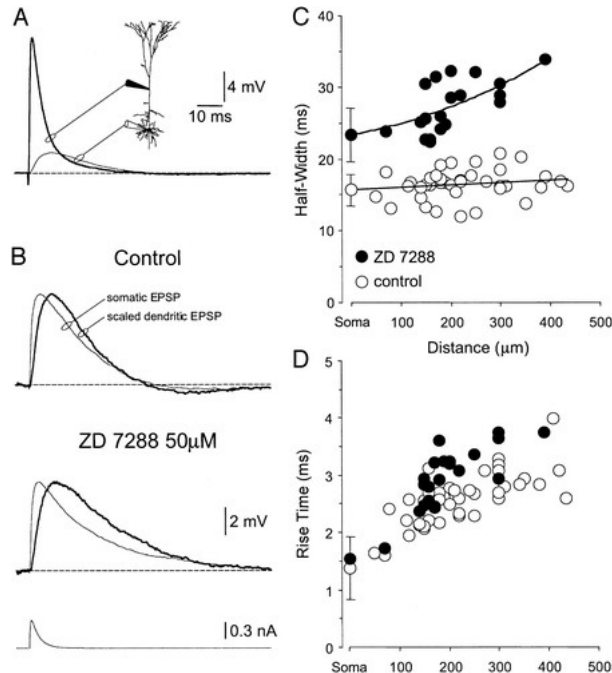


Figure 3.2: A) The graph shows the crossover between somatically recorded EPSP and voltage trace at source. It reveals high attenuation of dendritically injected propagated EPSP in the control case when I_h channels were present, B) Comparison of control case and blockage of I_h channels: Supplementation of ZD7288 ($50 \mu M$) led to blockage of the I_h channel and widened FWHM of somatically recorded signal, C) Blockage of I_h channels led to a non constant increase of signal FWHM with greater distance to the soma. Control shows the independence of signal FWHM from dendritic injection site, D) Both cases show an increase in signal rise time to the same extent. Source: [Williams and Stuart \(2000\)](#)

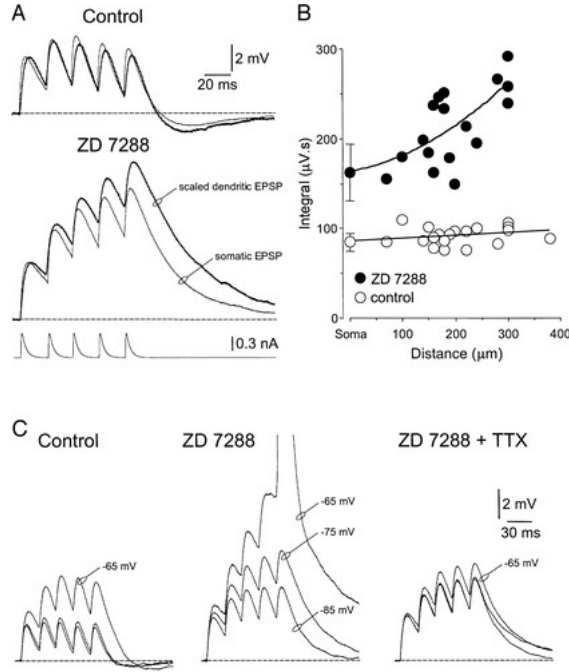


Figure 3.3: A) Dendritic injection site (thick line) was chosen 280 μm away from the soma. A train of EPSP was applied. This led to non significant temporal summation in the control case (presence of I_h). Supplementation of ZD7288 ($50 \mu\text{M}$) led to blockage of I_h channels and significant temporal summation occurred. B) The graph shows the dependence of the time voltage integral measured at the soma from the distance to the dendritic injection site. C) The figure shows the dependency of the degree of temporal summation from the membrane voltage for three different cases. Control: -65mV marks the depolarized somatic state. Incoming train of EPSP signals led to a higher voltage course due to moderate temporal summation of arriving signals. ZD7288: Supplementation of it led to blockage of I_h channels. Significant nonlinear temporal summation occurred, increasing with greater membrane voltage. TTX: Supplementation of TTX which is a sodium channel blocker led to removal of this nonlinear behaviour. Source: [Williams and Stuart \(2000\)](#)

K_s and K_f

The formula used to describe the distribution of the fast and slow inactivating potassium channel-types read,

$$G_{Ks}(x) := G_{Ks,dend} + G_{Ks,soma} e^{K_{s,slope} \cdot x}.$$

Same formula holds true for K_f ,

$$G_{Kf}(x) := G_{Kf,dend} + G_{Kf,soma} e^{K_{f,slope} \cdot x}.$$

Recall that $K_{s,slope}, K_{f,slope} < 0$ holds true.

Na^+

The distribution of the sodium channel type is defined by,

$$G_{Na}(x) := \begin{cases} G_{Na,soma} + x \frac{G_{Na,dend} - G_{Na,soma}}{Na_{dist}} & x \leq Na_{dist} \\ G_{Na,dend} & x > Na_{dist} \end{cases}$$

Obviously the distribution declines in a linear manner and comes to a halt at some distance.

Ca^{2+}

The set of distribution function of the subgroup of calcium channel declines linearly with further distance from soma. In contrast to the other channels its flux values are given in terms of permeabilities. The MVA channel distribution reads as follows,

$$P_{MVA}(x) := \begin{cases} P_{MVA,soma} + x \frac{P_{MVA,dend} - P_{MVA,soma}}{Ca_{MVA,dist}} & 0 \leq x \leq Ca_{MVA,dist} \\ P_{MVA,dend} & x > Ca_{MVA,dist} \end{cases}$$

The HVA channel distribution has the same distribution,

$$P_{HVA}(x) := \begin{cases} P_{HVA,soma} + x \frac{P_{HVA,dend} - P_{HVA,soma}}{Ca_{HVA,dist}} & 0 \leq x \leq Ca_{HVA,dist} \\ P_{HVA,dend} & x > Ca_{HVA,dist} \end{cases}$$

The distribution of the calcium-gate potassium channel K_{SK} reads as follows,

$$G_{SK}(x) := \begin{cases} G_{SK,soma} + x \frac{G_{SK,dend} - G_{SK,soma}}{SK_{dist}} & 0 \leq x \leq SK_{dist} \\ G_{SK,dend} & x > SK_{dist} \end{cases}$$

For the K_{BK} type it reads,

$$G_{BK}(x) := \begin{cases} G_{BK,soma} + x \frac{G_{BK,dend} - G_{BK,soma}}{BK_{dist}} & 0 \leq x \leq BK_{dist} \\ G_{BK,dend} & x > BK_{dist} \end{cases}$$

Considering BK_{dist} may reveal that its estimate is still bad conditioned due to high CV value. Further we may observe that the difference between $G_{BK,soma}$ and $G_{BK,dend}$ is quite small which also hints to some bad coniditon parameter space. Apart from the apical dendrites, the channel distribution in all the other morphological parts of the cell have been chosen uniform since the constraining procedure was applied to records from soma and apical dendrites.

3.2.2 Soma

Since the soma has small spatial extension, a uniform distribution of channels was assumed. The density of channels can be determined directly by continuity of the distributions from Chapter 3.2.1 and use of $x \rightarrow 0$.

3.2.3 Basal dendrites

The parameters are almost the same as in the soma with the only exception that,

$$G_{SK}(x) \equiv G_{SK,dend}, \\ G_{BK}(x) \equiv G_{BK,dend}.$$

This coincides with density values of the apical dendrites in the far distant region towards the apical tuft. This represents a non-continuous crossing from the soma to the basal dendrites since $G_{SK,dend} \approx \frac{1}{5} G_{SK,soma}$ holds true.

3.2.4 Axon

Since there was no recorded data for the axon, an artificial one was used (Mainen and Sejnowski, 1996). The axon is composed of the axon hillock, the axon initial segment and the Ranvier lacing ring which in turn consist of the nodes of Ranvier and myelin sheaths. The special feature is that the axon does not contain any of the calcium type channels.

Axon hillock, Initial segment and Nodes of Ranvier

Apart from the myelin sheaths, the axon has by far the highest values for sodium and potassium conductivity. It also explains why it is a preferred region for AP initiation. The IC_{50} threshold values of voltage-gated sodium channel activation were determined by a constraining procedure. From there, the parameter $Na_{shift,act}$ and $Na_{shift,inact}$ were determined in order to correct the threshold voltages for sodium activation and inactivation. These shift parameters were applied to the axon hillock, the axon initial segment and the nodes of Ranvier. Except for the myelin sheaths, almost all parameters were the same along the axon.

$$G_{Na}(x) \equiv G_{Na,node}, \\ G_{Ks}(x) \equiv G_{Ks,node}, \\ G_{Kf}(x) \equiv G_{Kf,node}, \\ G_{pas}(x) = \begin{cases} \frac{1}{r_m} & \text{for Hill and AIS} \\ G_{pas,node} & \text{for Node} \end{cases}. \quad (3.3)$$

x denotes the distance to the soma. The condition $G_{Na,node} \approx 100 \cdot G_{Na,soma}$ may explain why an AP is initiated preferably in the Nodes of Ranvier or the axon initial segment. In contrast to the axon hillock, both of them have a smaller diameter as we shall see later. Naturally, charge disbalance within the intracellular space leads to higher voltage deflections in segments of smaller diameter. This is because of the fact that the same amount of charge leads to higher voltage deflections in segments with lower volume.

Myelin sheaths

The distribution of channels along the myelinated parts of the axon are stated as follows,

$$\begin{aligned} G_{Na,myelin}(x) &\equiv G_{Na,soma}, \\ G_{Ks,myelin}(x) &\equiv G_{Ks,soma}, \\ G_{Kf,myelin}(x) &\equiv G_{Kf,soma}, \\ C_{m,myelin}(x) &= C_{m,myelin}, \\ G_{pas,myelin}(x) &= \frac{1}{r_m}. \end{aligned}$$

3.3 NEURON extracellular mechanism

NEURON provides the HOC library "xtra.hoc" in order to calculate compartmental current distribution.² We remind ourselves of the equation determining extracellular voltage in distance r_c to a point-source.

$$V_e(r_c) = \frac{\rho_e}{4\pi r} I_{el} = R_e(r_c) I_{el}.$$

$R_e(r_c)$ is called the transfer resistance for distance r_c . It is calculated by considering the specific resistance ρ_e of the extracellular homogeneous medium. When using the "xtra" mechanism it suffices to set following parameters for each compartment with distance r_c to point-source,

1. Set $R_e(r_c)$. r_c is the distance from point-source to considered compartment. Its choice is dependent on compartmental geometry in the following sense,
 - **cylinder/cone** Centerpoint of segment is used.
 - **soma** First the soma axis has to be aligned towards the point-source beforehand. This is done in order to assure that each compartment is at the same voltage level given the spherical electric field. Since the soma has great spatial expansion and therefore has high diameter, not the center of each segment is used but instead the distance towards the compartmental surface.
2. Setting the coordinates (x_c, y_c, z_c) of compartment centerpoint or surface which depends on the observation before.
3. Setting a pointer to the driving mechanisms of $i_{membrane}$ and $V_{e,n}$ of specified compartment.

3.4 Morphology

NEURON allows for cylindrical sections as well as truncated cones. For example, a truncated cone is defined by its 3-dimensional starting point and endpoint augmented by their

²Id: xtra.mod,v 1.4 2014/08/18 23:15:25 ted

respective circumference of circle.

$$\begin{aligned} p_{start} &= (x_s, y_s, z_s, d_s) \\ p_{end} &= (x_e, y_e, z_e, d_e) \end{aligned}$$

In the following we will detailly explain the morphological set up for the model which will subsequently be used to deduct results. Morphology of a real L5 pyramidal cell was taken from [Almog and Korngreen \(2014\)](#) and transferred to a self-developed Python interface. The interface makes it possible to manipulate some components. For example, rotating the soma in the 3-dimensional space is possible. This is also necessary in order to align the soma axis towards the point-source. Orientation of the axon is also freely selectable. All of the geometry was given in the notion of truncated cones, except the axon which was constructed artificially by cylinders.

3.4.1 Spines

As we already know, spines are small protrusions in the membrane of basal dendrites with length $2\mu m$. They aim to increase the area of the membrane. This can be modeled by two different approaches. Either you increase the area of the membrane or you increase the densities c_m and g_{pas} by a factor 2. The last one approach was used for the model used in this thesis.

3.4.2 Soma

Ideas on how to construct the soma were overtaken from [Fellner \(2017\)](#) and [Burian \(2017\)](#).

Geometry

The soma was built through staking of 20 truncated cones on top of each other in the attempt to approximate the real geometry in the best possible way. The situation is sketched in [Figure 3.4](#).

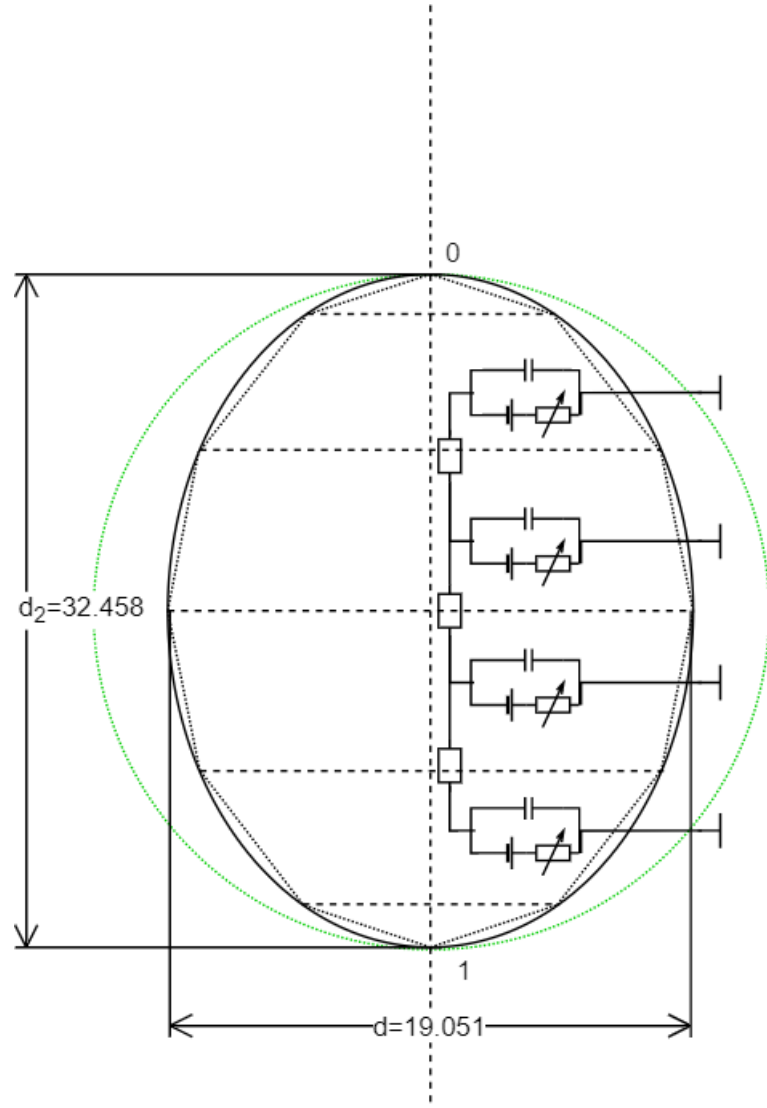


Figure 3.4: Discretized soma: The figure shows the cross-section of a spatially discretized soma. Given its pyramidal real life template, it is built in form of an ellipsoid. Its main axis has length d_2 and the minor axis has length d . The compartments are connected in serial to each other through intracellular resistance R_i . A second structure may be connected to the north- (0) or southpole (1) which prolongs the serially connected structure. In case that the second structure is connected somewhere in-between we have to consider a electrical star point connection. This could be for example the case when connecting the axon hillock to the soma.

Orientation

An extracellular point-source electrode is used to excite the neuron. In the concrete implementation, the centerpoint of the soma was taken as the zero point of the coordinate system while the compartments where stacked up along the y-axis. Since the soma itself has a relatively huge spatial expansion, the voltage gradient is quite high for close range stimulation. Therefore it is important to keep the sheathing surface of each compartment at same voltage-level. This makes calculations in connection with the xtra meachnsim as simple as possible, determining V_e for each compartment correctly. We remind ourself that the electric field is of spherical form. Demanding the conditions before, the only possible solution is to align the vertical soma axis through the coordinate of the extracellular point-source. In the concrete implementation this was done in several steps.

1. Build the soma geometry horizontally using the given 3D-morphology from [Almog and Korngreen \(2014\)](#) such that its axis is aligned to the y-axis.
2. Using the coordinates of the point-source electrode it is possible to calculate components of a 3-dimeniosnal rotation matrix which rotates any vector that points along the y-axis so that in retrospect it points to the direction of the specified coordinate.
3. Rotating the soma geometry by multiplication of 3d-coordinates with prespecified matrix.

The situatuion of alignment as well as correct assessment of extracellular voltage is sketched in [Figure 3.5](#).

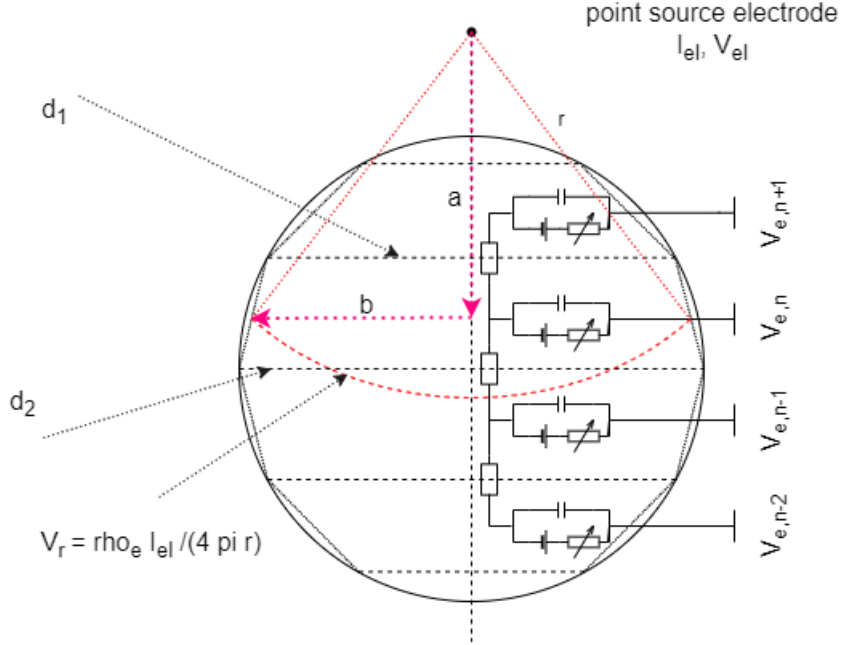


Figure 3.5: Stimulation of the discretized soma: The depiction shows the influence of an extracellular point-source electrode onto the compartments of the soma. The soma has spatial extent that is not negligible. Therefore we have to consider the distance $r = \sqrt{a^2 + b^2}$ in order to determine the correct extracellular voltage. This is in contrast to structures like the neurite or dendrite sections where distance is measured towards the midpoint of the segment. This is allowed since they have small spatial expansion which leads to a negligible error. Assuming that b is always measured at the midpoint of each compartment and d_1, d_2 denote the defining diameter of the considered cone, we can state $b = \frac{d_1+d_2}{4}$.

3.4.3 Axon

The axon was built up artificially by cylinders. In the concrete implementation the number of nodes can be adjusted while each node is followed by a myelinated section. The very first node of Ranvier is connected through the initial segment to the axon hillock. Geometry was specified by diameter and length. The diameters of the axon initial segment, nodes and myelinated sheaths were determined through an equation that relates to the cross-sectional area A_s of the most centric somatic compartment. The steps in determining the geometrical features are given as follows. All length units are set to μm .

$$d_{equiv} = \sqrt{\frac{A_s}{4\pi}} = \sqrt{\frac{r_s^2\pi}{4\pi}} = \frac{r_s}{2}$$

3 Methodology

Then we may calculate the diameter of the individual parts as follows,

$$d_{iseg} = \frac{d_{equiv}}{10}, d_{node} = \frac{d_{equiv} * 3}{40}, \quad d_{myelin} = \frac{d_{equiv}}{10}.$$

Length of each of the parts is given by,

$$L_{iseg} = 20, L_{node} = 1, L_{myelin} = 100.$$

Figure 3.6 visualizes the interconnection.

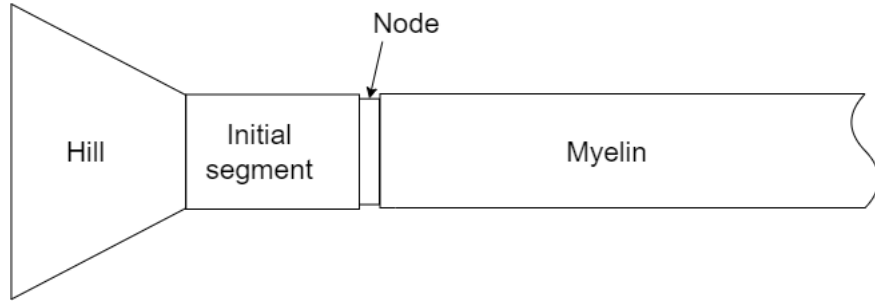


Figure 3.6: Axon morphology: Show the interconnection between axon hillock, initial segment, node of Ranvier and myelin sheath.

Extracellular field

The axon was excited by a spherical field. In contrast to the soma we can use the distance from point-source to compartment centerpoint in order to calculate the extracellular voltage drop. This approach does not produce high error and is sketched in **Figure 3.7**.

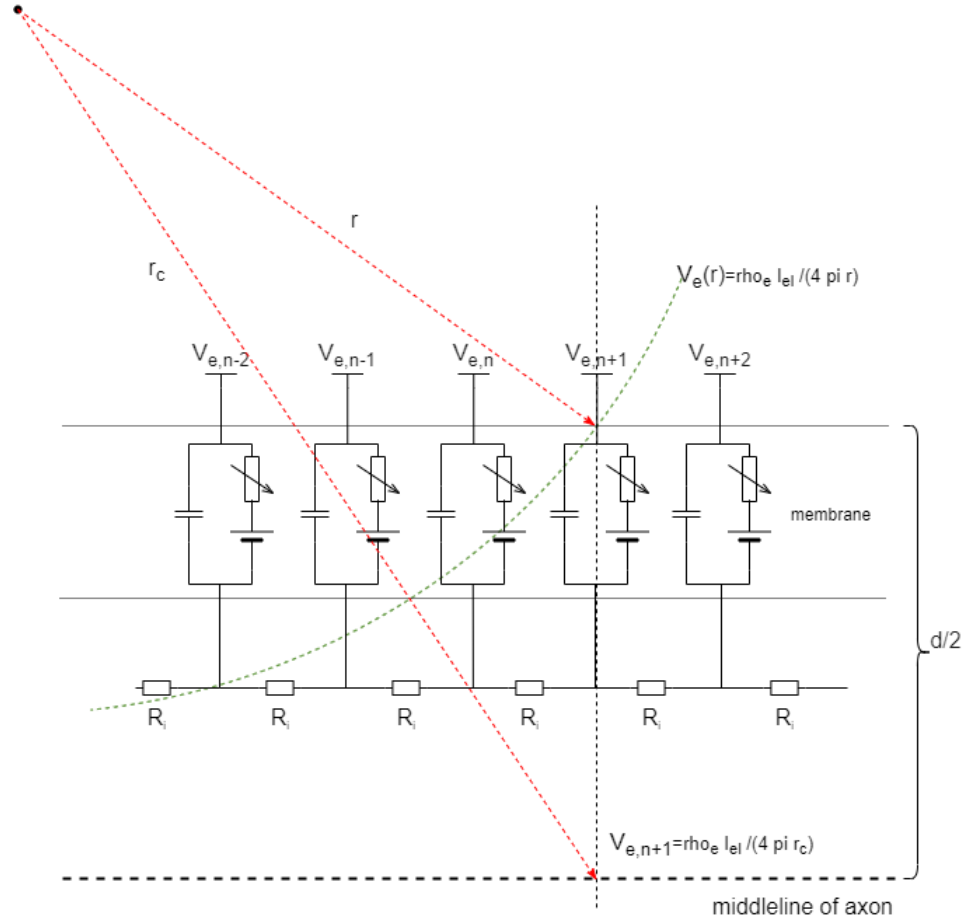


Figure 3.7: Discretized axon: The depiction shows the subdivision of the axon into its compartments. Extracellular compartment voltage is calculated based on the distance to the centerpoint of the considered segment. Since $d/2$ is small, the difference between $V_{e,n+1}$ and $V_e(r)$ can be neglected. Furthermore, the small gradient in transversal direction may also be ignored due to the small diameter. Therefore, taking the center of the compartment is a good approximation.

3.4.4 Axon Hillock

Geometry

The axon hillock originates from the soma and represents the interconnecting part between soma and axon. No morphological data was available for the axon hillock which is why it was built artificially. It was specified through two 3d-coordinates, both ends of a truncated

cone with following dimensions,

$$L_{hill} = 20\mu m,$$

$$d_{start} = 2d_{iseg} = \frac{d_{equiv}}{5},$$

$$d_{end} = d_{iseg} = \frac{d_{equiv}}{10}.$$

Orientation and Alignment

The axon hillock is aligned along the axis of the axon and therefore may also be rotated at will. Together with the nodes of Ranvier and the axon initial segment, it has by far the highest values for sodium and potassium conductivity of the whole neuron, which also explains the importance of correct alignment towards the soma. This is especially important for short-range stimulation which was not the focus of this project, still leaving that option. Since the pyramidal soma is not built as a perfect sphere but rather an ellipsoid, after rotation of both structures, attention must be paid to what somatic segment the axon hillock is connected. The situation and approach is sketched in [Figure 3.8](#).

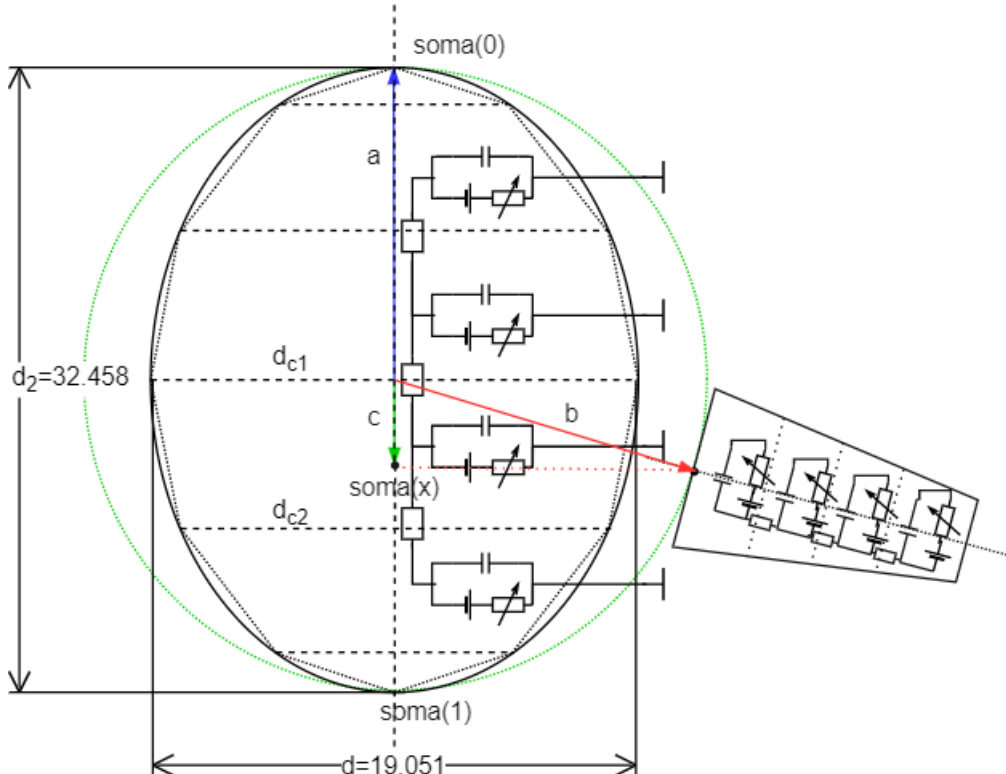


[Figure 3.8](#): Axon hillock alignment: The figure shows the circular alignment of the axon towards soma. The soma has ellipsoidal form with given axis lengths. *soma(0)* refers to the north- and *soma(1)* to the southpole. *soma(x)* with $0 \leq x \leq 1$ denotes the segment at relative arclength x .

Referring to [Figure 3.8](#), the axon was aligned and connected in four steps.

1. At first, the axon is stacked horizontally along the y-axis. Its first 3d-point coincides with the boarder of the green circle whose radius is $(r_{max} + r_{min})/2$ with $r_{max} = d_2/2$ and $r_{min} = d/2$.
2. Both, soma and axon are rotated according to specified angles around zero-point. Nevertheless, it suffices to analyze the relative angle between both structures, which is why we can leave the soma aligned with the y-axis for the purpose of illustration.
3. Now we construct vectors a and b by provided coordinates. Evaluation of the scalar product $a \cdot b = sgn(c \cdot a)|c|$ concludes the vertical distance between the center of axon hillock and zero point. Given c , by application of several norming and reparametrization steps it is simple to determine $x \in [0, 1]$ for $soma(x)$ and therefore the sought after somatic segment to which $hill(0)$ is connected to.

3.4.5 Dendrites

Geometry

The geometry of the dendrites was taken from [Almog and Korngreen \(2014\)](#). All dendritic sections originating from the soma were attached to its center-point.

Orientation and Alignment

The geometries of some few dendritic sections submerge into the one of the soma. Nevertheless, since dendritic morphology rather follows coincidence than a prescription and because dendrites do not have high conductivity, their connections to soma centerpoint were left as is. Correct placement is important for highly excitable structures like the axon hillock were for short-range stimulation, the distance to the point-source indeed plays an important role. The *cable length* which defines the electrotonic distance between two connected segments remains unaffected from shift in coordinates. Since the cable length determines intracellular resistance R_i , the intracellular properties are also independent from the choice of coordinates but solely depend on the logical connection between two segments.

4 Results

We used the model from Almog and Korngreen (2014) to deduct the results. We augmented it with an axon that consisted of 10 nodes of Ranvier with associated myelin sheaths. We studied the effects that intra- and extracellular stimulation have upon the different regions of the cell. We will keep an eye on calcium ion-dynamics and their implications for apical spiking generation.

4.1 Intracellular stimulation

For intracellular stimulation we will focus on the effects of intracellular square-wave stimulation. To be more precise, we will study the influence upon generation of dendritic spikes and AP-form in the soma. The goals we are pursuing are manifold and given through following questions.

- Is intracellular square-wave stimulation capable - with a duration of 10ms which is almost EPSP signal duration (14-20ms) - to initiate an AP in the apical dendrite itself? Does this AP manage to reach to soma?
- At what distance does this attempt succeed and what is the lower stimulation threshold for given distance? Both cases are of interest, dendritic AP-initiation at apical injection site as well as the soma itself.
- Same question can be raised for the basal dendrites.
- Referring to Almog and Korngreen (2014) modelling of voltage-gate calcium channels is a novel approach in contrast to preceding models which do not possess that dynamics. Therefore we should ask ourselves: Do AP spikes in the apical dendrites have properties of a calcium driven generation? At this point we remind ourself of the MVA channel with high time constant τ .
- Do basal dendrites have those properties too?
- What is the strength duration relation (SDuR) for axonal as well as for apical current injection?

To solve the first pair of questions an intracellular strength distance relation (SDR) was evaluated. In case for the apical dendrites, the path from the outermost apical dendrite in the apical tuft called apic[29] was recorded following the path of its predecessor all the way down to the soma. The morphological setting is sketched in Figure 4.1.

4 Results

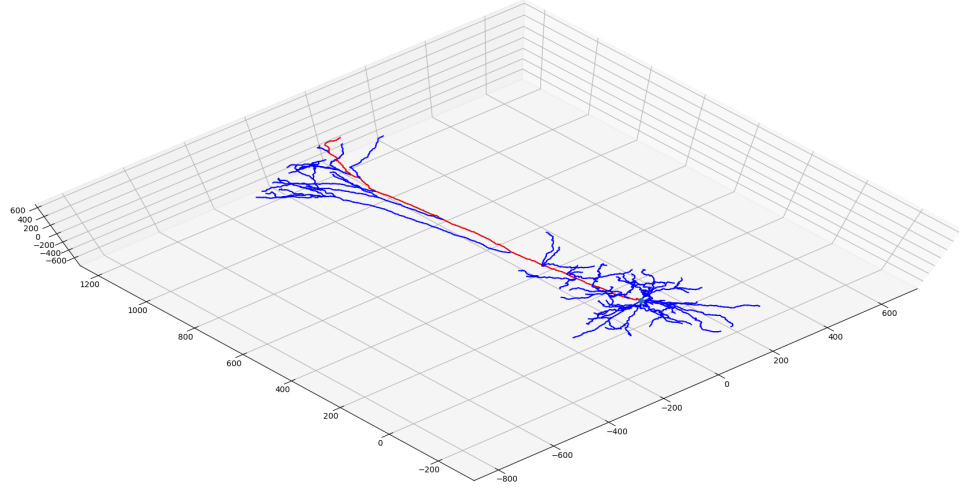


Figure 4.1: Apical path: The recorded apical path is marked in red. Especially in the case of extracellular stimulation it will give us a good overview over all the activities happening in the cell.

The path is given by following parent-child relationship starting off with the most distant child,

```
[apic[29], apic[25], apic[15], apic[14], apic[13],
apic[12], apic[11], apic[10], apic[9],
apic[8], apic[7], apic[6], apic[5], apic[4],
apic[3], apic[2], apic[1], apic[0], soma].
```

For the basal dendrites we conducted the same trial by choosing the most distant dendrite and following its precursors all the way down to the soma. The path is given by,

```
[dend[46], dend[44], dend[43], dend[42], dend[41], soma]
```

and sketched in [Figure 4.2](#).

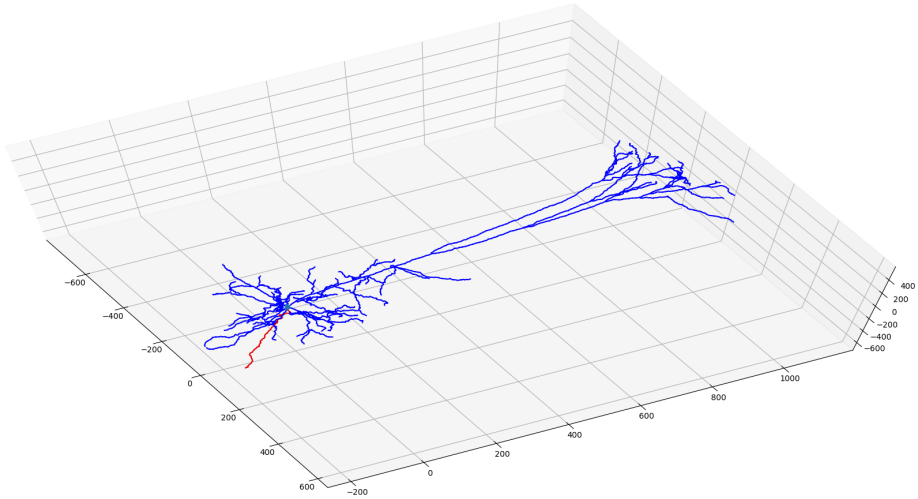


Figure 4.2: Basal path: The basal path that was chosen for the evaluation of the SDR for the case of basal dendrites, is marked in red.

For each of these paths an intracellular square-wave with 10ms duration was injected at midpoint of each section from the path. The distance from this point towards the center of the soma was determined to be the corresponding distance on the x-axis. The whole axon together with the axon initial segment and axon hillock was removed. Given their high excitability we did not want to initiate an AP there but focus solely on the aspects of dendritic driven AP-initiation in the soma. The results of the apical SDR are given in [Figure 4.3](#).

4 Results

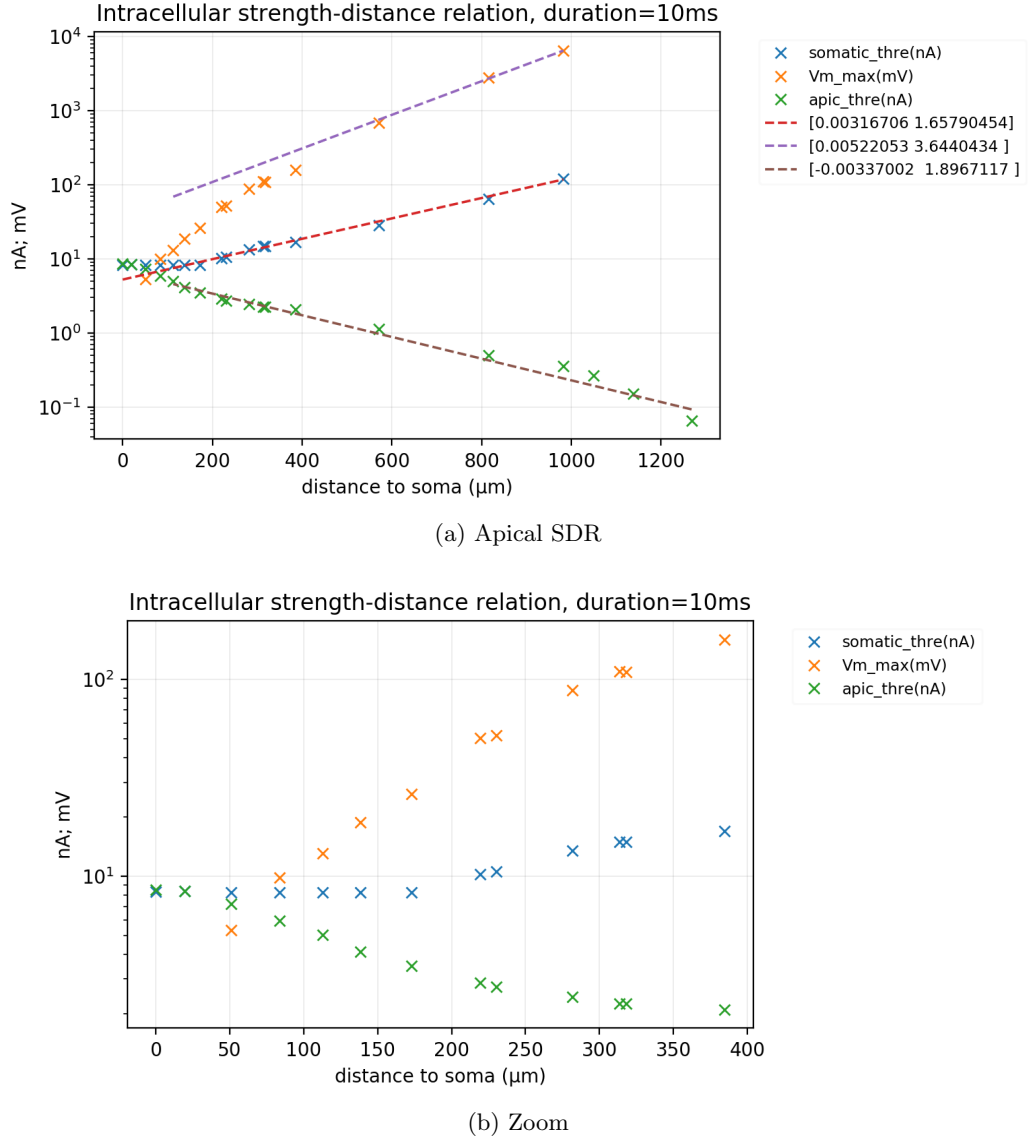


Figure 4.3: Apical SDR: The results show the threshold current as a function of the distance to the apical injection zone. The distance is determined by the distance of the iterated path of apical sections towards the soma. $apic_{thre}$ (green) is the lower threshold current of the apical dendrite injection site. $somatic_{thre}$ (blue) determines the somatic lower threshold current for the same injection site. Obviously the threshold value for the soma is always higher than that of the apical dendrites, and in contrast to the latter, monotonically increasing. Due to high somatic threshold values it is important to keep an eye on the membrane voltage at injection zone. $V_{m,max}$ (orange) denotes the membrane voltage at apical injection site which is necessary in order to reach somatic threshold strength. The parameters of the exponential fit are given by $[a, b]$ with its evaluating function e^{b+ax} .

Referring to [Figure 4.3](#) we want to mention a few things. The prominent crossover predicted in [Almog and Korngreen \(2014\)](#) did not occur which does not surprise. The paper used a duration of 50ms and decreased the conductivity of the axon by a factor of 10 instead of removing it. This still leaves a quite excitable structure. Nevertheless, all the other peculiarities are replicated most importantly that for higher distance it gets exponentially harder to initiate a somatic AP. We took a different approach by leaving the axon out justified by the fact that we want to solely focus on the behaviour of apical dendrites and their influence upon somatic AP, unperturbed by some axonal artifacts. When the axon was present, the axon initial segment which is quite close to the soma was always excited first leading to typical sodium driven AP initiation in the soma. The SDR for the basal dendritic path is sketched in [Figure 4.4](#)

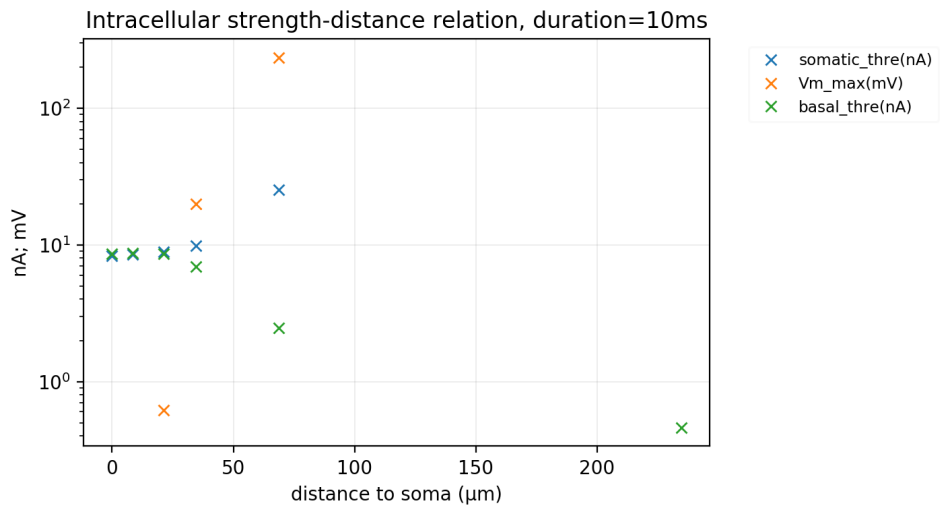


Figure 4.4: Basal SDR: Same procedure as in [Figure 4.3](#) was conducted. Obviously the path of basal dendrites is much scarcer than for the apical analogue since the basal dendrites are not spread that wide. What comes to our attention is that it is much harder for the basal dendrites to initiate an AP at the soma than it is the case for the apical ones. While $somatic_{thre}$ already reaches $10nA$ at a distance of $\approx 40\mu m$, for the apical type it is almost $230\mu m$.

We are also interested in what type of somatic AP is generated when comparing basal and apical injection site. What we wish for is to see a pronounced aspect of the calcium driven mechanism in the case of apical AP injection site. The subsequently simulated SDR give us a hint at which distance it is still possible to initiate a somatic AP without causing cell damage through high values of $V_{m,max}$. We will use $dend[43](39.02\mu m)$ from the basal path and $apic[7](232.41\mu m)$ from the apical path and compare its generated somatic AP-form. The duration will be set to $1.5ms$ for both trials since we want to focus on the ion-dynamics ignoring artifacts of too long stimulation. Since we want to better understand the results we plot several ion-dynamics which are listed as followed.

- **gna:** Plots the specific sodium conductivity which has a small time constant τ .

- **ica:** Plots the specific calcium current density. For apical excitation it will then be clear that there is a superimposed voltage-gated calcium ion mechanism with high time constant τ which leads to atypically long decline of calcium current in the apical dendrites. This will also explain the prominent voltage course of the soma in the case of apical injection site.
- **v:** Plots the voltage course.

In the following we will always plot metadata for deducted plots in order to increase its reproducibility.

- **sec** refers to the chosen site for intracellular stimulation which is usually taken at midpoint of the section if not mentioned otherwise.
- **del** denotes the stimulation delay.
- **dur** denotes the stimulation duration.
- **amp** denotes the stimulation strength.
- **[x,y,z]** denotes the position of the extracellular electrode whose influence is turned off for intracellular stimulation. Since the developed Python API is capable to conduct as many simultaneous stimulations as one wishes for, this information is always printed.
- **Legend** The legend always includes the soma. If present, some of the Ranvier nodes and most importantly for extracellular stimulation the recorded apical path. "apic[29],p=15; 1263.06um" for example decodes the information that apic[29] is the successor of its parental section apic[15]. This relationship is not directly but could be for example over several intervening sections. This truncates the apical path and maintains clarity of the plot. 1263.06um refers to the distance $apic[29](0.5), soma(0.5)$.

The results for the excitation of basal dendrites are given in [Figure 4.5](#).

4 Results

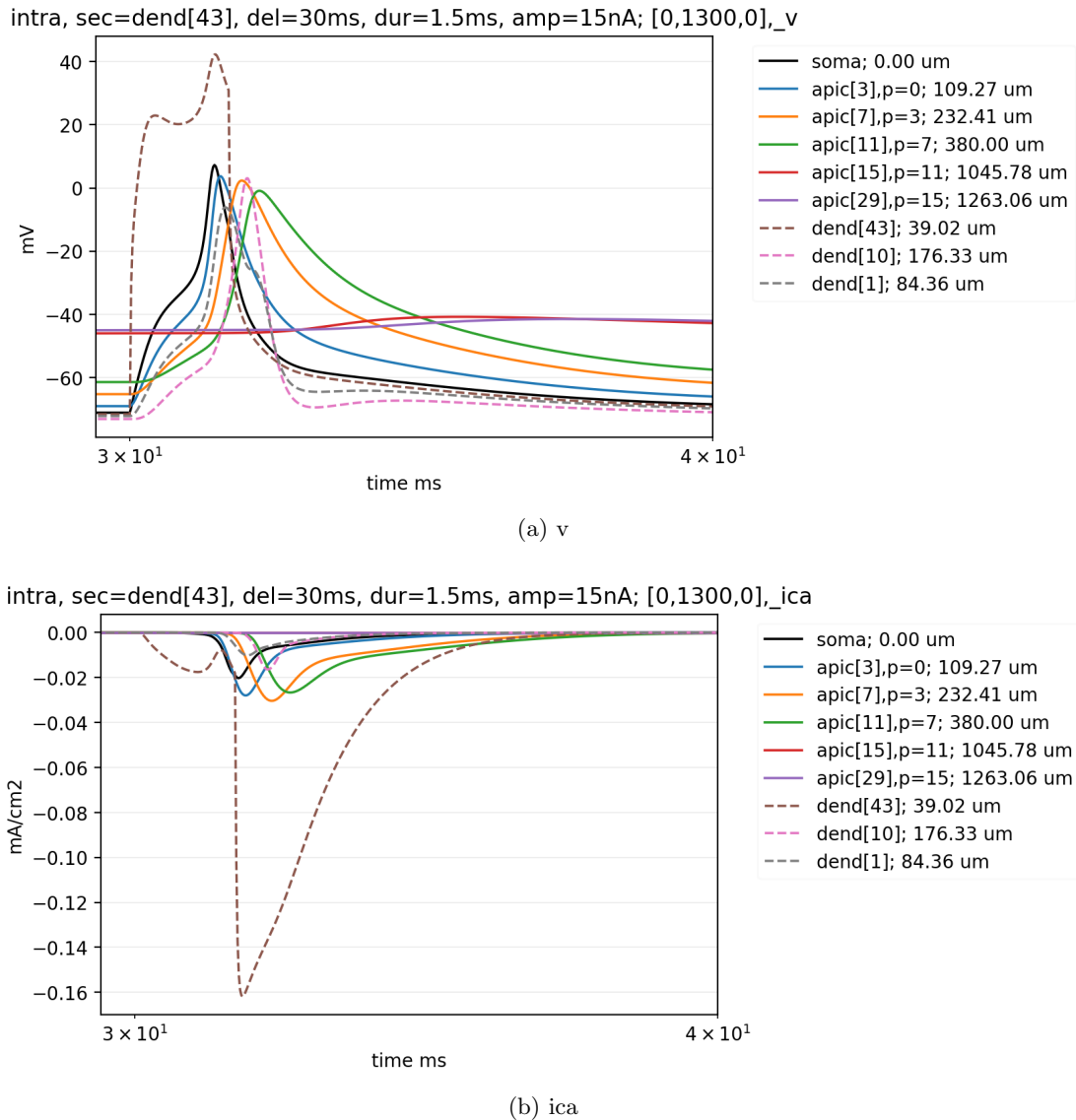


Figure 4.5

4 Results

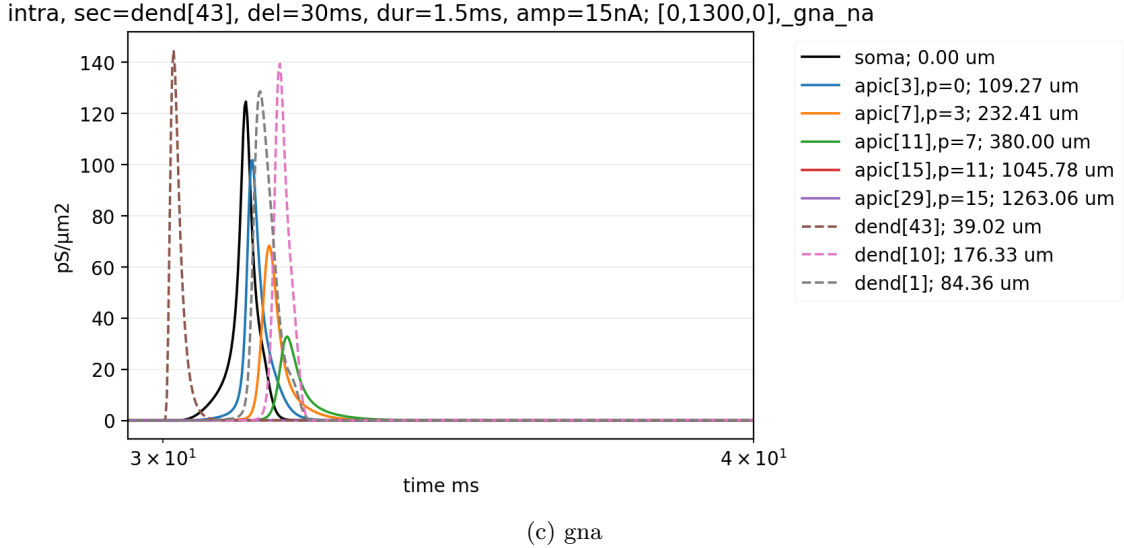


Figure 4.5: Basal dendrite injection site, somatic AP: a) Intacellular dendritic stimulation led to AP-firing in the soma, b) Calcium channels with their high time constant, c) Fast sodium current activation.

Referring to [Figure 4.5](#) there are still a few things to mention. What stands out is the difference in resting membrane voltage for each of the different sections which has something to do with the distribution of ion channels. Obviously, the further we go towards the apical tuft the value of V_{rest} increases. This peculiarity may be owed to the higher density of hyperpolarizing channels.

- (a) In this specific case, current injection into "dend[43](0.5)" led to AP-initiation in the dendrites, as well as in the soma itself, which than propagated some distance along the apical dendrites, nevertheless failing to propagate towards the apical tuft. We can also observe that the maximal-peak is diminishing along the apical path. This illustrates the almost electrotonical propagation of APs along the apical dendrites, given the increasing density of I_h channels.
- (b) Obviously there is still a bit influence from the appended apical dendrites, expressed in the kink of voltage curves in the course of the repolarization process. This can also be deducted from soma AP-form, where no clear hyperpolarization process seems to exist, and curve-form in the re- and hyperpolarized region seems to fit the kink of ica which otherwise couldnt't be explained by the curvature of gna processes in (c).
- (c) This electrotonical behaviour can also be deducted from the low values of gna . For comparison: specific sodium conductivity in the case of AP-propagation in node, axon initial segment and axon hillock usually lays at $\approx 8000 pS/\mu m^2$, as we will see.

The results for excitation of apical dendrites are given in [Figure 4.6](#).

4 Results

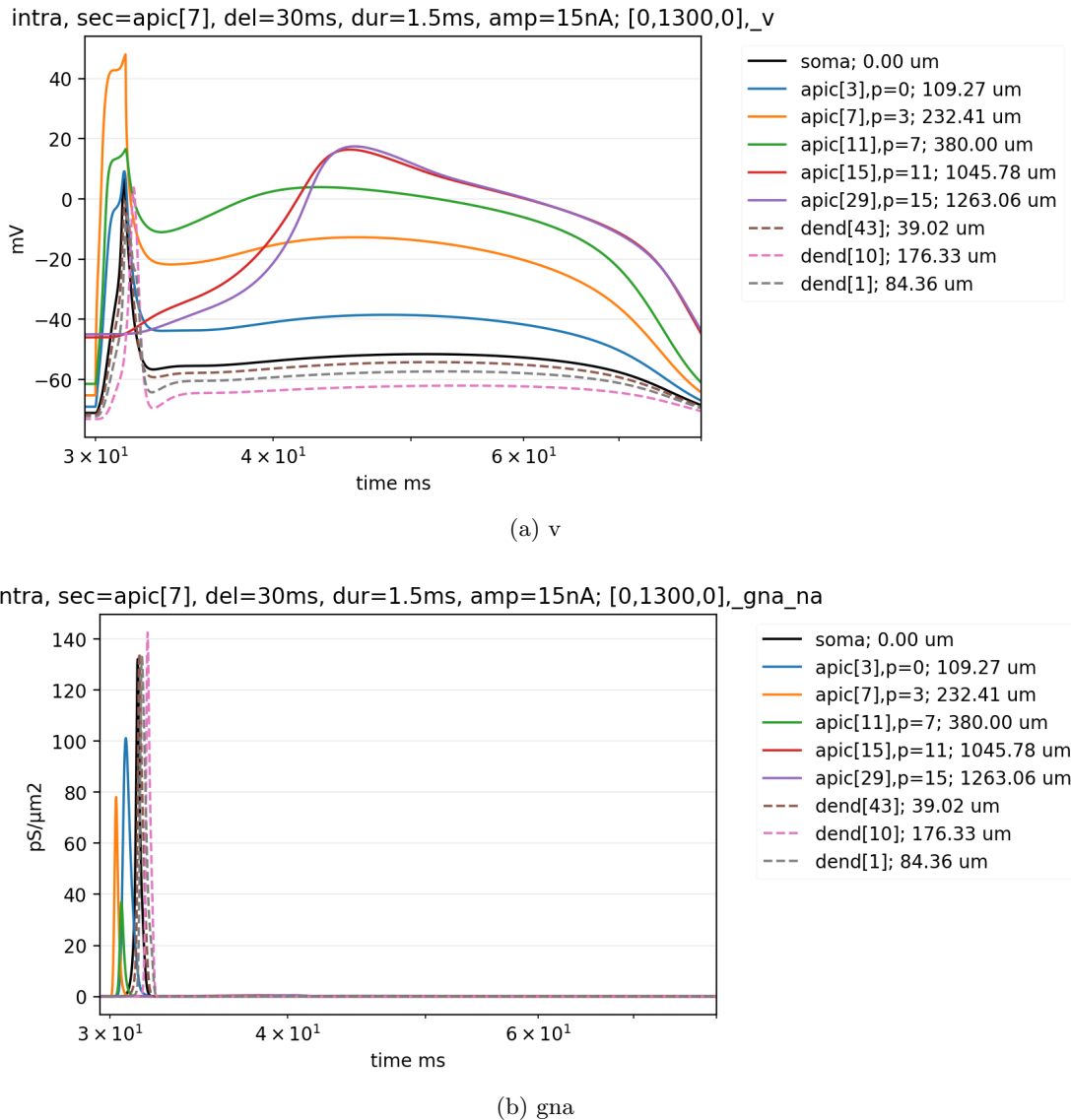


Figure 4.6

4 Results

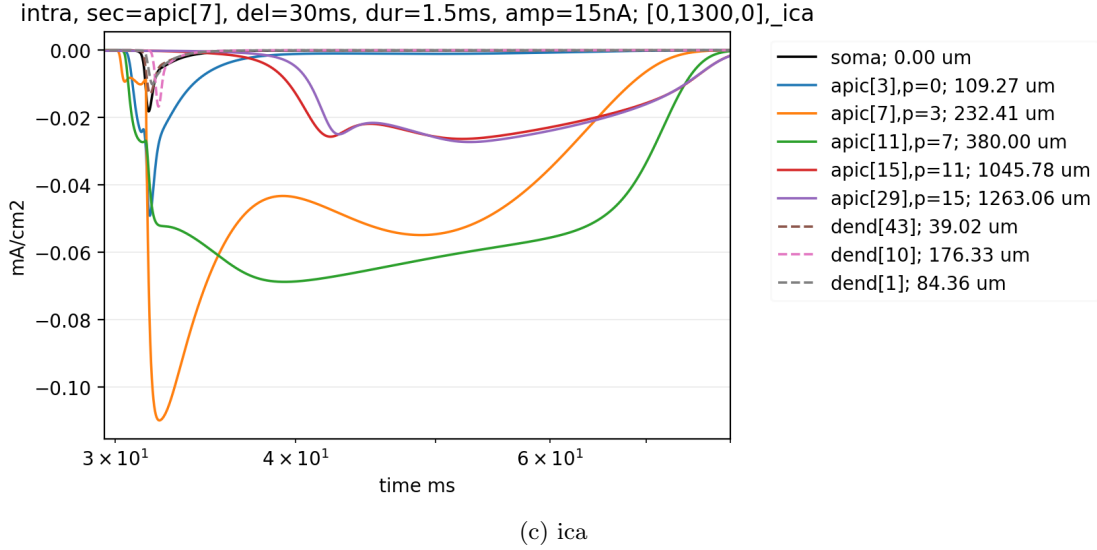


Figure 4.6: Apical dendrite injection site: Stimulation applied at apical injection site as expected leads to high influence of the calcium dynamics onto the somatic AP-form. It can be explained by the high time constant of HVA and MVA calcium channels. Nevertheless there are also some artifacts of temporal summation present. This is due to the fact that after an AP is generated at apic[7] it propagates towards the soma. There it gets amplified and reflected back to the apical dendrites were the arriving signal contributes to temporal summation.

Comparison of [Figure 4.6](#) and [Figure 4.5](#) reveals a pronounced influence of calcium dynamics in case of apical injection site. Proximal to the soma there are less of hyperpolarizing channels I_h present which would otherwise mitigate the effects of synaptic integration. From here until the end of the chapter we will incorporate the axon into the trials. What is also of interest is the relation between the time and minimal threshold strength it takes to initiate an AP. Thats why we evaluate a strength duration relation (SDuR). We will study two cases.

1. Evaluate at what strength a somatic AP is generated by excitation of the most distant *node[9](0.5)(954μm)* for given time durations.
2. Evaluate at what strength a somatic AP is generated by excitation of *apic[11](0.5)(380μm)* for given time durations.

We shall see that the axon initial segment is always excited first. In the case of AP initiation it then propagates towards the soma. Reasons on why the axon initial segment is a preferred candidate for AP initiation was discussed in [Section 3.2.4](#). The plots of both SDuR are given in [Figure 4.7](#).

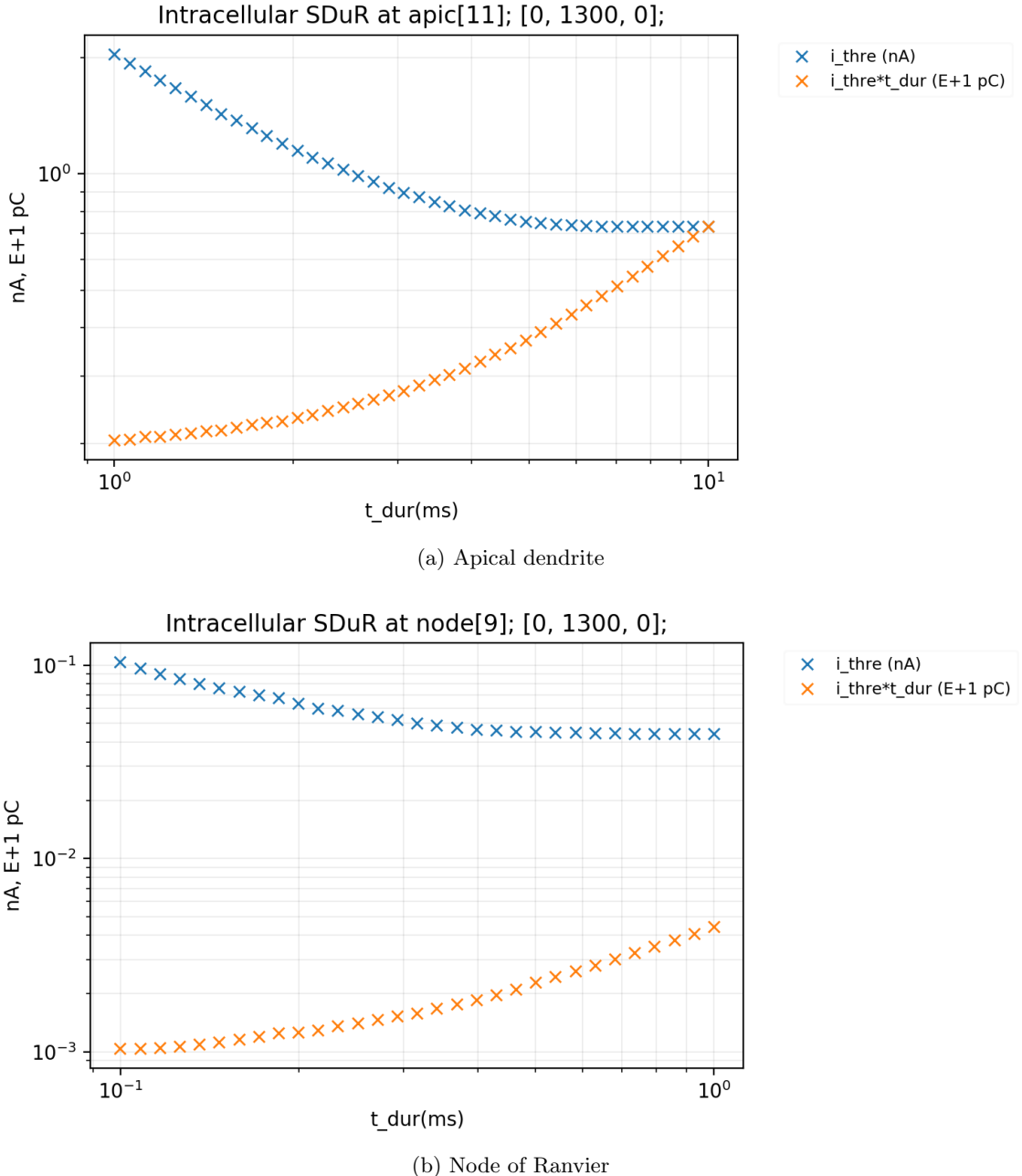


Figure 4.7: Intracellular SDuR: a) The Rheobase is 0.7nA. The injected charge $i_{thre} * t$ evaluates the charge that was injected for the duration of the stimulation. Since i_{thre} saturates at the Rheobase for high enough t_{dur} while t_{dur} increases this will gradually increase the slope of the orange curve. For $t_{dur} \gg 1$ this leads to $i_{thre} * t \propto t_{dur}$. b) For the most distant node it is obviously much easier to initiate an AP that eventually leads to somatic AP. Still it follows the same dynamics as in a). The Rheobase is 0.03nA.

4.2 Extracellular stimulation

We want to take a look at extracellular excitation. The point-source will be placed in long- and mid-range distance as well as lateral to the soma. Both stimulation types, anodic as well cathodic will be of interest. We want to study under which circumstances an AP is initiated in the axon initial segment as well as those circumstances that lead to AP initiation in the dendrites. The findings are quite interesting especially for AP initiation in the axon initial segment. Even for electrode placement in the mid-range distance, anodic stimulation managed to excite the axon initial segment. We will try do give an explanation for this phenomenon by considering the plots and stating physcial interpretations.

4.2.1 Long-range distance

For the first trial we chose (0,1300,0) as the position of the point-source electrode. This means that it was placed slightly above the apical tuft considering that the coordinates of one of the most distant apical dendrite apic[29] are approximately (10,1183,-11). Therefore the electrode had approximately $120\mu m$ distance towards the next apical dendrite. When stimulation was applied, we observed following phenomena.

1. Anodic stimulation led to hyperpolarization of apical dendrites in the near neighbourhood of the electrode. At the same time apical dendrites that are a bit further away were depolarized. It also led to depolarization of the somatic region in far distance to the electrode. The voltage distribution along the whole cell at the moment when stimulation halts is sketched in [Figure 4.8](#). The plots of voltage course for sub-threshold and AP initiation stimulation strength are given in [Figure 4.9](#). The effect that anodic stimulation led to excitation of the soma is quite interesting but may be explained as followed. The whole cell has wide spatial expansion along the y-axis. This means that the extracellular voltage V_e is much smaller at the soma than it is at the apical tuft. This is due to the voltage gradient produced by the point-source electrode. At the same time intracellular charge remains fairly constant. Since the intracellular medium is assumed to be a conductive medium with resistance R_i^1 , this leads to an intracellular electric field which points into the opposite direction and aims to compensate the one induced by the point-source. Since $\overline{V_{e,tuft}} > \overline{V_{e,soma}} > 0$ holds true, this leads to the effect that negative intracellular charge is attracted more towards the apical tuft than towards the soma.

$\overline{V_{e,i,tuft/soma}}$ denotes the mean intra- or extracellular voltage in the specified section. Since the mean intracellular voltage $\overline{V_i}$ remains fairly constant due to charge retention, this must be compensated by equalizing currents which augment the somatic space with more of positively charged ions. This leads to $\overline{V_{i,soma}} > \overline{V_{i,tuft}}$. Both of those effects lead to depolarizing effects on the soma.

2. Cathodic stimulation leads to hyperpolarization of the somatic region. This can be explained by the same mechanism, only reversed. In this constellation of far distant electrode and hyperpolarized soma, it is quite difficult to generate an AP through

¹ Hodgkin and Huxley (1952)

dendritic excitation in the apical tuft. The morphological situation is sketched in [Figure 4.10](#). Associated plots of voltage course are given in [Figure 4.11](#).

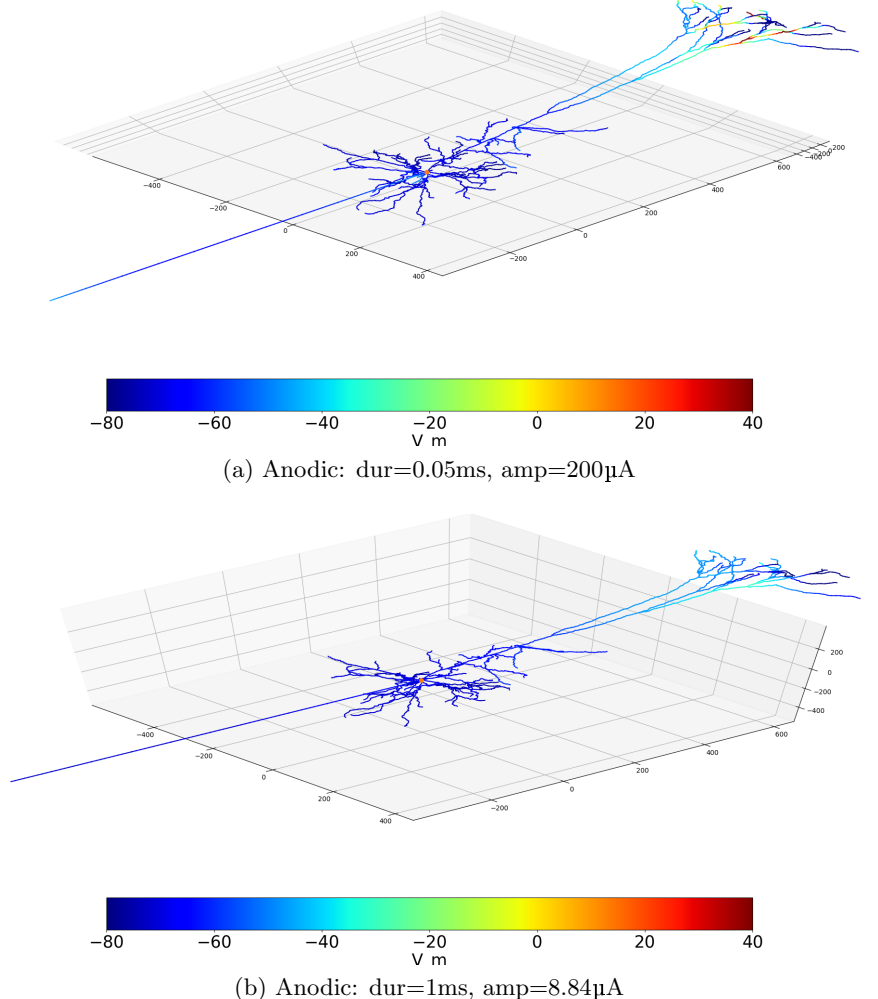


[Figure 4.8: Anodic Stimulation, coord=\(0,1300,0\):](#) Plots of the morphological voltage-distribution for long and short anodic stimulation duration with given threshold strength. As we can see clearly, the region surrounding the electrode gets hyperpolarized while apical dendrites neighbouring those sections get depolarized. It seems like that there is a grid-like distribution of de- and hyperpolarized zones present in the apical. The zones of depolarization seem to pile up in the branching regions of the apical tuft which may point to spatial summation. What still may not be seen clearly is that regions surrounding the soma are slightly lighter which points to depolarization of those. A detailed view is given in [Figure 4.9](#).

4 Results

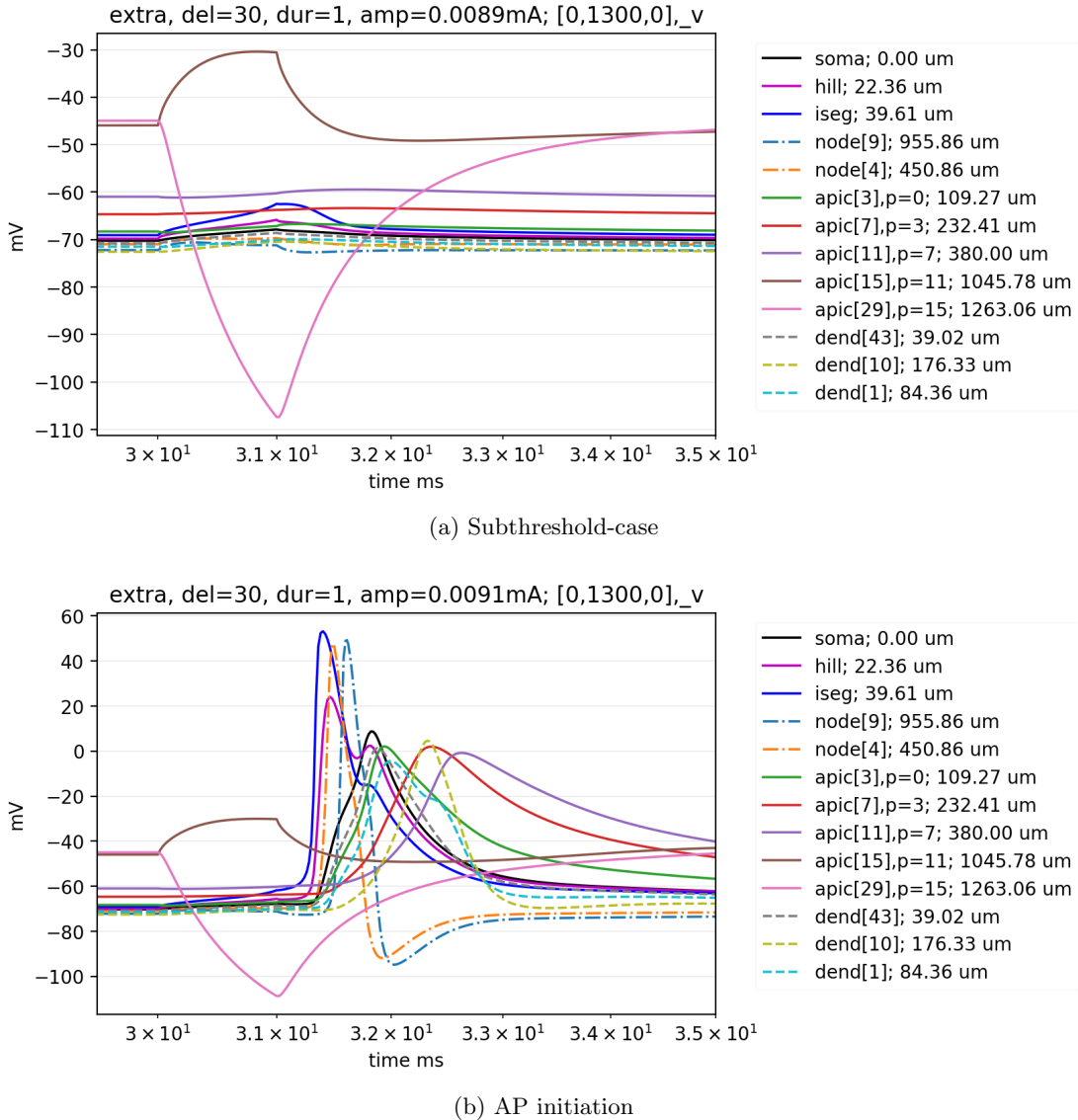
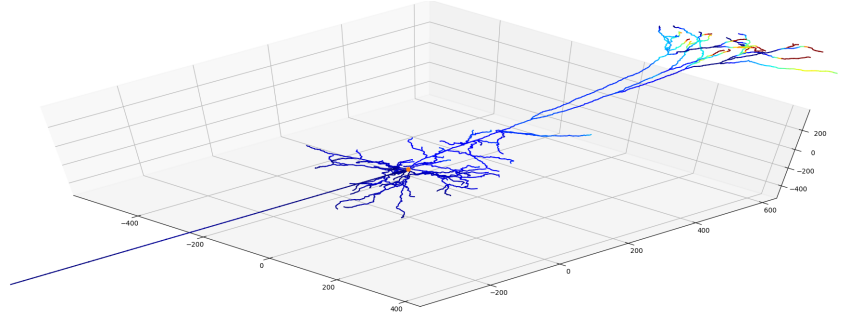
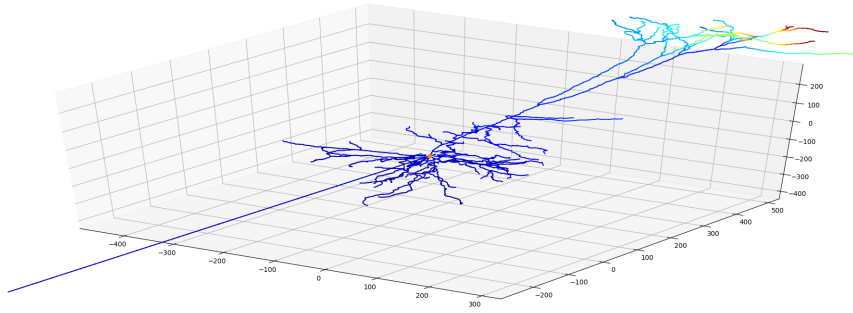


Figure 4.9: Anodic stimulation, coord=(0,1300,0): a) The subthreshold-case makes clear that the axon initial segment is the leading edge of depolarization. b) The depolarizing effect of anodic long-range distance excitation of the soma and its neighbourhood is obvious.

4 Results



(a) Cathodic: dur=0.05ms, amp=-200 μ A



(b) Cathodic: dur=1ms, amp=-11 μ A

Figure 4.10: Cathodic Stimulation, coord=(0,1300,0): Plots of the morphological voltage distribution for long and short cathodic stimulation duration with given threshold strength. As we can see clearly the region around the electrode gets depolarized. We can also identify a deep blue somatic region which indicates hyperpolarization.

4 Results

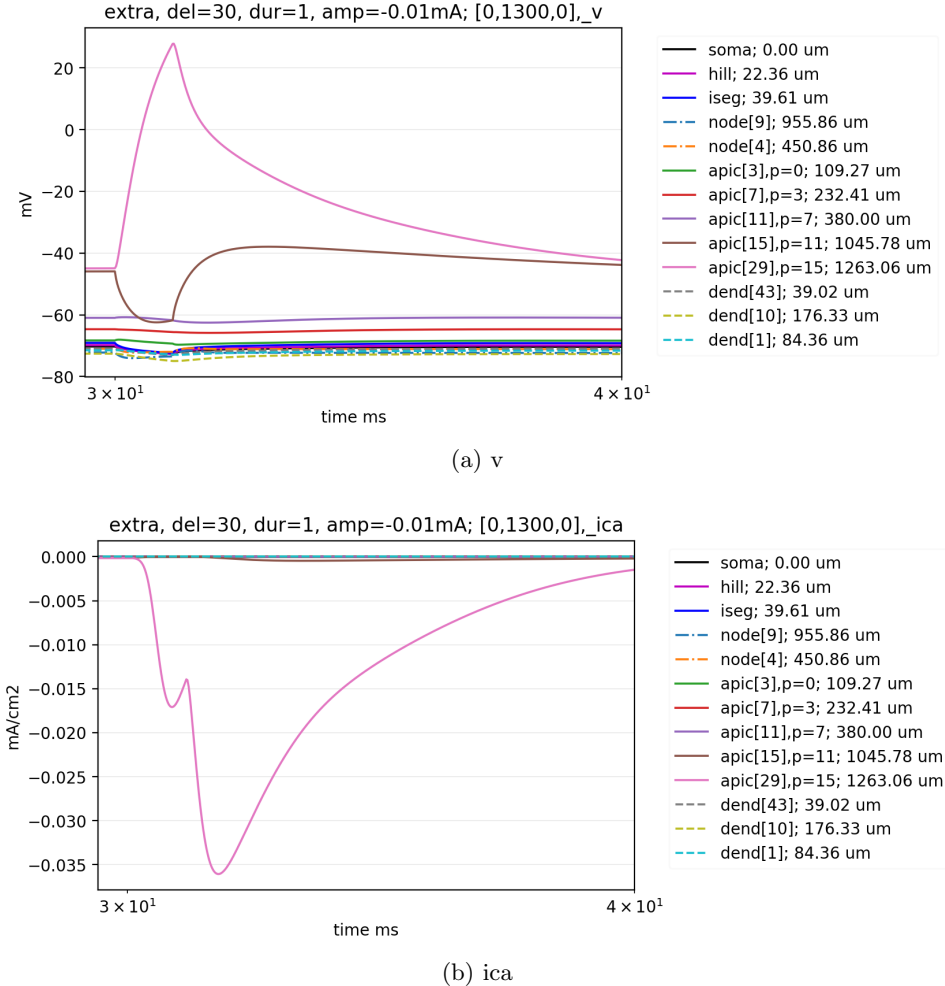


Figure 4.11: Cathodic Stimulation, coord=(0,1300,0): a) Hyperpolarization of the somatic region is obvious. Apical dendrites next to the electrode experience depolarization and furthermore dendritic spiking. Neighbouring regions of the apical path down the y-axis get hyperpolarized. b) Clearly shows the pronounced dynamics of the calcium mechanism at apic[29]. What we notice is a small change of direction right before stimulation comes to a halt. This is due to the effect of increasing V_m and the electric field that acts upon charged ions like calcium ions. Right before stimulation comes to a halt, the curve changes its direction pointing to north. As soon the stimulation is turned off, the influx of calcium ions again increases. The activity of the ion channel is only postponed. From the perspective of the HH formalism and its underlying differential equations we can say that the voltage time course sketches a homoclinic orbit in the phase space.

Summarizing those findings we chose to evaluate an anodic SDuR of the axon initial segment and a cathodic SDuR of apic[29]. The results are plotted in [Figure 4.12](#). At this

4 Results

distance it was not possible to initiate an somatic AP through cathodic excitation of the apical dendrites. Levels of membrane voltage in the near neighbourhood of the electrode would get too high which would lead to cellular damage.

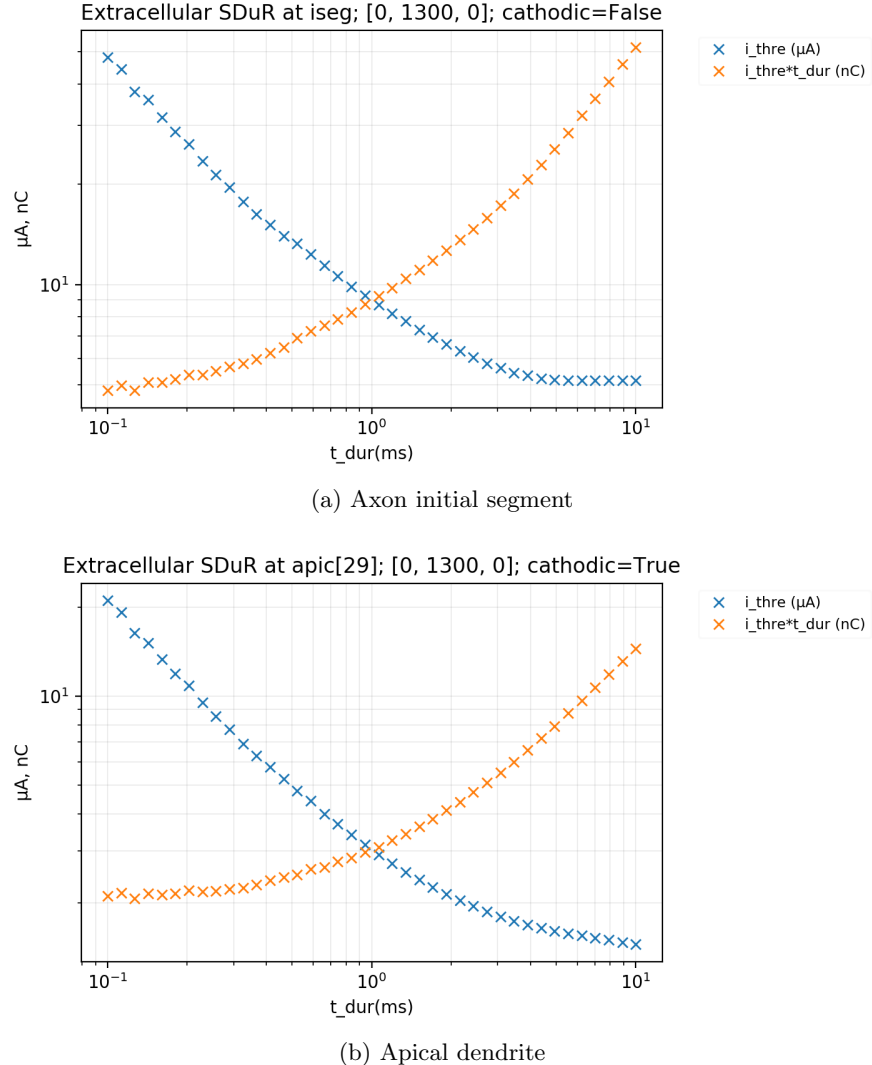


Figure 4.12: Extracellular SDuR (0,1300,0): a) Anodic excitation leads to firing of the axon initial segment. The threshold current (blue) is plotted together with the amount of charge (orange). For small times t_{dur} we can conclude that the charge remains almost constant. The Rheobase is $5\mu\text{A}$. b) The curve of the apical dendrite has the same declining behaviour. The Rheobase is at approximately $1.5\mu\text{A}$.

4.2.2 Mid-range distance

We would like to study the effects of mid-range distance stimulation upon the soma. For this purpose we chose (100,300,50) as the new coordinates for placement of the extracellular point-source. We study the effects of cathodic and anodic stimulation. The morphological distribution of membrane voltage for both cases right after stimulation comes to a halt, is sketched in [Figure 4.13](#). Findings were the following.

1. Cathodic stimulation leads to hyperpolarization of the somatic region. It also leads to AP initiation in the apical dendrites next to the electrode. The morphological setting is sketched in [Figure 4.13](#). apic[7] from the recorded apical path was closest to the electrode and got depolarized. Although the soma got hyperpolarized during the stimulation, right after stimulation comes to a halt, two scenarios occurred which led to AP initiation in the axon initial segment.
 - a) **scenario 1:** The axon initial segment fired after stimulation came to a halt despite none of the apical dendrites left the subthreshold region. The situation is discussed in [Figure 4.14](#). There were also several basal dendrites present proximal to the electrode. The voltage course of the first four basal dendrites closest to electrode together with their paths towards the soma, was recorded. This was done with the intention to systematically exclude that any influence may have originated from the basal dendrites that may have led to AP initiation in the axon initial segment. In the following we list the four closest basal dendrites together with their paths,

53 – 51 – 42 – *soma*,
 59 – 56 – 42 – *soma*,
 60 – 41 – *soma*,
 54 – 51 – 42 – *soma*.

The numbers refer to the ids of basal dendrites. Obviously the ids 42 and 41 are common predecessor. Therefore it suffices to consider only those two.

- b) **scenario 2:** The axon initial segment fired after stimulation comes to a halt with AP initiation in the apical dendrites happening beforehand. It is assumed that AP initiation in the apical dendrites facilitates the generation of an AP in the axon initial segment. Unlike scenario 1 the curve of calcium current of apic[7] is also much more prominent, unveiling the calcium mechanism with its high time constant. [Figure 4.15](#)
2. For anodic stimulation we could observe the same phenomena as for the case of long-range distance stimulation.

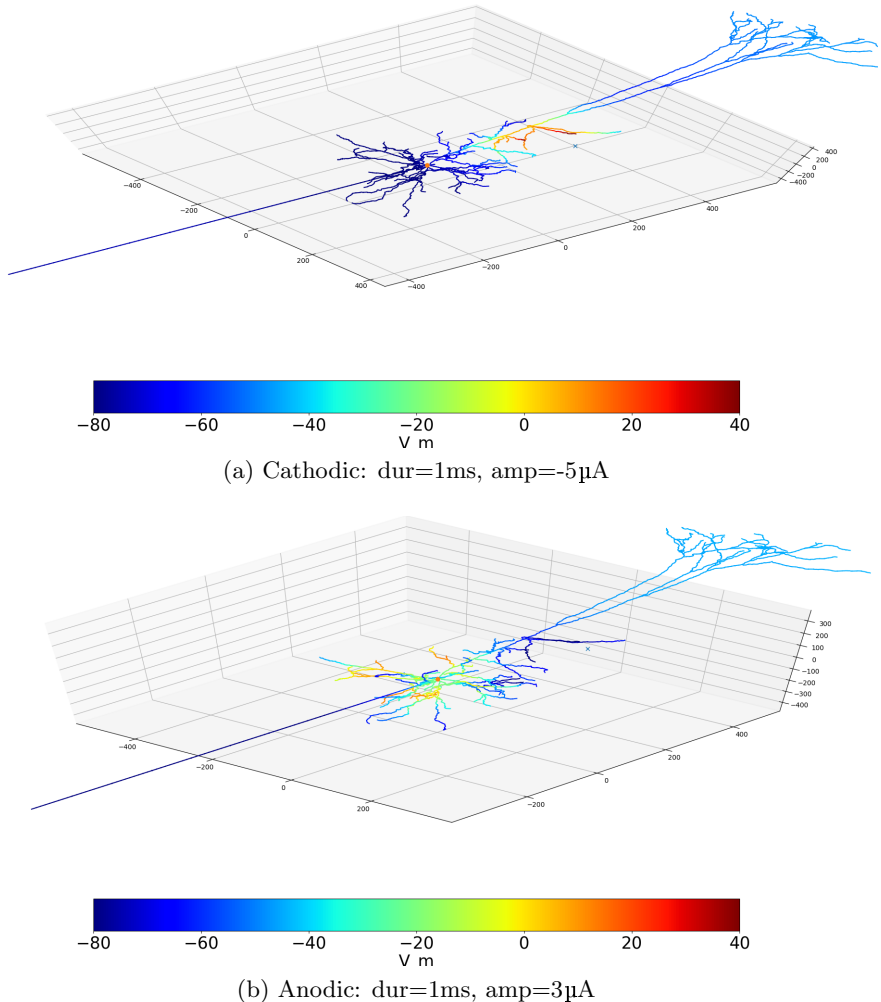


Figure 4.13: Morphological voltage-distribution, coord=(100,300,50): a) Cathodic excitation clearly depolarized the apical dendrites in the near neighbourhood of the point-source while structures further away got hyperpolarized. b) Anodic excitation led to hyperpolarization of the near neighbourhood surrounding the electrode and at the same time depolarizing the region around the soma.

4 Results

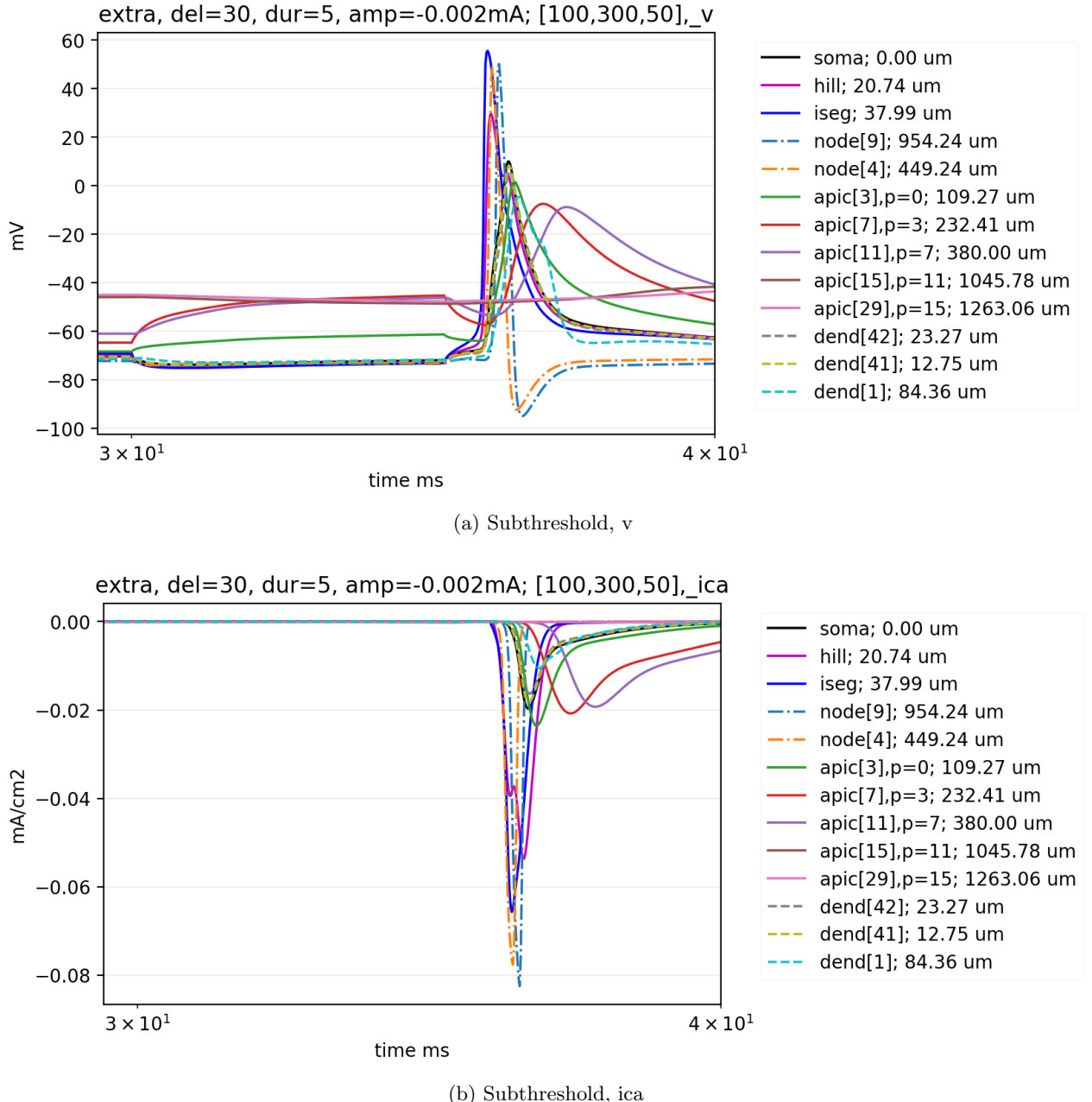


Figure 4.14: Cathodic stimulation scenario 1:

- After stimulation comes to a halt an AP is initiated in the axon initial segment. This happens although the somatic region was hyperpolarized beforehand. We suspect that the neighbouring apical dendrites facilitate the AP initiation in the axon initial segment through equalizing intracellular currents.
- Typical calcium current dynamics. The axon initial segment is the leading edge of channel activation.

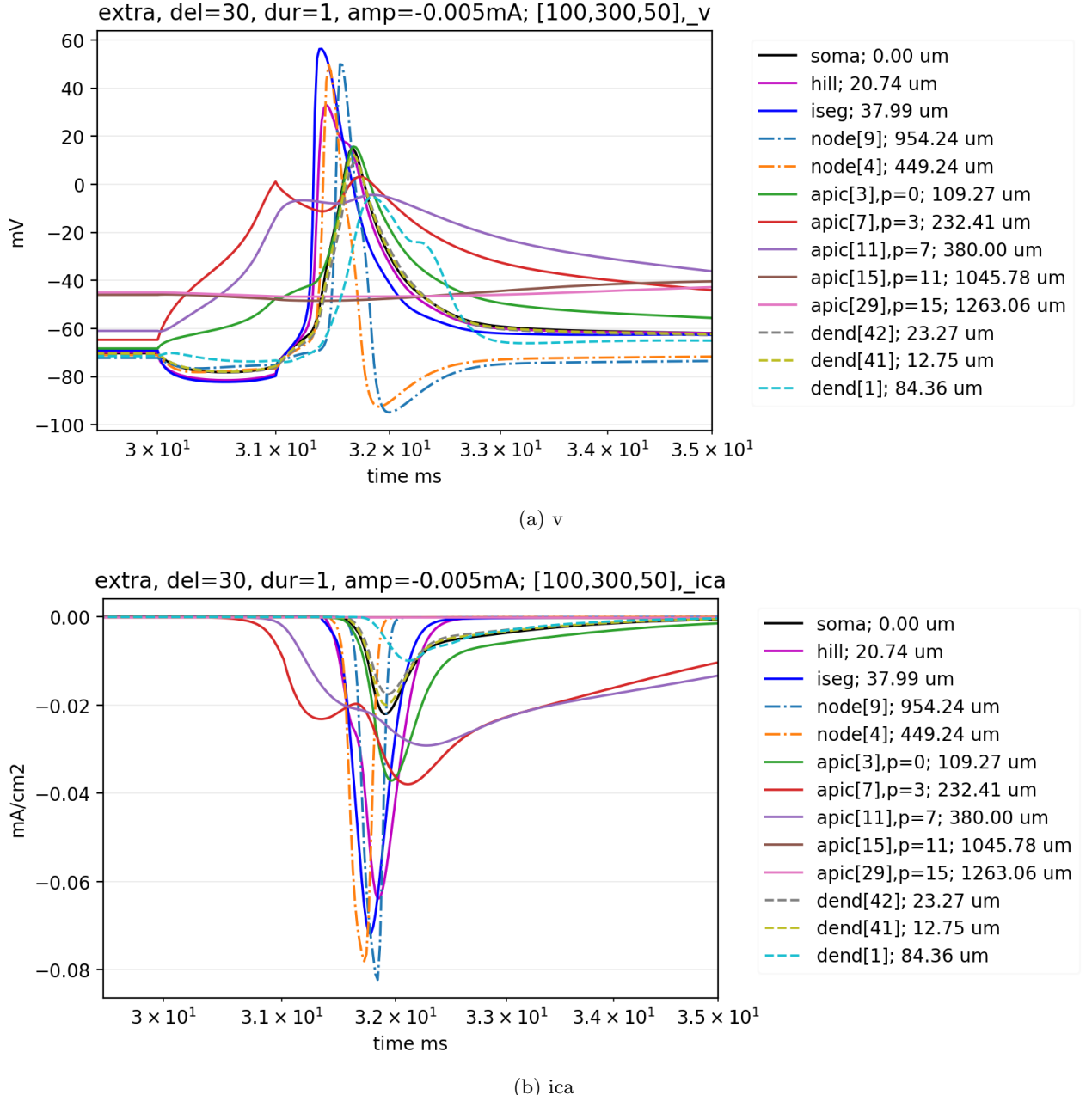


Figure 4.15: Cathodic stimulation scenario 2:

- a) The graph shows the hyperpolarization of the somatic region with beforehand AP initiation in the apcial dendrites. As soon stimulation comes to a halt, the axon initial segment fires. b) The peaks of calcium current are greater than for scenario 1. Furthermore, the calcium current dynamics start even before an AP was initiated in the initial sgement. This circumstance obviously leads to some kind of temporal summation which generates a second local maxima for apic[7] right after an AP was initiated in the axon initial segment.

4 Results

Combining those findings we evaluated the SDuR for direct anodic excitation of the axon initial segment as well as that of cathodic excitation with beforehand AP initiation in the apical dendrites, described by scenario 2.

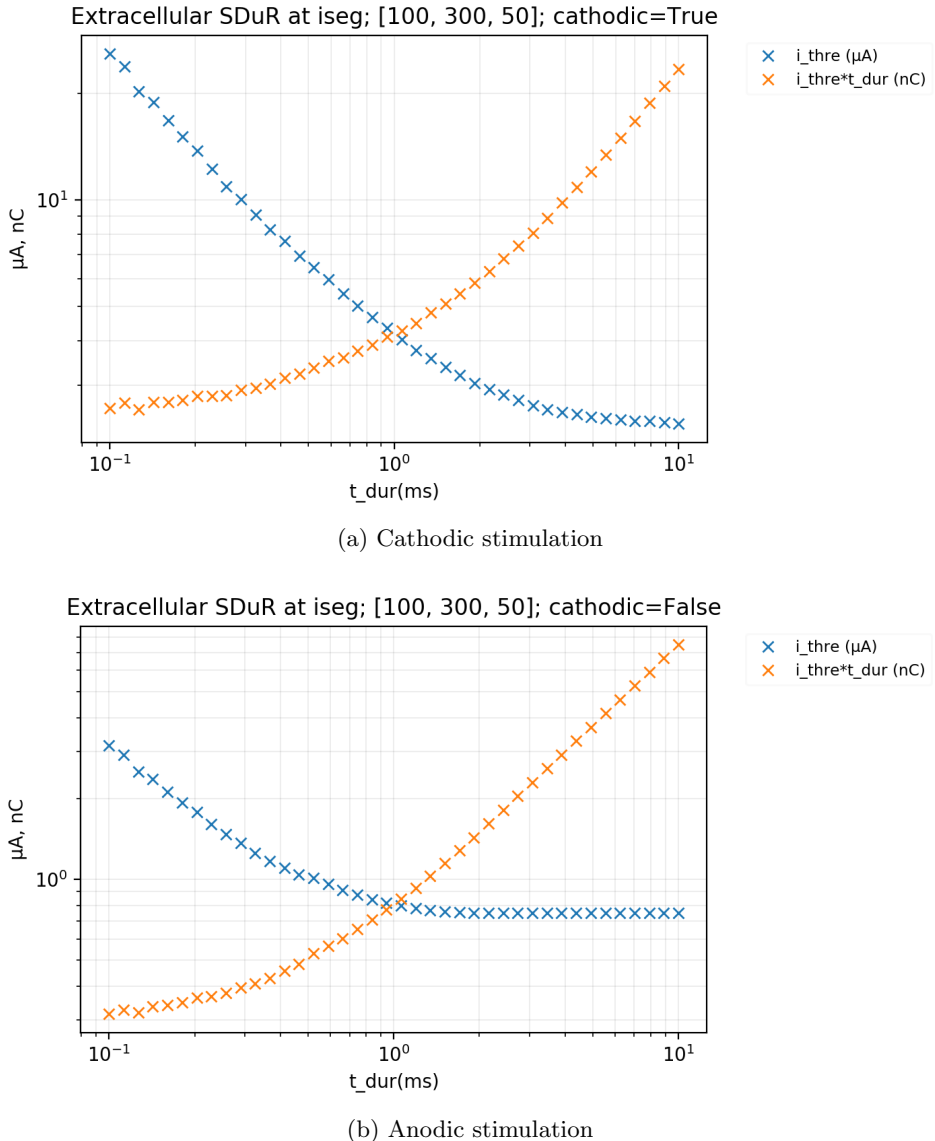


Figure 4.16: Extracellular SDuR (100,300,50) of the axon initial segment:

- a) Cathodic stimulation with threshold current and injected charge. The Rheobase is approximately $1\mu\text{A}$.
- b) Anodic stimulation leads to a Rheobase of $0.75\mu\text{A}$. AP initiation in the axon initial segment usually does not take that long.

4.2.3 Lateral to soma

Now we want to study the effects extracellular excitation has upon the basal dendrites and the nodes of Ranvier. For this purpose we chose the coordinates (300,0,0) for the placement of the electrode, lateral to the soma. We will keep an eye on the four basal dendrites closest to the electrode together with their paths towards the soma. A Python method was implemented in order to emit any number of closest dendrites in descending order (section with smallest distance first), given a tuple of 3d coordinates. We especially kept an eye on V_m for the closest dendrite in order not to reach cell damaging levels. In the following we list the four closest basal dendrites together with their paths

$4 - 1 - 0 - \text{soma},$
 $3 - 1 - 0 - \text{soma},$
 $58 - 56 - 42 - \text{soma},$
 $2 - 1 - 0 - \text{soma}.$

The numbers refer to the ids of basal dendrites. Obviously the dendrites with ids 42 and 1 are common predecessors. It suffices to record only those two together with number 4 denoting the closest dendrite. The morphological setting is sketched in [Figure 4.17](#).

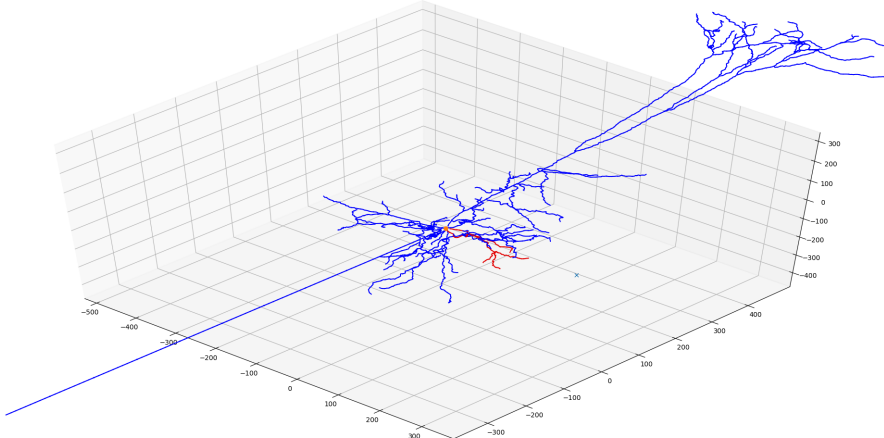


Figure 4.17: Trial, coord=(300,0,0):
Recorded paths of basal dendrites are marked in red.

During the trials we made following observations,

1. Cathodic stimulation led to hyperpolarization of far distant nodes in the axon. The axon initial segment got depolarized and generated an AP which then propagated further along the axon. The situation for the subthreshold-case and AP initiation process are visualized in [Figure 4.18](#).
2. Anodic stimulation led to hyperpolarization of the near somatic region as well as depolarization and subsequent AP initiation in the most distant node of Ranvier, node[9]. The situation is sketched in [Figure 4.19](#).

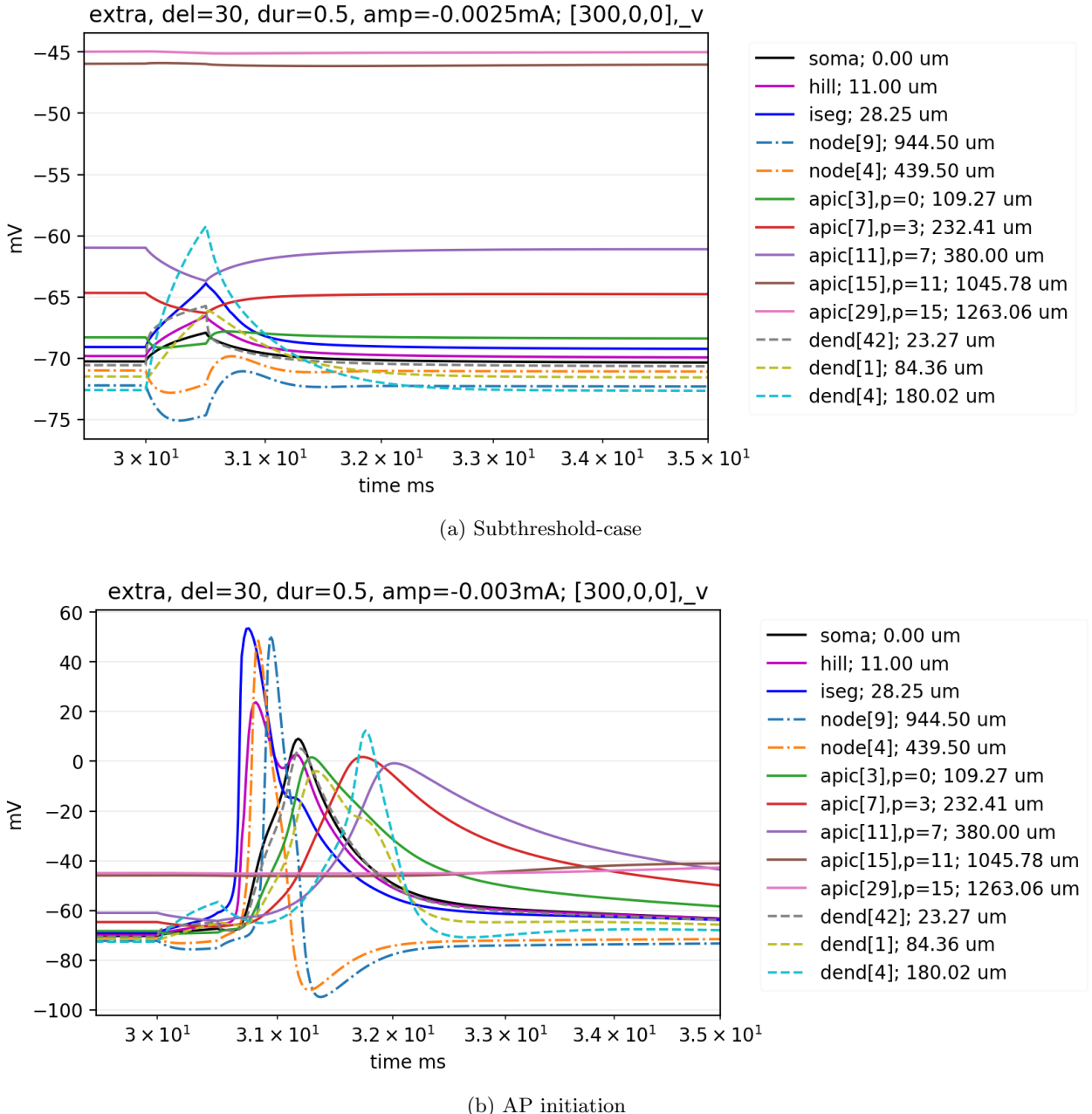


Figure 4.18: Cathodic stimulation, coord=(300,0,0): a) In the subthreshold-case it becomes clear that the axon initial segment is the leading edge of AP generation. b) The axon initial segment generates an AP that subsequently propagates along the axon. Furthermore, an AP could also be initiated in the basal dendrites.

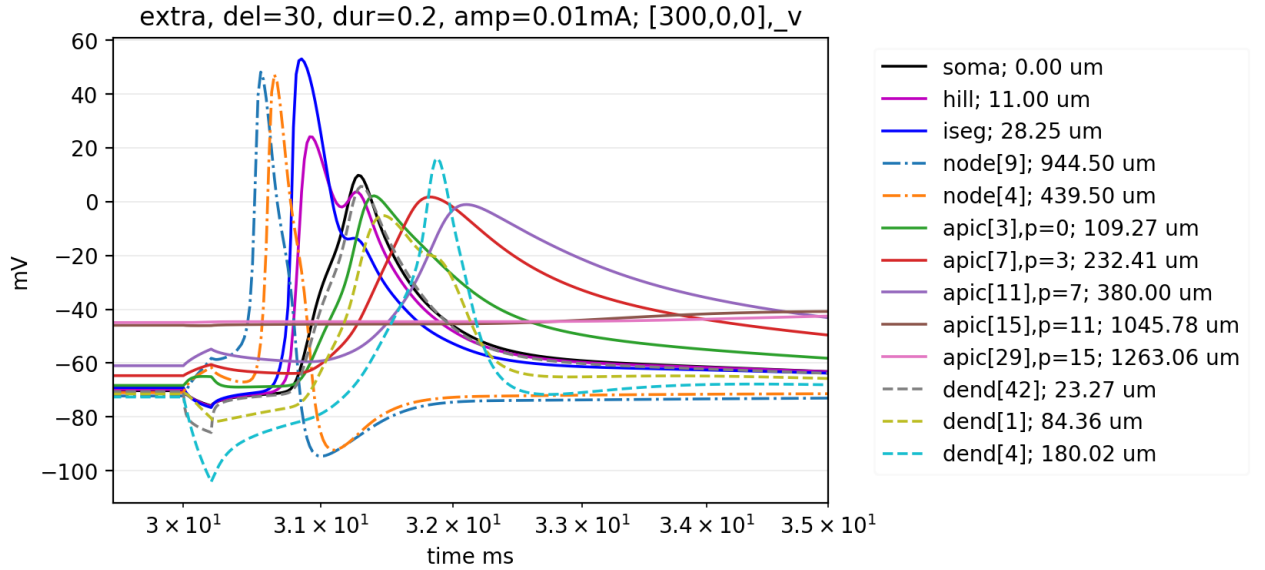


Figure 4.19: Anodic stimulation, coord=(300,0,0): Anodic stimulation led to initiation of an AP at the most distant axonal node node[9] which then propagated along the axon and got amplified in the axon initial segment. During stimulation the close neighbourhood of the soma gets hyperpolarized.

Summarizing those findings we chose to evaluate a cathodic SDuR of the axon initial segment and an anodic SDuR of node[9]. The results are the following [Figure 4.20](#).

4 Results

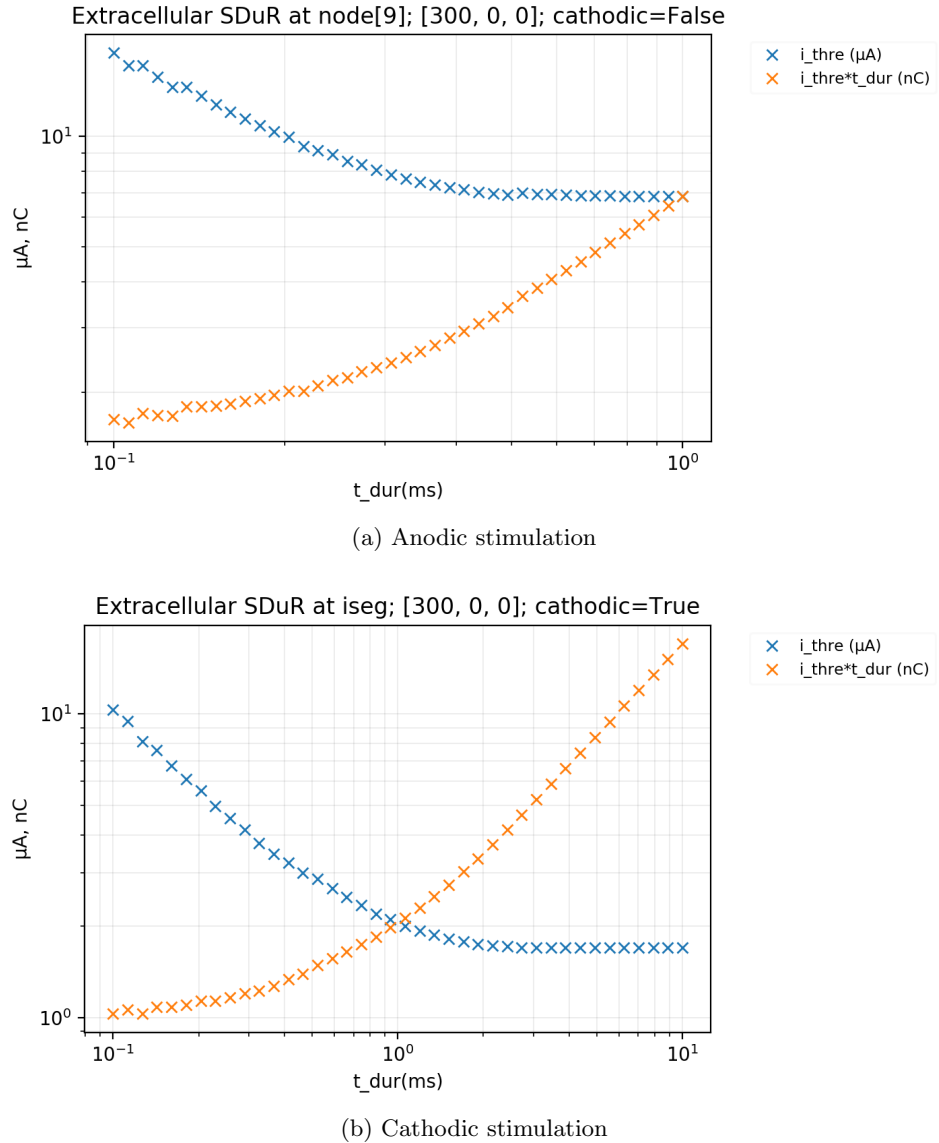


Figure 4.20: Extracellular SDuR (300,0,0):

- a) The Rheobase of the most distant node of the Ranvier lacing is reached quite fast at 0.5ms with a value of $7\mu\text{A}$.
- b) The Rheobase for the axon initial segment is reached at 2ms with value $1.7\mu\text{A}$. Obviously, cathodic stimulation is more efficient when it comes to excitation of the axon initial segment.

5 Discussion

In this work we enlightened the complex effects extracellular stimulation has upon a L5 pyramidal cell. There were a lot of ion-dynamics to keep an eye on. The probably most interesting and novel part was to observe the influence of the presence of calcium dynamics upon AP-form and calcium-spiking in the apical dendrites. The presence of the calcium mechanism and studying its dynamics allowed us to better comprehend the mechanisms behind propagation of AP in apical dendrites and synaptic integration.

5.1 Summary

We have observed several phenomena throughout the work depending on the chosen type of excitation.

For the case of intracellular stimulation we turned off the influence of the axon and especially that of the highly excitable axon initial segment. This was done with the aim to solely focus on the influence of AP initiation in the apical dendrites and its influence on the soma. A SDR was then evaluated by plotting the minimal threshold current as a function of the distance from the soma. Our findings confirmed the results from [Almog and Korngreen \(2014\)](#), that initiation of somatic AP through current injection in the apical dendrite gets almost exponentially harder with further distance from the soma. Still, in contrast to these results we used stimulation with duration of 10ms and instead of decreasing conductivity values of the axon by a factor of 10, we removed it completely. This naturally led to an increase of somatic threshold values by making it harder to initiate an AP in the soma without the presence of an axon.

By use of the strength distance relation we identified suitable regions for current injection into the apical dendrites for which the lower membrane threshold of the soma does not reach cell damaging levels. We clearly identified expected differences in somatic AP-form, depending whether basal or apical dendrites were excited. Somatic AP initiation through intracellular excitation of basal dendrites provided sodium driven form of somatic AP with fast declining tail. Excitement through current injection into an apical dendrite confirmed to have long-lasting effect on the somatic AP-form. It led to a small offset in membrane voltage for a duration of 20 to 30ms in the aftermath of an AP initiation. This behaviour is attributed to the peculiarity of backpropagating AP and the effects of temporal integration for apical dendrites which may be explained by the high time constant of the calcium dynamics.

The application of extracellular stimulation gave us some interesting insights on how hyper- as well as depolarized regions affected AP initiation in considered regions. In a more general view we studied if AP generated in the dendrites or axon managed to initiate an AP in the axon initial segment and consequently in the soma itself.

In the case of long-range distance stimulation the electrode was placed above the apical tuft. Cathodic stimulation led to dendritic spikes in the apical dendrites near the electrode and to hyperpolarization of regions further away, including the region surrounding the soma. Anodic stimulation led to depolarization of the soma and AP initiation in the axon initial segment. For mid-range distance stimulation the electrode was placed at almost midway along the apical ascending branch and with lateral offset to the soma. Cathodic stimulation led to AP initiation in nearby apical dendrites and to hyperpolarization of the region surrounding the soma together with the axon initial segment. Although the axon initial segment got hyperpolarized during stimulation as soon stimulation came to a halt, an AP was initiated in the latter. This was even the case although none of the apical dendrites generated an AP beforehand. This was observed for square-wave stimulation with a duration of 10ms.

In the case of lateral positioning of the electrode we addressed the behaviour of basal dendrites close to the electrode as well as that of the distant nodes of the axon. In the case of cathodic stimulation an AP was initiated in the axon initial segment. No AP was generated in the basal dendrites, still leaving the impression that they facilitated its generation in the axon initial segment. At the same time, the nodes of Ranvier got hyperpolarized. In the case of anodic stimulation, the somatic region got hyperpolarized during stimulation. At the same time the most distant node of the Ranvier lacing got depolarized and managed to initiate an AP.

5.2 Outlook

Very interesting phenomena occurred in the case of extracellular stimulation. This work makes an approach to enlighten those phenomena from a physical point of view and find explanations eliminating as much spurious correlation as possible. This has been done by recording clusters of somatic paths as well as use of Python methods that determine nearest sections to an electrode. Further we facilitated the functionality of morphological voltage-plots in order to assess if there was any odd behaviour somewhere in the cell. The deducted results may be an approach for further investigation.

Bibliography

- B. Alberts, A. Johnson, J. Lewis, D. Morgan, M. Raff, K. Roberts, P. Walter, J. Wilson, and T. Hunt. *Molecular biology of the cell*. WW Norton & Company, 2017.
- M. Almog and A. Korngreen. A quantitative description of dendritic conductances and its application to dendritic excitation in layer 5 pyramidal neurons. *Journal of Neuroscience*, 34(1):182–196, 2014. doi: 10.1523/JNEUROSCI.2896-13.2014.
- J. Bekkers. Pyramidal neurons. 12 2011. doi: 10.1016/j.cub.2011.10.037.
- T. Berger, M. E. Larkum, and H.-R. Lüscher. High i_h channel density in the distal apical dendrite of layer V pyramidal cells increases bidirectional attenuation of EPSPs. *Journal of Neurophysiology*, 85(2):855–868, 2001. doi: 10.1152/jn.2001.85.2.855.
- D. Boinagrov, S. Pangratz-Fuehrer, B. Suh, K. Mathieson, N. Naik, and D. Palanker. Upper threshold of extracellular neural stimulation. *Journal of neurophysiology*, 108(12), 2012. doi: <https://doi.org/10.1152/jn.01058.2011>.
- P. Booker, S. Whyte, and E. Ladusans. Long QT syndrome and anaesthesia. *British Journal of Anaesthesia*, 90(3):349–366, 2003.
- I. Burian. The upper threshold phenomenon in a pyramidal neuron stimulated with a multicompartment model. Master's thesis, Technical University Vienna, 2017.
- D. Chambers, C. Huang, and G. Matthews. *Basic physiology for anaesthetists*. Cambridge University Press, 2019.
- S. T. Destexhe A, Babloyantz A. Ionic mechanisms for intrinsic slow oscillations in thalamic relay neurons. *Biophysical journal*, 65(4):1538–52, 1993. doi: 10.1016/S0006-3495(93)81190-1.
- A. Fellner. Modelling block of excitation of a retinal ganglion cell stimulated with microelectrodes using python and neuron. Master's thesis, Technical University Vienna, 2017.
- D. E. Goldman. Potential, impedance, and rectification in membranes. *The Journal of general physiology*, 27(1):37–60, 1943.
- T. Guo, D. Tsai, S. Bai, J. Morley, G. Suaning, N. Lovell, and S. Dokos. Understanding the retina: A review of computational models of the retina from the single cell to the network level. *Critical reviews in biomedical engineering*, 42(5):419–36, 01 2014. doi: 10.1615/CritRevBiomedEng.2014011732.

BIBLIOGRAPHY

- M. Hines. Neuron - a program for simulation of nerve equations, 1993.
- A. L. Hodgkin and A. F. Huxley. A quantitative description of membrane current and its application to conduction and excitation in nerve. *The Journal of physiology*, 117(4): 500–544, 1952.
- N. Keren, N. Peled, and A. Korngreen. *Constraining Compartmental Models Using Multiple Voltage Recordings and Genetic Algorithms*, volume 94. 2005. doi: 10.1152/jn.00408.2005.
- N. Keren, D. Bar-Yehuda, and A. Korngreen. *Experimentally guided modelling of dendritic excitability in rat neocortical pyramidal neurones*, volume 587. 2009. doi: <https://doi.org/10.1113/jphysiol.2008.167130>.
- M. E. Larkum, T. Nevian, M. Sandler, A. Polksy, and J. Schiller. Synaptic integration in tuft dendrites of layer 5 pyramidal neurons: A new unifying principle. *Science*, 325 (5941):756–760, 2009. doi: 10.1126/science.1171958.
- A. Mahnam, S. M. R. Hashemi Golpayegani, and W. Grill. Measurement of the current–distance relationship using a novel refractory interaction technique. *Journal of neural engineering*, 6:036005, 07 2009. doi: 10.1088/1741-2560/6/3/036005.
- Z. F. Mainen and T. J. Sejnowski. Influence of dendritic structure on firing pattern in model neocortical neurons. *Nature*, 382(6589):363–366, 1996.
- H. Meffin, B. Tahayori, D. B. Grayden, and A. N. Burkitt. Modeling extracellular electrical stimulation: I. derivation and interpretation of neurite equations. *Journal of Neural Engineering*, 9(6):065005, nov 2012. doi: 10.1088/1741-2560/9/6/065005.
- W. R. J. Pivovarov A. S., Calahorro F. Na+/k+-pump and neurotransmitter membrane receptors. 19(1):1, 2018. doi: 10.1126/science.1171958.
- J. Ranck J. B. Which elements are excited in electrical stimulation of mammalian central nervous system: a review. *Brain research*, 98(3):417–440, 1975. doi: [https://doi.org/10.1016/0006-8993\(75\)90364-9](https://doi.org/10.1016/0006-8993(75)90364-9).
- F. Rattay. *Electrical Nerve Stimulation: Theory, Experiments and Applications*. Springer, 1990.
- F. Rattay, R. J. Greenberg, and S. Resatz. *Handbook of neuroprosthetic methods*. 01 2002.
- F. Rattay, L. Paredes, and R. Leao. Strength–duration relationship for intra- versus extracellular stimulation with microelectrodes. *Neuroscience*, 214:1–13, 2012. ISSN 0306-4522. doi: <https://doi.org/10.1016/j.neuroscience.2012.04.004>.
- N. Spruston. Pyramidal neurons: dendritic structure and synaptic integration. *Nature Reviews Neuroscience*, 9:206–221, 03 2008. doi: 10.1038/nrn2286.

BIBLIOGRAPHY

- X. Sun, X. Gu, and G. G. Haddad. Calcium influx via l- and n-type calcium channels activates a transient large-conductance ca₂₊-activated k⁺ current in mouse neocortical pyramidal neurons. *The Journal of neuroscience*, 23(9):3639–3648., 2003. doi: 10.1085/jgp.27.1.37.
- S. R. Williams and G. J. Stuart. Site independence of epsp time course is mediated by dendritic ih in neocortical pyramidal neurons. *Journal of Neurophysiology*, 83(5):3177–3182, 2000. doi: 10.1152/jn.2000.83.5.3177.
- J. Zhang. Basic neural units of the brain: Neurons, synapses and action potential, 2019.